Molecular Pharmacology Fast Forward. Published on April 2, 2020 as DOI: 10.1124/mol.119.118539
This article has not been copyedited and formatted. The final version may differ from this version.

Tubulin-Binding 3,5-Bis(styryl)pyrazoles as Lead Compounds for the Treatment of Castration-Resistant Prostate Cancer

Vivian W.Y. Liao,[#] Anuradha Kumari,[#] Rajeshwar Narlawar, Soma Vignarajan, David E. Hibbs, Dulal Panda, and Paul W. Groundwater

Sydney Pharmacy School, Faculty of Medicine and Health, The University of Sydney, Sydney, NSW 2006, Australia (VWYL, RN, DEH, PWG); Department of Biosciences and Bioengineering, Indian Institute of Technology Bombay, Mumbai 400076, India (AK, DP); Charles Perkins Centre, The University of Sydney, Sydney, NSW 2006, Australia (SV)

Molecular Pharmacology Fast Forward. Published on April 2, 2020 as DOI: 10.1124/mol.119.118539
This article has not been copyedited and formatted. The final version may differ from this version.

Running Title: Novel Tubulin-Binding 3,5-Bis(styryl)pyrazoles

Corresponding authors:

Paul W GROUNDWATER, Sydney Pharmacy School, Faculty of Medicine and Health, The University of Sydney, Sydney, NSW 2006, Australia; e-mail: paul.groundwater@sydney.edu.au

Dulal PANDA, Department of Biosciences and Bioengineering, Indian Institute of Technology Bombay, Mumbai 400076, India; e-mail: panda@iitb.ac.in

Text pages: 26

Tables: 5

Figures: 14

References: 39

Abstract: 232 words

Introduction: 347 words

Discussion: 796 words

Molecular Pharmacology Fast Forward. Published on April 2, 2020 as DOI: 10.1124/mol.119.118539
This article has not been copyedited and formatted. The final version may differ from this version.

Abstract

The microtubule-binding taxanes, docetaxel, and cabazitaxel, are administered intravenously for the treatment of castration-resistant prostate cancer (CRPC) as the oral administration of these drugs is largely hampered by their low and highly variable bioavailabilities. Using a simple, rapid, and environmentally friendly, microwave-assisted protocol, we have synthesized a number of 3,5-bis(styryl)pyrazoles **2a-l**, thus allowing for their screening for anti-proliferative activity in the androgen-independent PC3 prostate cancer cell line. Surprisingly, two of these structurally simple 3,5-bis(styryl)pyrazoles (**2a** and **2l**) had GI_{50} values in the low micromolar range in the PC3 cell line and were thus selected for extensive further biological evaluation (apoptosis and cell cycle analysis, and effects on tubulin and microtubules). Our findings from these studies show that 3,5-bis[(1*E*)-2(2,6-dichlorophenyl)ethenyl]-1*H*-pyrazole **2l** (i) caused significant effects on the cell cycle in PC3 cells, with the vast majority of treated cells in the G_2/M phase (89%), (ii) induces cell death in PC3 cells even after the removal of the compound, (iii) binds to tubulin (K_d 0.4 ± 0.1 μM) and inhibits tubulin polymerization *in vitro*, (iv) had no effect upon the polymerization of the bacterial cell division protein FtsZ (a homolog of tubulin), (v) is competitive with paclitaxel for binding to tubulin but not with vinblastine, crocin, or colchicine, and (vi) leads to microtubule depolymerization in PC3 cells. Taken together, these results suggest that 3,5-bis(styryl)pyrazoles warrant further investigation as lead compounds for the treatment of CRPC.

Significance statement

The taxanes are important components of prostate cancer chemotherapy regimens, but their oral administration is hampered by very low and highly variable oral bioavailabilities resulting from their poor absorption, poor solubility, high first-pass metabolism, and efficient efflux by P-glycoprotein. New chemical entities (NCEs) for the treatment of prostate cancer are thus required

Molecular Pharmacology Fast Forward. Published on April 2, 2020 as DOI: 10.1124/mol.119.118539
This article has not been copyedited and formatted. The final version may differ from this version.

and we report here the synthesis and investigation of the mechanism of action of some bis(styryl)pyrazoles, demonstrating their potential as lead compounds for the treatment of prostate cancer.

Introduction

Globally, prostate cancer is the second most common male cancer in terms of incidence, and fifth in terms of mortality, with over 300,000 men dying from the disease every year (Todd et al., 2018). Tumour growth in the early stages of prostate cancer is androgen-dependent, so the typical treatment for early metastatic prostate cancer is androgen deprivation therapy with a gonadotropin-releasing hormone analogue such as leuprolide, often in combination with an anti-androgen such as flutamide (Crawford et al., 1989; Garnick, 1997, Taplin and Balk, 2004). As the disease progresses, however, molecular and cellular changes occur so that cancer becomes androgen-independent / hormone refractory (termed castration-resistant prostate cancer [CRPC]) and unresponsive to current hormone therapy (Todd et al., 2018; Feldman and Feldman, 2001). This form of prostate cancer is aggressive, highly metastatic, is associated with poor prognosis (mean survival time of 18-24 months) (Abouelfadel and Crawford, 2008) and there is no effective treatment (Karantanos et al., 2013).

Paclitaxel has been used in the treatment of prostate cancer, and the semi-synthetic taxanes, docetaxel, and cabazitaxel, are administered intravenously for the treatment of castration-resistant prostate cancer (CRPC). The oral administration of these drugs is hampered by their low and highly variable bioavailabilities (Torne et al., 2010), which are due to their poor absorption (a result of their poor solubilities), efficient efflux by P-glycoprotein (P-gp), which is abundant in the gastrointestinal tract, and high first-pass metabolism by CYP450s, CYP2C8 and 3A4.

Molecular Pharmacology Fast Forward. Published on April 2, 2020 as DOI: 10.1124/mol.119.118539
This article has not been copyedited and formatted. The final version may differ from this version.

We report here the discovery of a 3,5-bis(styryl)pyrazole analogue **2l** which induces cell death in PC3 cells (Pululkuri et al., 2005; Schmitt et al., 2014) even after the removal of the compound. The compound binds to tubulin (K_d 0.4 ± 0.1 μM), inhibits tubulin polymerization *in vitro* (with no effect upon the polymerization of the bacterial homolog *Spn*FtsZ or on the activity of alkaline phosphatase). Pyrazole **2l** is competitive with paclitaxel for binding to tubulin (but not with vinblastine, crocin, or colchicine) and treatment with pyrazole **2l** results in microtubule depolymerization in PC3 cells, suggesting the further investigation of these 3,5-bis(styryl)pyrazoles as lead compounds for the treatment of CRPC.

Materials and Methods

General synthetic chemistry procedures

The 3,5-bis(styryl)pyrazoles **2a-l** were synthesized from the curcuminoids **1** (Supplemental Methods) using a CEM Discover SP microwave synthesis system. The spectroscopic and analytical data for pyrazoles **2a** (Amolins et al., 2009; Mayadevi et al., 2012), **2b** (Amolins et al., 2009) and **2k** (Luo et al., 2013) were identical to that reported previously. Melting points were determined on a Stuart Scientific SMP10 apparatus. IR spectra were obtained on a FTIR-8400S Shimadzu system, using NaCl plates and values are recorded as wave-numbers (cm^{-1}). ^{1}H and ^{13}C NMR spectra were recorded at 400 and 100 MHz, respectively, on a Varian 400-MR magnetic resonance spectrometer, with chemical shifts (δ) reported in parts per million (ppm). Spectra were acquired in solutions of deuterated solvents and the residual solvent peaks were used as internal references; 7.24 ppm ($CDCl_3$), 2.50 ppm (DMSO-d_6), 2.05 ppm (acetone-d_6) and 3.31 ppm (methanol-d_4). Low-resolution electrospray ionization (ESI) mass spectrometry was performed on a TSQ Quantum Access Max LCMS/MS (Thomas R Watson Mass Spectrometry Laboratory, Sydney Pharmacy School, The University of Sydney) and high-resolution mass spectroscopy was

Molecular Pharmacology Fast Forward. Published on April 2, 2020 as DOI: 10.1124/mol.119.118539
This article has not been copyedited and formatted. The final version may differ from this version.

performed on a Bruker 7T Fourier transform ion cyclotron resonance mass spectrometer (Mass Spectrometry Unit, School of Chemistry, The University of Sydney). Elemental analysis was performed on a Thermo Flash 2000 Elemental Analyser (Campbell Microanalytical Laboratory, University of Otago, New Zealand). All reagents were commercially available and purchased from Sigma Aldrich (Castle Hill, Sydney, Australia), Alfa Aesar (VWR, Australia). Solvents were purchased from Chem-Supply (Australia) and were used as received. Flash column chromatography was performed using Grace Davison (LC604 40-63 µm) Davisil chromatographic silica media. Thin layer chromatography (TLC) was performed using Grace Davidson Reveleris, aluminum-backed TLC plates (UV254).

General experimental procedure for the synthesis of pyrazoles 2a-l

Pyrazole derivatives **2a-l** were synthesized using a modification of the method of Mayadevi *et al*. (2012). Curcuminoids **1** (1.0 mmol) were dissolved in DMF (1 mL). Acetic acid (1 mL) and hydrazine monohydrate (0.2 mL) were added to the solution in a microwave synthesizer tube. The mixture was placed in the microwave reactor and heated at 80 ˚C for 5 minutes with rapid stirring. The reaction was cooled then added dropwise to stirred water (100 mL). The solid was collected by filtration, purified by flash chromatography using a gradient mobile phase of ethyl acetate and hexane (1:4 to 1:1) and then recrystallized from ethanol. Spectroscopic and analytical data for the pyrazoles are provided in the Supplemental Methods.

General experimental procedure for the degradation studies

HiPerSolv® CHROMANORM® LC-MS grade acetonitrile and methanol were purchased from VWR International. HPLC grade glacial acetic acid was purchased from Fisher Scientific, UK. Ultrapure water was obtained with a SG, Ultra Clear water system. The chromatographic separation

Molecular Pharmacology Fast Forward. Published on April 2, 2020 as DOI: 10.1124/mol.119.118539
This article has not been copyedited and formatted. The final version may differ from this version.

was performed on a Aquacil C_{18} column (2.1 × 100 mm, 5 µm particle size, Thermo Scientific, USA).

An orbital mixter incubator (Ratek instruments, Australia) was used for the degradation study at 37 ˚C and 200 rpm. The HPLC analysis was carried out on a Shimadzu UFLC prominence system, consisting of a DGU-20A5R degassing unit, an LC-20AD pump, a SIL-20AHT autosampler, a SPD-M20A photodiode array (PDA) detector, and a PC with LabSolutions CS software for data acquisition and processing.

Chromatographic conditions and preparation of standards

The chromatographic method was adapted from Jayaprakasha *et al*. (2002). The mobile phase consisted of varying gradients of acetonitrile (A) and 2 % aq. acetic acid solution (B), with a flow rate of 0.75 mL/min. The total run time was 25 minutes, the last 10 minutes equilibrating the column for the next run. The wavelength of detection was the λ_{max} of each compound (**2a**; 325 nm; **2l** 300 nm). The injection volume was 10 µL. Table 1 summarizes the chromatographic conditions used for each of the compounds.

Methanolic standard stock solutions (1 mg/mL) were prepared for each of the analyzed compounds. The stock solutions were diluted in methanol to obtain concentrations of 0.01, 0.02, 0.03, 0.04, 0.05, and 0.06 mg/mL. For less concentrated standard samples of **2a** and **2l**, a 1 µg/mL standard stock was prepared from the 1 mg/mL stock and the stock solutions were diluted in methanol to obtain 100, 50, 20, 10, 5, and 2 ng/mL solutions. All standards were freshly prepared from the stock solutions on the day of analysis. The stock solutions were stored at -20 ˚C. The AUC versus the concentration of each compound standards was plotted and fitted with linear regression analysis using GraphPad Prism to calculate the slope, intercept, and correlation coefficient and thus determine the linearity of the standard curve (Supplemental Tables 1 and 2).

Molecular Pharmacology Fast Forward. Published on April 2, 2020 as DOI: 10.1124/mol.119.118539
This article has not been copyedited and formatted. The final version may differ from this version.

For reproducibility, the experiment was repeated three times, on three separate days, with freshly prepared standard solutions for each compound.

Degradation study

The degradation study was carried out according to the method outlined by Tønnesen and Karlsen (1985). Compounds **2a** and **2l** were dissolved in methanol (1 mg/mL concentration). The methanolic solution (100 μL) of the compounds was then added to pre-warmed PBS (900 μL, 37 ˚C) and placed in the orbital incubator. At time points of 1, 2, 4, 8, 12, 24, 48, and 72 hours, 100 μL of the solution was removed and extracted twice with ethyl acetate (2 × 200 μL). The ethyl acetate extracts were combined, evaporated and the residues were redissolved in methanol (200 μL) for HPLC analysis. 10 μL of the original methanolic solutions were removed, evaporated and redissolved in methanol (200 μL) and this was taken as t = 0. The area under the curve (AUC) is the total absorbance of the compound at that given concentration and was used for quantification. The degradation profiles of each of the compounds are expressed as percentages of compounds remaining in PBS at the sampled time, with the AUC at t = 0 taken as 100 %.

The detection and quantification limits for analogues **2a** and **2l** were calculated according to the method outlined in the guidelines of International Committee on Harmonization (2005) using the following formulae:

$$\text{Detection limit} = 3.3\sigma/\text{slope}$$

$$\text{Quantification limit} = 10\sigma/\text{slope}$$

Where σ is the standard deviation of errors in regression of the standard curve generated upon linear regression fitting of the average values of three standard curves (n = 3).

Molecular Pharmacology Fast Forward. Published on April 2, 2020 as DOI: 10.1124/mol.119.118539
This article has not been copyedited and formatted. The final version may differ from this version.

The detection and quantification limits for **2a** and **2l** were verified by injecting multiple samples (n = 6) at the concentrations of the detection and quantification limits. The accuracy is expressed as the percentage of the standard deviation divided by mean values of the six AUC values determined from the injected samples.

General experimental procedure for the *in vitro* testing

RPMI-1640, phosphate buffered saline (PBS), trypsin/EDTA 10 × solution, and 3-(4,5-dimethyl-2-thiazolyl)-2,5-diphenyl-2*H*-tetrazolium bromide (MTT) were purchased from Sigma Aldrich (Castle Hill, Sydney, Australia). Foetal bovine serum (FBS) of Australian origin was purchased from Bovogen. PC3 cells were purchased from ATCC (Cat. No. CRL-1435). Muse® Count & Viability Assay Kit, Muse® Annexin V & Dead Cell Assay kit and Muse® Cell Cycle Assay Kit were purchased from Millipore, Australia**.** A CLARIOstar® microplate reader was used to measure the absorbance of MTT formazan at 540 nm. A Muse™ Cell Analyzer (Merck, Millipore) was used to conduct the Annexin V apoptosis and cell cycle analysis assays.

Anti-proliferative assay

PC3 cells were grown in RPMI-1640 supplemented with 10 % FBS to ~70-80 % confluency before seeding. Anti-proliferative activity was determined by the MTT colorimetric assay (Mosmann, 1983). The MTT stock solution (12 mM) was prepared by dissolving 3-(4,5-dimethylthiazol-2-yl)-2,5-diphenyltetrazolium bromide in PBS (5 mg/mL) filtered through a 0.2 µm syringe filter.

The pyrazoles and methotrexate were dissolved in DMSO to make a 200 mM stock. PC3 cells were seeded in 96-well plates at 3,000 cells/well and incubated for 24 hours. The DMSO stock solutions were diluted in 10 % FBS supplemented RPMI 1640 media; six concentrations of each of the test compounds were added to wells (in triplicate) with the final DMSO concentration of less than 0.1

Molecular Pharmacology Fast Forward. Published on April 2, 2020 as DOI: 10.1124/mol.119.118539
This article has not been copyedited and formatted. The final version may differ from this version.

% in each well. 0.1 % of DMSO in RPMI medium, was also prepared and used as a vehicle control for each plate and represents 100% growth in this assay. The plates were then incubated for 72 hours (T_{72}).

After 72 hours, the medium was removed from each well and was replaced with 10 % MTT stock solution in serum and phenol red-free RPMI 1640 medium (100 µL/ well). The plates were then incubated for 3 hours at 37 ˚C before removing the medium and replacing it with DMSO (50 µL/ well). After mixing, the plates were placed in the microplate reader and the absorbance was determined. A control plate was prepared in the same way as above and read 24 hours (T_0) after seeding. The experiment was repeated at least three times on three separate days to give n = 3.

The percentage of inhibition of cell growth was then calculated using the following formula:

$$\% \text{ Growth inhibition} = 100 - \left(\left(\frac{Abs\ (T_{72}) - Ab\ \ (T_0)}{Abs\ (DMSO) - Abs\ (T_0)} \right) \times 100 \right)$$

GraphPad Prism was used to determine the GI_{50} values using a non-linear regression fit after first transforming concentrations to log scale values. All results were representative of three independent experiments conducted on three separate days.

Annexin V / propidium iodide apoptosis assay

PC3 cells were seeded in 6-well plates at cell densities of 100,000 cells per well and incubated for 24 hours. The pyrazoles **2a** and **2l** were added to the wells at their GI_{50} concentration. 0.1 % of DMSO in RPMI medium was used as a vehicle control. The cells were incubated for 72 hours, then they were trypsinized, centrifuged, stained with the Muse™ Annexin V/Dead Cell kit according to manufacturer's instructions and then analyzed using, Muse™ Cell Analyzer. The experiment was

Molecular Pharmacology Fast Forward. Published on April 2, 2020 as DOI: 10.1124/mol.119.118539
This article has not been copyedited and formatted. The final version may differ from this version.

conducted in duplicate, with data acquisition of 4000 events and the experiment was repeated three times on three separate days to give n = 3.

A set of experiments was performed following the same procedure as above but after 72 hours of drug treatment, the medium containing the pyrazoles was removed and replaced with fresh medium and the cells were incubated for a further 72 hours. Cells were then trypsinized, stained with the Muse™ Annexin V/Dead Cell kit, and analysed using the Muse™ Cell Analyzer. The experiment was conducted in duplicate, with data acquisition of 4000 events and the experiment was repeated three times on three separate days to give n = 3.

Cell cycle analysis

PC3 cells were treated in the same way as in the apoptosis assay except, after trypsinization, cells were counted, centrifuged and fixed with cold ethanol solution 70 % (v/v) at 1×10^6 cells/mL. The cells were left to fix overnight at -20 °C, then centrifuged, stained with the Muse™ Cell Cycle kit according to the manufacturer's instructions and then analyzed using the Muse™ Cell Analyzer. The experiment was conducted in duplicate with data acquisition of 5000 events and the experiment was repeated at least four times on four separate days, to give n = 4.

Experimental procedure for the tubulin and microtubule studies

The determination of the effects of the pyrazoles on the assembly kinetics of tubulin *in vitro*, the dissociation constant (K_d) for the binding of the analogues to tubulin, and effect on microtubules in cells were performed as described previously (Panda et al., 2005)

Tubulin purification

Tubulin was isolated from goat brain by two cycles of polymerization and depolymerization as described previously (Panda et al., 2005).

Molecular Pharmacology Fast Forward. Published on April 2, 2020 as DOI: 10.1124/mol.119.118539
This article has not been copyedited and formatted. The final version may differ from this version.

Light scattering

Tubulin (12 μM) was incubated with different concentrations of **2a** and **2l** in PEM (50 mM PIPES, 1 mM EGTA and 3 mM $MgCl_2$) buffer, pH 6.8 on ice for 10 minutes. After 10 minutes of incubation, 10% DMSO and 1 mM GTP was added to the reaction mixture and polymerization was monitored at 37 °C in a spectrophotometer, Spectramax M2^e, at 350 nm for 30 minutes. The experiment was repeated three times and the percentage inhibition of tubulin polymerization was calculated. The IC_{50} of polymerization was determined by fitting the data in dose-response inhibition curve in the GraphPad Prism Software.

Sedimentation assay

Tubulin (12 μM) was polymerized at 37 °C for 30 minutes in the presence and the absence of **2a** and **2l** as in light scattering. After 30 minutes, the polymerized microtubules were pelleted by centrifuging it at 33000 g, 30 °C for 30 minutes. The supernatant was separated and the amount of polymerized microtubules was calculated by loading the supernatant and pellet on the SDS-PAGE gel followed by intensity quantification of bands by ImageJ or by quantifying the supernatant protein concentration by Bradford's assay.

Determination of dissociation constant

Tubulin (2 μM) was incubated with and without different concentrations of **2a** or **2l** in 25 mM PIPES buffer pH 6.8 for 10 minutes at room temperature. After incubation, the spectra of tryptophan emission was recorded in a spectrofluorometer (JASCO FP-6500, Tokyo, Japan) by exciting the sample at 295 nm and recording the spectra. The fluorescence intensity at λ_{max} was noted and it was fitted in the following equation in GraphPad Prism software to determine the K_d.

$$\Delta F = \Delta Fmax \times \frac{([P_0]+[L_0]+K_d)-\sqrt{([P_0]+[L_0]+K_d)^2-4[P_0][L_0]}}{2[P_0]}$$

Molecular Pharmacology Fast Forward. Published on April 2, 2020 as DOI: 10.1124/mol.119.118539
This article has not been copyedited and formatted. The final version may differ from this version.

Where ΔF_{max} is the highest fluorescence intensity, P_0 is the concentration of protein and L_0 is the concentration of **2a** or **2l**.

Determination of tubulin binding site of pyrazole 2l

Competitive inhibition with colchicine

Tubulin (5 μM) was incubated without or with 10 and 20 μM of **2l** on ice for 10 min in 25 mM PIPES buffer pH 6.8 and then, incubated with 10 μM colchicine for 45 min at 37 °C. The fluorescence spectra (370 – 500 nm) were monitored using a fluorescence spectrophotometer (JASCO FP-6500, Tokyo, Japan) with excitation of the samples at 340 nm.

Competitive inhibition with vinblastine and crocin

First, we examined whether **2l** could inhibit the binding of vinblastine to tubulin using BODIPY-FL-Vinblastine, a fluorescent analogue of vinblastine (Lin and Chen, 2013). Tubulin (3 μM) was incubated with 200 nM of BODIPY-FL-vinblastine (Thermo Scientific; cat. no. V12390) on ice for 10 min in 25 mM PIPES buffer pH 6.8. The reaction mixture was then incubated without or with 1 and 5 μM of **2l** for 10 min on ice. The change in fluorescence of BODIPY-FL-Vinblastine was observed in a spectrofluorometer (JASCO FP-6500, Tokyo, Japan) by exciting at 488 nm and taking emission spectra from 498 nm to 540 nm.

Recently, it has been reported that vinblastine and crocin share their binding sites on tubulin (Sawant *et al*., 2019; Hire *et al*.; 2017). Therefore, we examined whether **2l** could inhibit the binding of crocin to tubulin. Crocin (5 μM) was incubated with 10 μM tubulin for 10 min on ice in PEM buffer pH 6.8. The reaction mixture was then incubated with 10 μM 2l for 10 min on ice and then change in O.D from 410 nm – 500 nm was observed in a spectrophotometer (JASCO, V-730).

Molecular Pharmacology Fast Forward. Published on April 2, 2020 as DOI: 10.1124/mol.119.118539
This article has not been copyedited and formatted. The final version may differ from this version.

Docking of 2l with tubulin

The structure of **2l** was drawn in PubChem Sketcher (V2.4) and the PDB coordinates of **2l** were generated in PRODRG server (Schuttelkopf et al., 2004). The Autodock Vina tool was used for docking of **2l** on tubulin (Trott and Olson, 2010) as described previously (Rane et al., 2017, Hura et al., 2018). The crystal structure of tubulin (PDB ID 5LYJ) was used for docking **2l** with tubulin. The coordinates of all other proteins and molecules (tubulin-tyrosine ligase, CA-4, glycerol, stathmin, *etc*.) in 5LYJ, except one α and one β subunit of tubulin were deleted using PyMOL (DeLano, 2002). The final coordinates used for docking had one α subunit, one β subunit, one GDP, one GTP, one calcium ion and two magnesium ions. Initially global docking was performed by covering the whole molecule in a grid box of 72 × 102 × 100 Å, with grid spacing of 1 Å. The global docking was performed 5 times with exhaustiveness of 100 (the number of times the calculation is repeated) and each set of docking produced 9 conformations. The greatest number of conformations were found to interact with two sites on the protein (16 conformations at the interface of the α- and β-dimers and 19 conformations at the taxol site) (Jaghoori et al., 2016). These two sites were thus chosen to perform local docking, which was performed in a grid box of 72 × 56 × 58 Å for colchicine and 126 × 86 × 82 Å for epothilone, with a grid spacing of 0.375 Å. The conformation with minimum binding energy was chosen to analyse the interaction with tubulin. Control docking with epothilone was performed in a similar way to validate the docking protocol. The coordinates of epothilone and colchicine were obtained from their PDB structures 4O4I and 1SA0, respectively. The interaction of the docked conformers with tubulin was further analyzed in UCSF Chimera version 1.11 (Pettersen *et al*., 2004) to determine the amino acid residues in the binding pocket and the residues within 4 Å of **2l** to determine the possible hydrogen bonding interactions.

Molecular Pharmacology Fast Forward. Published on April 2, 2020 as DOI: 10.1124/mol.119.118539
This article has not been copyedited and formatted. The final version may differ from this version.

Competitive inhibition with paclitaxel

Tubulin (12 μM) was incubated with different concentrations (0, 2, 5, 10, 20 and 30 μM) of **2l** for 10 min on ice in PEM buffer pH 6.8. Different concentrations (2, 5 and 7 μM) of paclitaxel was added to the reaction mixtures for each concentration of **2l** and incubated for 10 minutes on ice. The polymerization reaction was monitored immediately after adding 1 mM GTP in Spectramax M2e by taking O.D at 350 nm. The percentage inhibition of tubulin polymerization versus concentration of **2l** was plotted in a Lineweaver-Burk plot at different concentrations of paclitaxel to determine the nature of inhibition.

Effects of 2l on the polymerization of *Streptococcus pneumoniae* FtsZ

Purified FtsZ (10 μM) was polymerized in the presence of 1 mM GTP at 37 °C as described previously (Dhaked et al, 2019). The polymerization reaction was monitored in a spectrofluorometer (JASCO FP-6500, Tokyo, Japan) with the wavelength for both excitation and the emission at 400 nm. Polymerization of SpnFtsz was also observed with prior incubation of the protein with 20 μM **2a** and **2l** in ice for 10 minutes.

Alkaline phosphatase assay

2 U of alkaline phosphatase was taken in glycine-NaOH buffer pH 10.4 with 1 mM $MgCl_2$ and 0.1 mM $ZnCl_2$. 250 μM of *para*-nitrophenylphosphate (PNPP) was mixed with the reaction mixture in a cuvette. The reaction mixture was immediately put in a spectrophotometer and the conversion of the yellow coloured product was monitored by taking the O.D at 410 nm. A similar experiment was performed with both **2a** and **2l** by incubating 20 μM each of **2a** and **2l** for 10 minutes with alkaline phosphatase on ice.

Sulphorhodamine B (SRB) assay

Molecular Pharmacology Fast Forward. Published on April 2, 2020 as DOI: 10.1124/mol.119.118539
This article has not been copyedited and formatted. The final version may differ from this version.

The GI_{50} in HeLa cells was determined by SRB assay as described previously (Vichai and Kirtikara, 2006). Briefly, HeLa cells were seeded in TC treated 96-well plate (10,000 cells/well). After attachment, the cells were treated with different concentrations of **2a** and **2l** and incubated for 24 hours followed by fixation with 50% trichloroacetic acid for 1 hour at 4 °C. The plates were then washed, dried and stained with 0.4% SRB for 1 hour at room temperature. After drying of the plates, the dye was dissolved in 10 mM Tris pH 10.5 and the absorbance was measured at 520 nm in Spectramax M2^e. The percentage inhibition of cell proliferation at each concentration was determined by the formula,

$$\%\ Inhibition\ of\ cell\ proliferation = 100 - \left\{\left(\frac{N_t - N_0}{N_c - N_0}\right) \times 100\right\}$$

Where N_t is O.D of the wells where **2a** or **2l** was added. N_0 is the O.D of the wells at the time of **2a** or **2l** addition, and N_c is the O.D of the wells of 0.1% DMSO treatment. This percentage inhibition was then fitted in dose-response inhibition curve in GraphPad Prism software.

Immunofluorescence microscopy

The coverslips were first coated with poly-L-lysine and then cells were added onto coverslips (25000 cells/well) for attachment. After attachment, cells were treated with different concentrations of **2a** and **2l** and incubated for 24 hours. Cells were then fixed with 4% formaldehyde and permeabilized with 100% chilled methanol. 2% BSA was used for blocking the non-specific binding of the antibody and then the anti-α-tubulin antibody (Sigma) was added to cells and incubated for 3 hours at 37 °C. After washing of primary antibody secondary antibody tagged with FITC (Sigma) was added to the cells and incubated for 1.5 hours. The coverslips were mounted on clean glass slides using the mounting media having DAPI, purchased from vector laboratories, and observed under a fluorescence microscope (Yokogawa CSU-XI).

Molecular Pharmacology Fast Forward. Published on April 2, 2020 as DOI: 10.1124/mol.119.118539
This article has not been copyedited and formatted. The final version may differ from this version.

Live-dead assay

The percentage of the live and dead cell was determined by PI staining. The cells were seeded up to 50% confluency in T25 flasks and then incubated with 4 and 8 μM of **2a** and **2l** for 24 hours. The cells were trypsinized, pelleted and resuspended in PBS with a final concentration of cells approximately 1 million per mL. The cells were stained with PI and then analyzed by flow cytometry for PI positive and PI negative cells. 10,000 cells were counted in each case. The experiment was repeated three times.

Statistical analysis

'±' represents standard deviation (S.D.) and p values were calculated using Student's t-test.

Results

Synthetic chemistry

The synthesis of the bis(styryl)pyrazoles **2a-l** takes advantage of our recently described microwave-assisted synthesis of curcuminoids (Groundwater et al., 2017), in which the total reaction time was shortened to 10 minutes and the analytically pure compounds were mostly obtained by the simple recrystallization from ethanol of the crude solid obtained from the acid hydrolysis of the boron-containing intermediate. The ready availability of these synthetic intermediates **1a-l** lead to the preparation of non-curcuminoid analogues such as 3,5-bis(stryryl)pyrazole analogues **2a-l** for biological evaluation, Scheme 1, *via* the cyclization with hydrazine in an acid-catalyzed microwave-assisted condensation, to generate the respective **2a-l** (Scheme 1).

Anti-proliferative activity of 3,5-bis(styryl)pyrazoles 2a-l in PC3 cells

Molecular Pharmacology Fast Forward. Published on April 2, 2020 as DOI: 10.1124/mol.119.118539
This article has not been copyedited and formatted. The final version may differ from this version.

The growth inhibitory effect of all the 3,5-bis(styryl)pyrazoles **2a-l** on the PC3 cell line was determined by the MTT assay (Table 2) which was validated by the trypan blue exclusion cell count. Methotrexate was used as a positive control, with a GI_{50} value (obtained in this study) of 0.012 ± 0.008 μM, which is within the ranges of the reported GI_{50} values in PC3 cells for methotrexate (0.001 – 0.1 μM) (Serova et al., 2010; Derenne et al., 2010; Marques et al., 2010). Two compounds (**2a** and **2l**) had GI_{50} values in the low micromolar range (< 2.5 μM) (Supplemental Figure 1) and were thus selected for further biological evaluation, as well as degradation and solubility studies.

Degradation studies

We evaluated the stability and solubility of the two analogues selected for extensive biological testing, **2a** and **2l**, under simulated physiological conditions (pH 7.4, 37 ˚C), and the degradation kinetics are summarized in Figure 1. After 24 hours under the simulated physiological conditions, 10 % of analogue **2a** remained, while 71 % of analogue **2l** remained after 72 hours (Supplemental Figures 2 and 3).

The effect of 3,5-bis(styryl)pyrazoles 2a and 2l on the induction of apoptosis in PC3 cells

The two selected analogues (**2a** and **2l**) did not induce apoptosis at their GI_{50} concentrations, as determined by the annexin V / propidium iodide (PI) apoptosis assay. PC3 cells were treated at the GI_{50} of analogues **2a** and **2l**, with cells treated with DMSO (0.01 %) as the vehicle control. The cells were then incubated for 72 hours, stained with annexin V/PI, and analyzed. The representative dot plots depicting the results from this apoptosis assay are shown in Figure 2; cells treated with and without these compounds maintained more than 90 % viability, indicating that they did not undergo apoptosis when treated at the GI_{50} concentrations. However, the cells died after treatment with higher concentrations of **2a** and **2l** (4 and 8 μM), as shown by the increasing number of PI

Molecular Pharmacology Fast Forward. Published on April 2, 2020 as DOI: 10.1124/mol.119.118539
This article has not been copyedited and formatted. The final version may differ from this version.

positive cells after PI staining and counting 10,000 cells by flow cytometry (Figure 3, Table 4). In addition, we quantified the extent of apoptosis in three other cell lines, namely lung carcinoma (A549), skin melanoma (B16F10) and liver carcinoma (Huh-7) at similar concentrations of **2a** and **2l**. The compounds induced apoptosis in all three cell lines in a concentration dependent manner (Supplemental Figure 4 and Supplemental Table 3).

The effect of 3,5-bis(styryl)pyrazoles 2a and 2l on the cell cycle of PC3 cells

A cell cycle analysis was conducted in order to determine the effects of 3,5-bis(styryl)pyrazoles **2a** and **2l** on cell division. PC3 cells were treated for 72 hours at the GI_{50}s of these compounds, with cells treated with 0.01 % of DMSO used as the vehicle control. The cell cycle analysis showed a significant increase in the percentage of cells in the G_2/M phase when treated with the 3,5-bis(styryl)pyrazoles at their GI_{50} concentrations, in comparison to the control (Figure 4; Supplemental Table 4).

Assessment of the outcome of mitotic arrest induced by 3,5-bis(styryl)pyrazoles 2a and 2l.

In order to evaluate the potential of 3,5-bis(styryl)pyrazoles **2a** and **2l** as effective agents for the treatment of CRPC, we examined whether cell death results from mitotic arrest in PC3 cells. PC3 cells were treated for 72 hours with 3,5-bis(styryl)pyrazoles **2a** and **2l** (at their GI_{50}s) and the medium containing the compounds was then removed and replaced with fresh medium. The cells were incubated for a further 72 hours before being stained with annexin V / PI and analysed. The percentage of cell death 72 hours after the removal of **2a** and **2l** (Table 3 and Supplemental Figure 5) was lower than the mitotic block after 72 hours treatment with **2a** and **2l** (Supplemental Table 4), suggesting that the effects of the compounds on PC3 cells are reversible.

Molecular Pharmacology Fast Forward. Published on April 2, 2020 as DOI: 10.1124/mol.119.118539
This article has not been copyedited and formatted. The final version may differ from this version.

Determination of the effect of 3,5-bis(styryl)pyrazoles 2a and 2l on tubulin polymerization. Since both the compounds, **2a** and **2l,** caused a mitotic block, a characteristic of most anti-tubulin agents (Mukhtar et al., 2014), the effect of **2a** and **2l** on tubulin was investigated. 3,5-Bis(styryl)pyrazole **2l** inhibited the polymerization of purified tubulin (Figure 5), inhibiting both the rate and extent of tubulin assembly, as monitored by light scattering. The extent of inhibition of tubulin polymerization by the compound was also determined by the sedimentation assay (Supplemental Figure 6). The half maximal inhibitory concentration (IC_{50}) of 3,5-bis(styryl)pyrazole **2l** for tubulin polymerization was found to be 4.7 ± 1.2 μM by light scattering and 4 ± 1.5 μM by the sedimentation assay.

The effect of analogue **2a** on the polymerization of purified tubulin was also determined by light scattering and sedimentation assay (Supplemental Figure 7). Unlike the pyrazole **2l**, analogue **2a** was not able to inhibit the tubulin polymerization *in vitro* (Supplemental Figure 7).

Effect of 3,5-bis(styryl)pyrazoles 2a and 2l on microtubules of PC3 cells

Next, the effects of 3,5-bis(styryl)pyrazoles **2a** and **2l** on the microtubules of PC3 cells were examined by fluorescence microscopy. Cells were seeded on poly-L-lysine coated coverslips and treated with 4 and 8 μM of **2a** or **2l**. Both the compounds caused the depolymerization of the interphase microtubules in PC3 cells (Figure 6a) as in the control cells, thread-like microtubule structures can be seen which were well spread in the cytoplasm of the cells. These thread-like structures were not properly visible in cells treated with **2a** and **2l**, indicating that the interphase microtubules were depolymerized by the treatment with these drugs (Figure 6a). Although both **2a** and **2l** also strongly depolymerized spindle microtubules and caused the formation of abnormal spindles in PC3 cells (Figure 6b), the effects of **2l** on interphase microtubules were more pronounced (Supplemental Figure 8a). A normal mitotic cell with spindle microtubules is shown

Molecular Pharmacology Fast Forward. Published on April 2, 2020 as DOI: 10.1124/mol.119.118539
This article has not been copyedited and formatted. The final version may differ from this version.

in the Figure 6b control panel (arrow). In treated cells, abnormal multipolar spindles can be seen and the number of mitotic cells per field increased significantly after the treatment with **2a** and **2l** which also confirms that these compounds cause mitotic block (Figure 6b, Supplemental Figure 8b). In the control cells, DNA is aligned on the metaphase plate (arranged more compactly in a straight line [arrow]) while after treatment the DNA is scattered and unable to align. We also determined the effect of **2a** and **2l** on the microtubules of HeLa cells. The GI_{50} of **2a** and **2l** was determined to be 2.6 ± 1.2 and 2.4 ± 0.5 μM, respectively (Supplemental Figure 9 a-b). Both **2a** and **2l** depolymerized interphase and spindle microtubules in HeLa cells (Supplemental Figure 9 c-d), with the depolymerization of microtubules by **2l** being more pronounced than that produced by **2a** (Supplemental Figure 10a). The population of mitotic cells also increased upon treatment with **2a** and **2l,** suggesting that the compounds cause mitotic block (Supplemental Figure 10b).

Kinetics of microtubule depolymerization and cell death after treatment of PC3 cells with 3,5-bis(styryl)pyrazole 2a

To examine whether or not microtubules are the primary targets of **2a** and **2l**, we compared the kinetics of microtubule disassembly and cell death upon treatment with both compounds. PC3 cells were incubated without or with either 4 and 8 μM of **2a** and **2l** for 2 and 4 hours. The fluorescence intensity of microtubules was found to be strongly reduced after both 2 and 4 hour treatment with **2a** and **2l** (Figure 7, Supplemental Figure 11). The fluorescence intensity of microtubules in vehicle treated cells was determined to be 1525 ± 229 (a.u.), dropping to 1054 ± 112 and 913 ± 105 (a.u.) after treatment with 4 μM **2a** for 2 and 4 hours, respectively, and 825 ± 61 and 771 ± 54 (a.u.) after treatment with 4 μM **2l** for 2 and 4 hours, respectively (Figure 7, Supplemental Figure 11). The fluorescence intensity of the microtubules was reduced by 54 and 57% in the presence of 8 μM **2a** for 2 and 4 hours, and 41% and 72% in the presence of 8 μM **2l** for 2 and 4 hours,

Molecular Pharmacology Fast Forward. Published on April 2, 2020 as DOI: 10.1124/mol.119.118539
This article has not been copyedited and formatted. The final version may differ from this version.

respectively (Figure 7, Supplemental Figure 11). These results indicate that treatment with both **2a** and **2l** led to the formation of depolymerized microtubules within a short time period. In contrast, treatment with 4 and 8 μM **2a** and **2l**, for 2 or 4 hours, did not induce cell death in PC3 cells (Figure 8 and Supplemental Table 5), indicating that the depolymerization of microtubules preceded cell death upon treatment with **2a** or **2l**, and that microtubules are the primary targets of both **2a** and **2l** in PC3 cells.

Binding of 3,5-bis(styryl)pyrazole 2l to tubulin

Since **2a** and **2l** caused microtubule depolymerization, we characterized the binding of **2a** and **2l** with tubulin; the binding of **2l** with tubulin was examined by monitoring the tryptophan fluorescence of tubulin (Bhattacharyya et al., 2010). The fluorescence of tubulin was found to be reduced in the presence of **2l** indicating that the compound binds to tubulin (Figure 9). The change in the fluorescence intensity of tubulin in the presence of **2l** was plotted in a binding isotherm, which yielded a dissociation constant (K_d) of 0.4 ± 0.1 μM for the binding interaction.

The binding affinity of **2a** to tubulin was also determined (Supplemental Figure 12) and it was found that it binds to tubulin with a much weaker affinity (K_d, 4.6 ± 1.1 μM) than **2l (**K_d, 0.4 ± 0.1 μM), a possible explanation for the weak effect of **2a** on the polymerization of purified tubulin and interphase cellular microtubules.

Determination of binding site of 3,5-bis(styryl)pyrazole 2l on tubulin

Pyrazole **2l** binds to tubulin with higher affinity than **2a** and we have determined the binding site of **2l** on tubulin. Tubulin has three well-defined binding sites for small molecules; the taxane, vinca alkaloid, and colchicine sites (Supplemental Figure 13). Compounds that bind to the vinca alkaloid

Molecular Pharmacology Fast Forward. Published on April 2, 2020 as DOI: 10.1124/mol.119.118539
This article has not been copyedited and formatted. The final version may differ from this version.

and colchicine sites generally destabilize microtubules so we first checked the binding of **2l** to these binding sites.

The fluorescence intensity of colchicine and BODIPY-FL-vinblastine increases upon binding to tubulin, while the absorbance of crocin, a vinca domain binder, increases upon binding to tubulin. If **2l** inhibits the binding of colchicine to tubulin, the fluorescence of colchicine-tubulin complex should be reduced in the presence of **2l**. However, the prior incubation of **2l** with tubulin did not reduce the fluorescence of colchicine-tubulin complex, indicating that **2l** does not bind to the colchicine site on tubulin (Supplemental Figure 14a). To check the binding of **2l** at the vinblastine site, we used BODIPY-FL-vinblastine and crocin. There was no change in the fluorescence of the BODIPY-FL-vinblastine-tubulin complex or the absorbance of the crocin-tubulin complex, respectively, upon prior incubation with **2l**, indicating that **2l** does not bind to the vinblastine site on tubulin (Supplemental Figure 14b,c).

Consequently, in order to determine the putative binding site, we performed molecular docking with the tubulin crystal structure (PDB ID 5LYJ) as described previously (Rane et al., 2017, Hura et al., 2018). We found that most conformations of **2l** were interacting with two distinct sites on tubulin; the paclitaxel binding site on β-tubulin (Figure 10) and the interface of the α- and β-tubulin heterodimer (Supplemental Figure 15), near the colchicine site. To further validate the docking, we docked epothilone, a paclitaxel site binder, with tubulin. The RMSD of the docked conformation of epothilone to the epothilone conformation present in complex with tubulin (PDB ID 404I) was found to be 1 Å, confirming that the docking protocols were appropriate (Figure 11) (Hura et al., 2018). Since competitive binding data with colchicine showed that **2l** does not bind to the colchicine site (Supplemental Figure 14a), we further analysed the docking data only for paclitaxel site.

Molecular Pharmacology Fast Forward. Published on April 2, 2020 as DOI: 10.1124/mol.119.118539
This article has not been copyedited and formatted. The final version may differ from this version.

We found that **2l** possibly forms 2 hydrogen bonds in the paclitaxel binding site, with the peptide backbone of T273 (2.2 Å) and P271 (2.6 Å) (Figure 12). Further analysis of the docking gave the binding energy of **2l** with tubulin, which was found to be -8.4 kcal/mol, while that of epothilone was found to be -9.1 kcal/mol. Taxol also forms a similar hydrogen bond with the peptide backbone of T273 (3.0 Å)**.** In addition, paclitaxel also forms other hydrogen bonds, with R358 (3.3 Å), Q278 (3.4 Å), H226 (2.6 Å) and the peptide backbone of R358 (3.1 Å) (Snyder et al., 2001; Yadava et al., 2015).

We also analyzed the binding pocket of both epothilone and **2l** on beta-tubulin and found that there were 12 residues which are common to both **2l** and epothilone (Table 5) showing that **2l** and epothilone share the same binding pocket. Since the taxol binding pocket has hydrophobic residues in the H7 helix, M loop and β strand of S7, S9-10 (Ranade et al., 2016), it is possible that **2l** also makes some hydrophobic interactions within the binding pocket.

To elucidate the binding site of **2l** on tubulin, we performed a competitive inhibition experiment of **2l** with paclitaxel. The effects of **2l** on the polymerization of tubulin in the presence of different concentrations of paclitaxel were determined. **2l** exerted a stronger inhibitory effect on tubulin polymerization in the presence of low concentrations of paclitaxel. The percentage inhibition at each concentration of taxol was plotted in the Michaelis–Menten equation (Figure 13a). The resulting curves showed a typical competitive inhibition pattern, where V_{max} (maximum percentage of inhibition) remains unchanged ($p > 0.05$). Furthermore, the Lineweaver-Burk plot indicated that the nature of inhibition is competitive (Figure 13b) as the plot shows that the affinity of the substrate **2l** changes with changes in the paclitaxel concentration, as suggested by a decrease in the x-intercept with increasing concentration of paclitaxel.

Determination of the effect of 3,5-bis(styryl)pyrazoles 2a and 2l on FtsZ

Molecular Pharmacology Fast Forward. Published on April 2, 2020 as DOI: 10.1124/mol.119.118539
This article has not been copyedited and formatted. The final version may differ from this version.

3,5-Bis(styryl)pyrazoles, **2a** and **2l,** neither inhibited the polymerization of FtsZ (a bacterial homolog of tubulin) nor the enzymatic activity of alkaline phosphatase (Figure 14) suggesting that the compounds are not PAINS.

Discussion

A range of 3,5-bis(styryl)pyrazole analogues **2a-l** have been prepared using a very simple environmentally-friendly microwave-assisted protocol, allowing the rapid and clean generation of analogues in minutes without the need for multiple chromatographic steps for purification. All analogues were screened for anti-proliferative activity in the PC3 (androgen-independent) prostate cancer cell line and two analogues (**2a** and **2l**) with GI_{50} values in the low micromolar range were selected for further biological evaluation. 3,5-Bis(styryl)pyrazole **2a** was the most potent compound in the study of the anti-proliferative activity in PC3 cells (GI_{50} 0.85 ± 0.34 μM), while the novel analogue **2l** was also selected for further biological evaluation (Supplemental Figure 1); it has been shown in other studies that analogue **2a** has GI_{50} values of 5.6 μM (in PC3 cells) (Fuchs et al., 2009), 4.19 μM and 0.25 μM in breast cancer cell lines, MCF-7 and SKBR3, respectively (Amolins et al., 2009). The GI_{50} of **2a** and **2l** against human cervical cancer (HeLa) cells was determined to be 2.6 ± 1.2 and 2.4 ± 0.5 μM, respectively (Supplemental Figure 9).

In a stability study, we found that after 72 hours only 1 % of derivative **2a** remained, in comparison to the 71% of analogue **2l** which remained. The instability of **2a** at pH 7.4 may be due to the presence of the *para*-hydroxy group; a detailed study of the mechanism of degradation of **1a** under physiological conditions suggested that the major degradation pathway is auto-oxidation due to the presence of this group (Gordon et al., 2015). As **2a** is a derivative of **1a**, it too could undergo similar auto-oxidation, leading to rapid degradation. Although the GI_{50} of **2a** is less than that of **2l**, **2l** might thus be a better lead than **2a**. Neither of these analogues induced apoptosis at their

Molecular Pharmacology Fast Forward. Published on April 2, 2020 as DOI: 10.1124/mol.119.118539
This article has not been copyedited and formatted. The final version may differ from this version.

GI_{50} concentration but, as can be seen from the cell cycle histograms in Figure 4, both caused significant effects on the cell cycle, with the vast majority of treated cells in the G_2/M phase (89.6 and 89.3 %, respectively), suggesting that these analogues inhibit PC3 cell growth as a result of G_2/M arrest. With no cell division, as a result of G_2/M arrest, the percentage of cells in the G_0/G_1 phase decreases and this, in turn, reduces the number of cells in the S phase.

We next examined whether cell death results from mitotic arrest in PC3 cells. The results showed that the tested compounds caused greater cell death in PC3 cells than the control (Table 3; Supplemental Figure 5). Analogue **2a** had the least effect on PC3 cells 72 hours after removal, despite showing G_2/M arrest in the cell cycle analysis, indicating that cells treated with this analogue may either have divided or remained in a senescing state. Treatment with analogue **2l** led to the greatest total percentage of dead PC3 cells. Analysis of the cell cycle in cells treated with analogue **2l** showed that this compound resulted in the greatest percentage of cells in the G_2/M phase, indicating that the arrested cells undergo significant mitotic death.

There are three possible main outcomes from drug-mediated mitotic arrest upon drug removal (Yamada and Gorbsky, 2006), the cells divide (they may recover, leading to normal cell division or divide with abnormalities in the genome), the cells may remain in a senescent state, in which they are metabolically active but do not undergo further cell division, or cell death may be triggered, either by necrosis or apoptosis.

3,5-Bis(styryl)pyrazole **2l** inhibited the polymerization of purified tubulin (Figure 5), inhibiting both the rate and extent of tubulin assembly, as monitored by light scattering and sedimentation assay. Extensive testing of the effects of these pyrazoles on tubulin and microtubules showed that **2l** binds to tubulin tightly with a K_d of 0.4 ± 0.1 μM and inhibits the assembly of purified tubulin with no effect on the assembly of FtsZ, a bacterial homologue of tubulin which shows the specific

Molecular Pharmacology Fast Forward. Published on April 2, 2020 as DOI: 10.1124/mol.119.118539
This article has not been copyedited and formatted. The final version may differ from this version.

binding of **2l** to tubulin only. Treatment with both pyrazoles **2a** and **2l** caused depolymerization of the microtubules in PC3 and HeLa cells. We also found that, although **2l** depolymerizes microtubules, it shares its binding site on tubulin with paclitaxel. Paclitaxel is a known microtubule polymerizing agent and paclitaxel site binders generally stabilize microtubules, however, few tubulin binding small molecules such as estramustine (Laing et al., 1997) and griseofulvin (Rathinasamy et al., 2010) are reported to share their binding sites with paclitaxel but to destabilize microtubules. In summary, we have identified a potential lead which could be the basis for future optimization in the search for novel agents for the treatment of CRPC. Both pyrazoles exert similar effects on HeLa cells (Supplemental Figure 9), GI_{50}s of 2.6 ± 1.2 μM (**2a**) and 2.4 ± 0.5 μM (**2l**), through their interactions with tubulin and the depolymerization of microtubules in cells.

Acknowledgements

We thank Drs Donna Lai and Sheng Hua at the Molecular Biology Facility, Bosch Institute for their technical support. We also thank CRNTS, IIT Bombay for kindly providing a spinning disc confocal microscope and FACS facility.

Authorship contributions

Participated in research design: Vivian W.Y. Liao, Anuradha Kumari, Rajeshwar Narlawar, Soma Vignarajan, David E. Hibbs, Dulal Panda, Paul W. Groundwater

Conducted experiments: Vivian W.Y. Liao, Anuradha Kumari, Rajeshwar Narlawar

Contributed new reagents or tools: Vivian W.Y. Liao, Anuradha Kumari, Rajeshwar Narlawar

Performed data analysis: Vivian W.Y. Liao, Anuradha Kumari, Soma Vignarajan, David E. Hibbs, Dulal Panda, Paul W. Groundwater

Wrote or contributed to the writing of the manuscript: Vivian W.Y. Liao, Anuradha Kumari, David E. Hibbs, Dulal Panda, Paul W. Groundwater

References

Abouelfadel, Z and Crawford, ED (2008) Leuprorelin depot injection: patient considerations in the management of prostatic cancer. *Ther. Clin. Risk Manag.* **4**:513.

Amolins, MW, Peterson, LB and Blagg, BSJ (2009) Synthesis and evaluation of electron-rich curcumin analogues. *Bioorg. Med. Chem.* **17**:360-367.

Bhattacharyya, B, Kapoor, S and Panda, D (2010) Fluorescence Spectroscopic Methods to Analyze Drug-Tubulin Interactions. In Microtubules, in Vitro: Microtubules, in Vitro (Wilson, L and Correia, JJ, eds.). pp. 301-329, Elsevier Academic Press Inc, San Diego

Crawford, ED, Eisenberger, MA, McLeod, DG, Spaulding, JT, Benson, R, Dorr, FA, Blumenstein, BA, Davis, MA and Goodman, PJ (1989) A controlled trial of leuprolide with and without flutamide in prostatic carcinoma. *N. Engl. J. Med.* **321**: 419-424

DeLano, WL, (2002) The PyMOL molecular graphics system, Version 1.1; *Schrodinger LLC*

Derenne, A, Gasper, R and Goormaghtigh, E (2010) Monitoring of metabolism perturbation in prostate PC-3 cancer cells by sub-lethal concentrations of methotrexate. *J. Spectrosc.* **24**: 55-60

Dhaked, HPS, Ray, Shashikant, R, Battaje, RR, Banerjee, A and Panda. D (2019) Regulation of *Streptococcus pneumoniae* FtsZ assembly by divalent cations: paradoxical effects of Ca^{2+} on the nucleation and bundling of FtsZ polymers. *FEBS Journal*, 14928

Feldman, BJ and Feldman, D (2001) The development of androgen-independent prostate cancer. *Nature Rev. Cancer* **1**: 34-45.

Fuchs, JR, Pandit, B, Bhasin, D, Etter, JP, Regan, N, Abdelhamid, D, Li, C, Lin, J and Li, P-K (2009) Structure–activity relationship studies of curcumin analogues. *Bioorg. Med. Chem. Lett.* **19**: 2065-2069.

Garnick, MB (1997) Hormonal therapy in the management of prostate cancer: from Huggins to the present. *Urology* **49**: 5-15.

Gordon, ON, Luis, PB, Sintim, HO and Schneider, C (2015). Unraveling curcumin degradation: autoxidation proceeds through spiroepoxide and vinylether intermediates en route to the main bicyclopentadione. *J. Biol. Chem.* **290**: 4817–4828.

Groundwater, PW, Narlawar, R, Liao, VWY, Bhattacharya, A, Srivastava, S, Kunal, K, Doddareddy, M, Oza, PM, Mamidi, R, Marrs, ECL, Perry, JD, Hibbs, DE and Panda, D (2017) A Carbocyclic Curcumin Inhibits Proliferation of Gram-Positive Bacteria by Targeting FtsZ. *Biochemistry* **56**: 514-524

Hire, RR, Srivastava, S, Davis, MB, Konreddy, AK and Panda, D (2017) Antiproliferative activity of crocin involves trageting of microtubules in breast cancer cells. *Sci. Rep.* **7**: 44984.

Hura, N, Naaz, A, Prassanawar, SS, Guchhait, SK, Panda D (2018) Drug clinical agent molecular hybrdid: Synthesis of diaryl(trifluoromethyl)pyrazoles as tubulin targeting anticancer agents. *ACS Omega***. 3**: 1955-1969

ICH Harmonised Tripartite Guideline Validation of Analytical Procedures: Text and Methodology Q2 (R1) (2005) International Conference on Harmonization (https://www.ich.org/fileadmin/Public_Web_Site/ICH_Products/Guidelines/Quality/Q2_R1/Step4/Q2_R1__Guideline.pdf)

Jaghoori, MM, Bleijlevens and Olabarriaga, SD (2016) 1001 ways to run AutoDock Vina for virtual screening. *J. Computer-Aided Mol Design*. **30**: 237-249

Jayaprakasha, GK, Jagan Mohan Rao, L and Sakariah, KK (2002) Improved HPLC Method for the Determination of Curcumin, Demethoxycurcumin, and Bisdemethoxycurcumin. *J. Agric. Food Chem.* **50**: 3668-3672.

Karantanos, T, Corn, P and Thompson, T (2013) Prostate cancer progression after androgen deprivation therapy: mechanisms of castrate resistance and novel therapeutic approaches. *Oncogene* **32**: 5501-5511.

Lin, W and Chen, T (2013) A vinblastinefluorescent probe for pregnane X receptor in a time-resolved fluorescence resonance enegry transfer assay, *Anal. Biochem.* **443**: 252-260.

Luo, JX, Ding, W, Zhang, YQ, Yang, ZG, Li, Y and Ding, LJ (2013) Semisynthesis and acaricidal activities of isoxazole and pyrazole derivatives of a natural product bisdemethoxycurcumin. *J. Pestic. Sci*. **38**: 214-219.

Marques, SM, Enyedy, ÉA, Supuran, CT, Krupenko, NI, Krupenko, SA and Amélia Santos, M (2010) Pteridine–sulfonamide conjugates as dual inhibitors of carbonic anhydrases and

dihydrofolate reductase with potential antitumor activity. *Bioorg. Med. Chem.* **18**: 5081-5089.

Mayadevi, M, Sherin, DR, Keerthi, VS, Rajasekharan, KN and Omkumar, RV (2012) Curcumin is an inhibitor of calcium/calmodulin dependent protein kinase II. *Bioorg. Med. Chem.* **20**: 6040-6047.

Mosmann, T (1983) Rapid colorimetric assay for cellular growth and survival: Application to proliferation and cytotoxicity assays. *J. Immunol. Methods* **65**: 55-63.

Mukhtar, E, Adhami, VM and Mukhtar, H (2014) Targeting Microtubules by Natural Agents for Cancer Therapy. *Mol. Cancer Ther.* **13**: 275-284.

Panda, D, Rathinasamy, K, Santra, MK and Wilson, L (2005) Kinetic suppression of microtubule dynamic instability by griseofulvin: Implications for its possible use in the treatment of cancer. *Proc. Natl. Acad. Sci. U.S.A.* **102**: 9878-9883.

Pettersen, EF, Goddard, TD, Huang, CC, Couch, GS, Greenblatt, DM Meng, EC and Ferrin TE (2004) UCSF Chimera – a visualization system for exploratory research and analysis. *J. Comput. Chem.* **25**: 1605-1612.

Pulukuri, SM, Gondi, CS, Lakka, SS, Jutla, A, Estes, N, Gujrati, M and Rao, JS (2005) RNA interference-directed knockdown of urokinase plasminogen activator and urokinase plasminogen activator receptor inhibits prostate cancer cell invasion, survival, and tumorigenicity in vivo. *J. Biol. Chem.* **280**: 36529-36540.

Ranade, AR, Higgins, LA, Markowski, TW, Glaser, N, Kashin, D, Bai, R, Hong, KH, Hamel, E, Hofle, G and Georg, GI (2016) Characterizing the epothilone binding site on β-tubulin by photoaffinity labeling: Identification of β-tubulin peptides TARGSQQY and TSRGSQQY as targets of an epothilone photoprobe for polymrized tubulin. *J. Med. Chem*. **59**: 3499-3514

Rane, JS, Bhaumik, P, Panda, D (2017) Curcumin inhibits tau aggregation and disintegrates preformed tau filaments *in vitro. J. Alzheimer's Disease*. **60:** 999-1014

Sawant, AV, Srivastave, S, Prassanawar, SS, Bhattacharyya, B and Panda, D (2019) Crocin, a carotenoid, suppresses spindle microtubule dynamics and activates the mitotic checkpoint by binding to tubulin. *Biochem. Pharmacol.* **163**: 32-45.

Schmitt, J, Noble, A, Otsuka, M, Berry, P, Maitland, N and Rumsby, M (2014) Phorbol ester stimulates ethanolamine release from the metastatic basal prostate cancer cell line PC3 but not from prostate epithelial cell lines LNCaP and P4E6. *Br. J. Cancer* **111**: 1646-1656.

Schuttelkopf, AW, van Alten, DMF. (2004) PRODRG: A tool for high throughput crystallography of ptotrin-ligad complexes. *Acta Crytallogr*. **60**: 1355-1363

Serova, M, Bieche, I, Sablin, M, Pronk, G, Vidaud, M, Cvitkovic, ., Faivre, S and Raymond, E (2010) Single agent and combination studies of pralatrexate and molecular correlates of sensitivity. *Br. J. Cancer* **104**, 272-280.

Snyder, J. P., Nettles, J. H., Cornett, B., Downing, K. H., & Nogales, E. (2001). The binding conformation of Taxol in β-tubulin: a model based on electron crystallographic density. *PNAS*. **98**: 5312-5316.

Taplin, ME and Balk, SP (2004) Androgen receptor: a key molecule in the progression of prostate cancer to hormone independence. *J. Cell. Biochem*. **91**: 483-190.

Todd, A, Groundwater, PW and Gill, JH (2018) Anticancer Therapeutics: From Drug Discovery to Clinical Applications. John Wiley & Sons Ltd., Chichester, UK, ISBN 978-1-118-62212-4.

Tønnesen, HH and Karlsen, J (1985) Studies on curcumin and curcuminoids. *Z. Lebensm. Unters. Forsch.* **180**: 402-404.

Trott, O and Olson AJ (2010) AutoDock Vina: improving the speed and accuracy of docking with a new scoring function, efficient optimization, and multithreading. *J. Comput. Chem*. **31**: 455-61

Vichai, V and Kirtikara, K (2006) Sulforhodamine B colorimetric assay for cytotoxicity screening. *Nature Protoc*. **1**: 1112-1116.

Yadava, U., Gupta, H., & Roychoudhury, M. (2015). Stabilization of microtubules by taxane diterpenoids: insight from docking and MD simulations. *J. Biol. Phys*. **41**: 117-133.

Yamada, HY and Gorbsky, GJ (2006) Spindle checkpoint function and cellular sensitivity to antimitotic drugs. *Mol. Cancer Ther.* **5**: 2963-2969.

Molecular Pharmacology Fast Forward. Published on April 2, 2020 as DOI: 10.1124/mol.119.118539
This article has not been copyedited and formatted. The final version may differ from this version.

Footnotes

[#] These authors contributed equally to this work.

This work was partially supported by a grant from Department of Biotechnology (BT/PR14618/BRB/10/1418/2015), Government of India and partly by JC Bose fellowship (JCB/2019/000016), Department of Science and Technology, Government of India to DP.

Molecular Pharmacology Fast Forward. Published on April 2, 2020 as DOI: 10.1124/mol.119.118539
This article has not been copyedited and formatted. The final version may differ from this version.

Scheme and Figure Legends

Scheme 1 Synthesis of 3,5-bis(styryl)pyrazoles **2a-l**. Reagents and conditions: (a) $NH_2NH_2 \bullet H_2O$, AcOH, DMF, microwave, 80 ˚C, 5 mins. For detailed experimental protocols and spectroscopic information, see Supplemental Methods.

Figure 1 Representative degradation profiles of pyrazoles **2a** and **2l** in PBS (pH 7.4) at 37 ˚C in darkness over a period of 72 hours. Residual concentrations of each compound are expressed as percentages with respect to the concentration at time zero (t = 0, 100 %).

Figure 2 Representative dot plots from the annexin V/PI apoptosis assay of PC3 cells treated with the GI_{50} concentrations of **2a** and **2l** for 72 hours. DMSO (0.01 %) was used as the vehicle control.

Figure 3 Live dead assay to determine the percentage of cell death after treatment with **(a)** 0.1% DMSO; **(b) 2a** (4 μM); **(c) 2a** (8 μM); **(d) 2l** (4 μM); and **(e) 2l** (8 μM). The blue dots represent the PI negative (live) cells and magenta dots represent PI positive (dead) cells. The experiment was repeated three times and the quantitation is represented as mean ± standard deviation of three independent sets in Table 4.

Figure 4 Representative cell cycle histograms for PC3 cells 72 hours after treatment with vehicle control (0.01 % of DMSO) and GI_{50} concentrations of analogues **2a** and **2l**; where blue, magenta and green represent the numbers of cells in the G_0/G_1, S and G_2/M phases, respectively.

Figure 5 Inhibition of tubulin polymerization by 3,5-bis(styryl)pyrazole **2l** monitored by light scattering. Tubulin (12 μM) was polymerized in the presence of 10% DMSO and 1 mM GTP without (●) or with 2 (■), 5 (▲), 10 (▼), 20 (♦), and 30 (★) μM **2l**. The polymerization kinetics were followed by light scattering at 350 nm. The experiment was repeated three times. **(a)** Representative graph of the light scattering of tubulin in the presence and absence of **2l**; **(b)** The

Molecular Pharmacology Fast Forward. Published on April 2, 2020 as DOI: 10.1124/mol.119.118539
This article has not been copyedited and formatted. The final version may differ from this version.

inhibition of tubulin polymerization at different concentrations of **2l**. Error bars represent standard deviation.

Figure 6 Effect of **2l** and **2a** on microtubules of PC3 cells. **(a)** Interphase microtubules of PC3 cells before and after the treatment with 4 and 8 μM of **2a** and **2l** (grey scale image); **(b)** Mitotic microtubules (green) and corresponding DNA (grey scale image). Scale bar is 10 μm.

Figure 7 Effects of **2l** and **2a** on microtubules of PC3 cells after 2 and 4 hours of **2a** and **2l** treatment. Interphase microtubules (green) of PC3 cells before and after the short exposure of 4 and 8 μM of **2a** and **2l**. DNA (blue) was stained with Hoechst 33258. Scale bar is 10 μm.

Figure 8 Live dead assay to determine the percentage of cell death after treatment with 4 and 8 μM of **2a** and **2l** for 2 and 4 hours. The experiment was repeated three times and the quantitation is represented as mean ± standard deviation of three independent sets in Supplemental Table 5.

Figure 9 Determination of the dissociation constant (K_d) of the tubulin-**2l** complex. **(a)** The fluorescence of tubulin reduced with increasing concentration of **2l**; 0 (●), 0.1 (■), 0.2 (▲), 0.5 (▼), 1.5 (○), 2 (□) and 5 (Δ) μM; **(b)** The difference in the fluorescence intensity (at 340 nm) of tubulin in the presence of various concentrations of the compound was fitted in a binding equation. The experiment was repeated three times.

Figure 10 Docking of **2l** on tubulin. **(a)** structure of **2l** shown in red sticks; **(b)** conformation of **2l** (red sticks) docked with beta-tubulin (blue ribbon) with least binding energy; **(c)** docked conformation of epothilone (yellow sticks) and **2l** (red sticks) with beta-tubulin (blue ribbons) showing epothilone and **2l** goes to the same binding pocket on beta-tubulin; **(d)** magnified view of overlap between **2l** and epothilone after docking.

Molecular Pharmacology Fast Forward. Published on April 2, 2020 as DOI: 10.1124/mol.119.118539
This article has not been copyedited and formatted. The final version may differ from this version.

Figure 11 Docking of epothilone with tubulin; **(a)** crystal structure of epothilone (green sticks); **(b)** docked conformation of epothilone (yellow sticks) with beta-tubulin (blue ribbon) **(c)** RMSD of the crystal structure (green) and docked conformation (yellow) of epothilone.

Figure 12 Residues within 4 Å of **2l** (red sticks) on beta-tubulin (blue ribbon) showing two possible hydrogen bonds.

Figure 13 Determination of the nature of inhibition of **2l** by paclitaxel. (**a**) Percentage inhibition data fitted in Michaelis–Menten equation. (**b**) Lineweaver-Burk plot for 3 (●), 5 (■) and 7 (▲) μM paclitaxel concentration showing that the nature of inhibition is competitive. The experiment was repeated three times and error bars represent standard deviation.

Figure 14 The specificity of **2a** and **2l**. **(a)** Polymerization of FtsZ in the absence (●) and presence of 20 μM **2a** (▲) and **2l** (■); **(b)** activity of alkaline phosphatase in the presence and absence of 20 μM of **2a** and **2l**.

Molecular Pharmacology Fast Forward. Published on April 2, 2020 as DOI: 10.1124/mol.119.118539
This article has not been copyedited and formatted. The final version may differ from this version.

TABLE 1

HPLC conditions for each of the compounds analyzed; A, acetonitrile; B, 2% aq. acetic acid solution.

Compound	**Solvent gradient % A**		
	0-15 mins (linear gradient)	**15-20 mins (linear gradient)**	**20-25 mins (isocratic re-equilibration)**
2a	30–70	70-30	30
2l	60–80	80-60	60

Molecular Pharmacology Fast Forward. Published on April 2, 2020 as DOI: 10.1124/mol.119.118539
This article has not been copyedited and formatted. The final version may differ from this version.

TABLE 2

GI_{50} values of 3,5-bis(styryl)pyrazoles **2a-l** in PC3 cells[a]

Compound	GI_{50} (μM)
Methotrexate	0.012 ± 0.008
2a	0.85 ± 0.34
2b	39.8 ± 7.8
2c	3.4 ± 0.1
2d	77.8 ± 6.7
2e	69.3 ± 9.4
2f	> 500[b]
2g	4.1 ± 0.14
2h	26.9 ± 1.7
2i	39.8 ± 7.8
2j	24.2 ± 0.5
2k	28.9 ± 2.5
2l	2.21 ± 0.33

[a]Data represent the mean ± standard deviation of three independent replicates (n = 3). [b]Compound showed no growth inhibitory activity in PC3 cells at the highest tested concentration (500 μM).

Molecular Pharmacology Fast Forward. Published on April 2, 2020 as DOI: 10.1124/mol.119.118539
This article has not been copyedited and formatted. The final version may differ from this version.

TABLE 3

Percentage of live and dead PC3 cells 72 hours after the removal of the 3,5-bis(styryl)pyrazoles **2a** and **2l**.[a]

Compound	% Live cells	% Dead cells
Control	95.7 ± 2.2	3.9 ±1.9
2a	86.7 ± 3.5	12.3 ± 3.7
2l	67.5 ± 9.1	29.4 ± 9.8

[a]Data represent the mean ± standard deviation of three independent replicates (n = 3)

Molecular Pharmacology Fast Forward. Published on April 2, 2020 as DOI: 10.1124/mol.119.118539
This article has not been copyedited and formatted. The final version may differ from this version.

TABLE 4

Quantification of percentage of live and dead cells after treatment with bis(styryl)pyrazoles **2a** and **2l**.

Compound	% Dead cells
Control	15.4 ±1.2
2a (4 μM)	35.9 ± 8.9
2a (8 μM)	54.5 ± 12.2
2l (4 μM)	49.4 ± 10.8
2l (8 μM)	47.4 ± 6.0

Molecular Pharmacology Fast Forward. Published on April 2, 2020 as DOI: 10.1124/mol.119.118539
This article has not been copyedited and formatted. The final version may differ from this version.

TABLE 5

Residues within 4 Å of the binding pocket of **2l,** epothilone and paclitaxel

Molecule	**Common Residues**	**Uncommon Residues**
Epothilone	**β-tubulin residues** D223, H226, L227, A230, F269, P271, T273, L360,	**β-tubulin residues** L214, L272, S274, R275, R281, L283, Y280, Q278, Q279, G276
2l		**β-tubulin residues-** L214, L216, L272, S274, R275, P357, **R358**
Paclitaxel		V22, D25, S233, **R358**, Q278

Molecular Pharmacology Fast Forward. Published on April 2, 2020 as DOI: 10.1124/mol.119.118539
This article has not been copyedited and formatted. The final version may differ from this version.

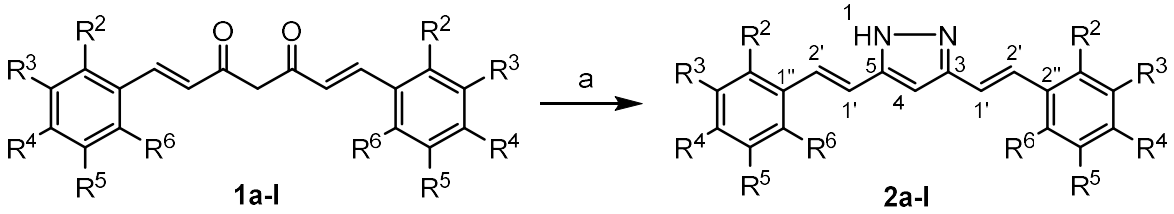

a $R^2 = R^5 = R^6 = H$, $R^3 = OMe$, $R^4 = OH$
b $R^2 = R^5 = R^6 = H$, $R^3 = R^4 = OMe$
c $R^2 = R^5 = R^6 = H$, $R^3 = OEt$, $R^4 = OH$
d $R^2 = R^5 = R^6 = H$, $R^3 = OH$, $R^4 = OMe$
e $R^2 = R^5 = R^6 = H$, $R^3 = OMe$, $R^4 = OEt$
f $R^2 = R^3 = R^5 = R^6 = H$, $R^4 = Me$
g $R^2 = OMe$, $R^3 = R^4 = R^5 = R^6 = H$
h $R^2 = R^4 = R^5 = R^6 = H$, $R^3 = OMe$
i $R^2 = R^3 = R^5 = R^6 = H$, $R^4 = OMe$
j $R^2 = R^4 = R^5 = R^6 = H$, $R^3 = OH$
k $R^2 = R^3 = R^5 = R^6 = H$, $R^4 = OH$
l $R^2 = R^6 = Cl$, $R^3 = R^4 = R^5 = H$

Scheme 1

Molecular Pharmacology Fast Forward. Published on April 2, 2020 as DOI: 10.1124/mol.119.118539
This article has not been copyedited and formatted. The final version may differ from this version.

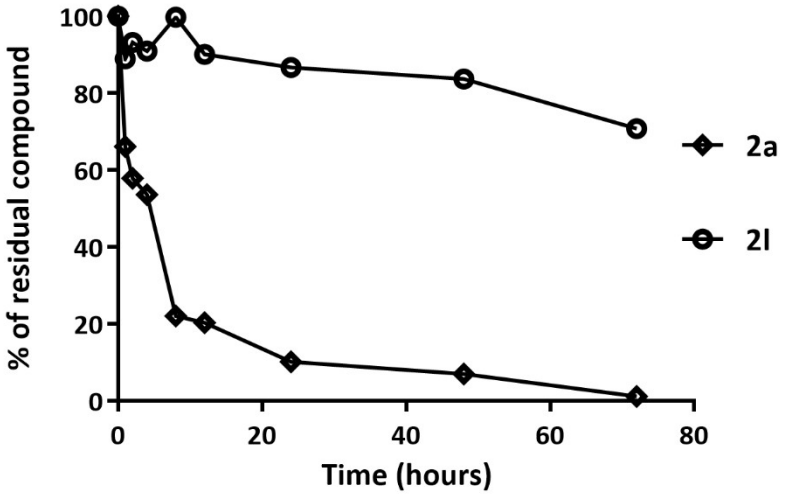

Figure 1

Molecular Pharmacology Fast Forward. Published on April 2, 2020 as DOI: 10.1124/mol.119.118539
This article has not been copyedited and formatted. The final version may differ from this version.

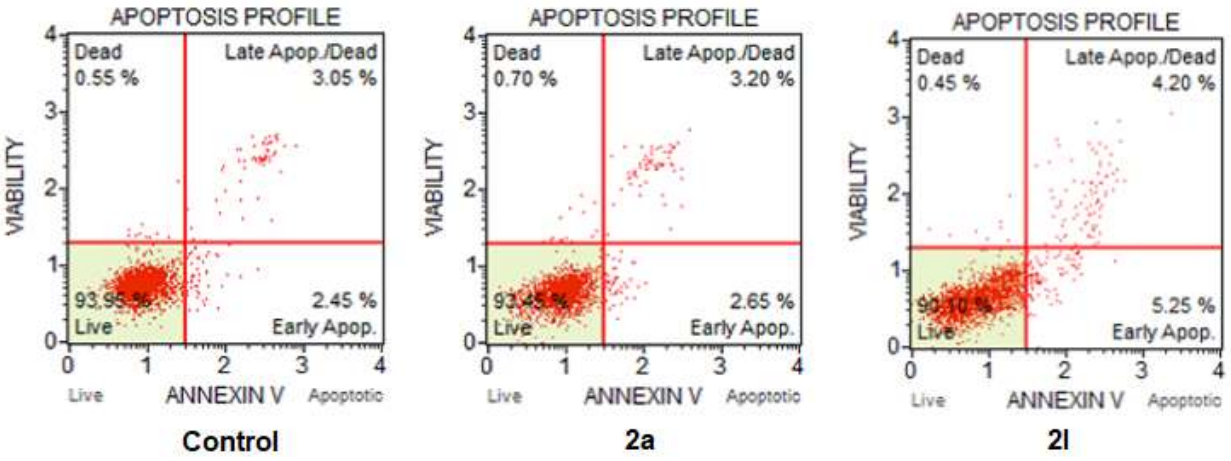

Figure 2

Molecular Pharmacology Fast Forward. Published on April 2, 2020 as DOI: 10.1124/mol.119.118539
This article has not been copyedited and formatted. The final version may differ from this version.

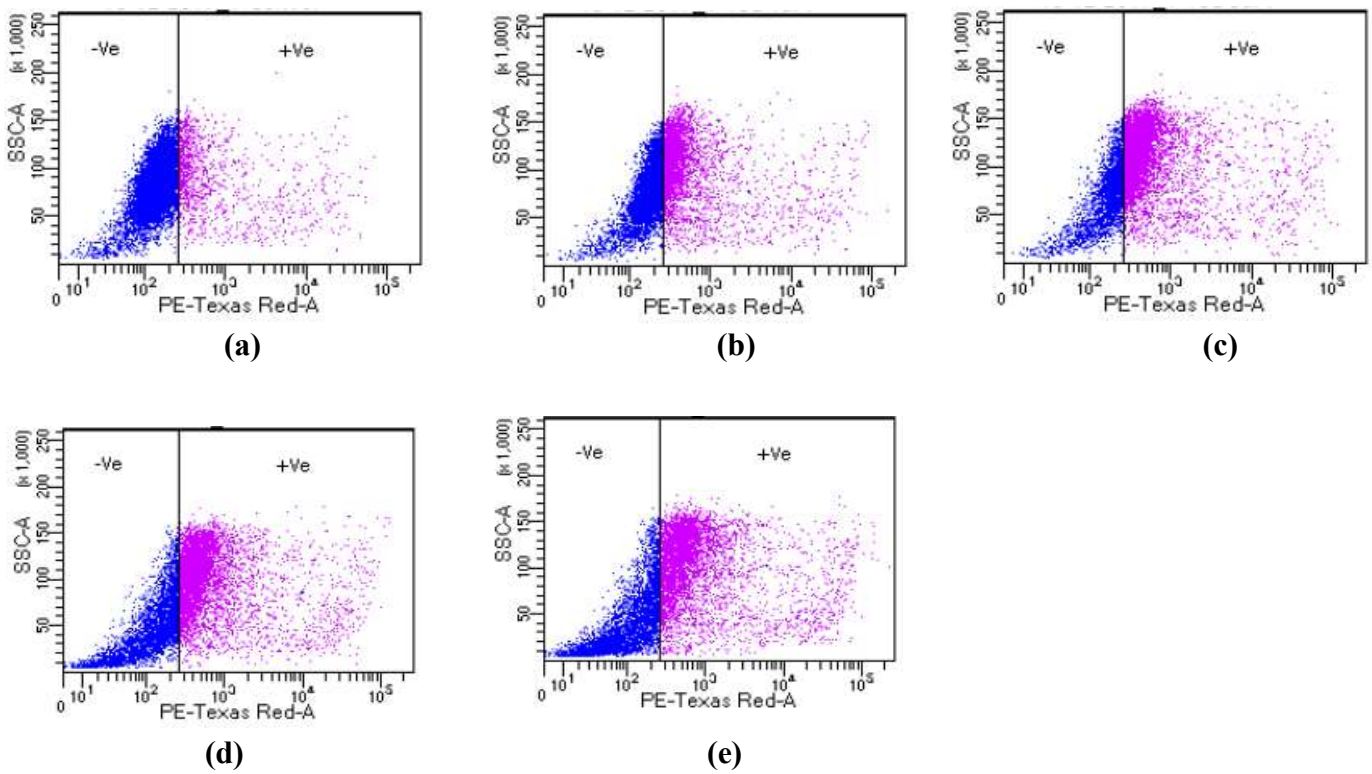

Figure 3

Molecular Pharmacology Fast Forward. Published on April 2, 2020 as DOI: 10.1124/mol.119.118539
This article has not been copyedited and formatted. The final version may differ from this version.

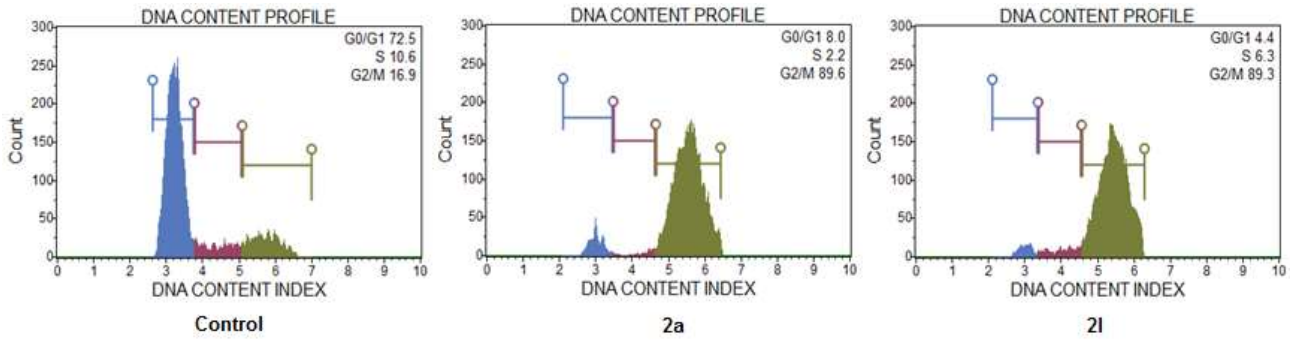

Figure 4

Molecular Pharmacology Fast Forward. Published on April 2, 2020 as DOI: 10.1124/mol.119.118539
This article has not been copyedited and formatted. The final version may differ from this version.

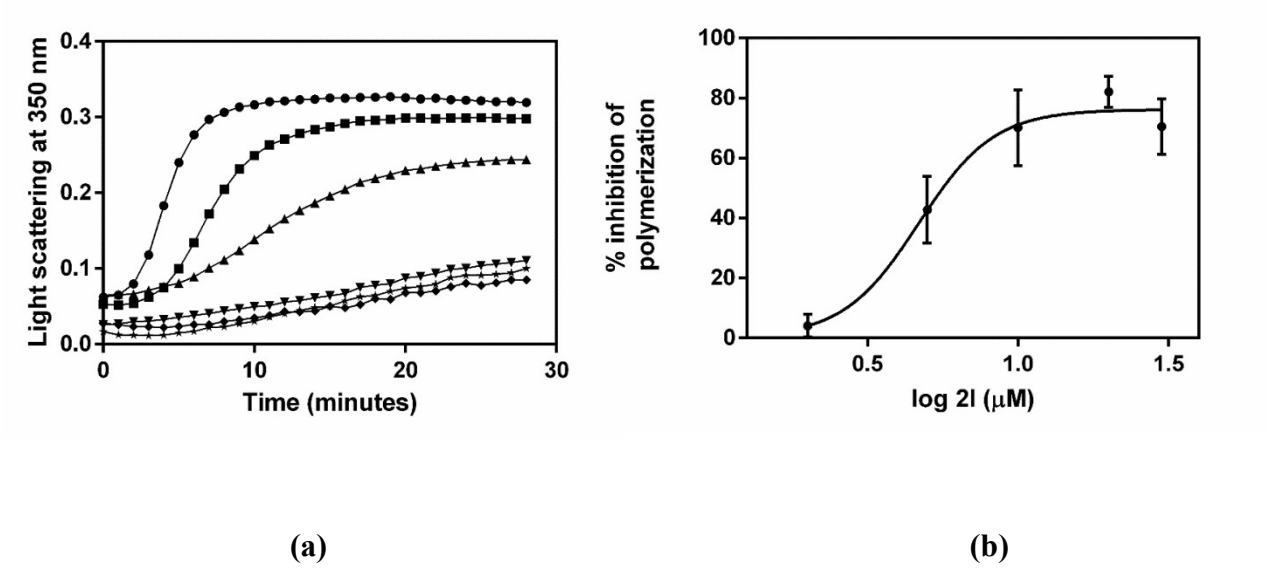

(a) **(b)**

Figure 5

Molecular Pharmacology Fast Forward. Published on April 2, 2020 as DOI: 10.1124/mol.119.118539
This article has not been copyedited and formatted. The final version may differ from this version.

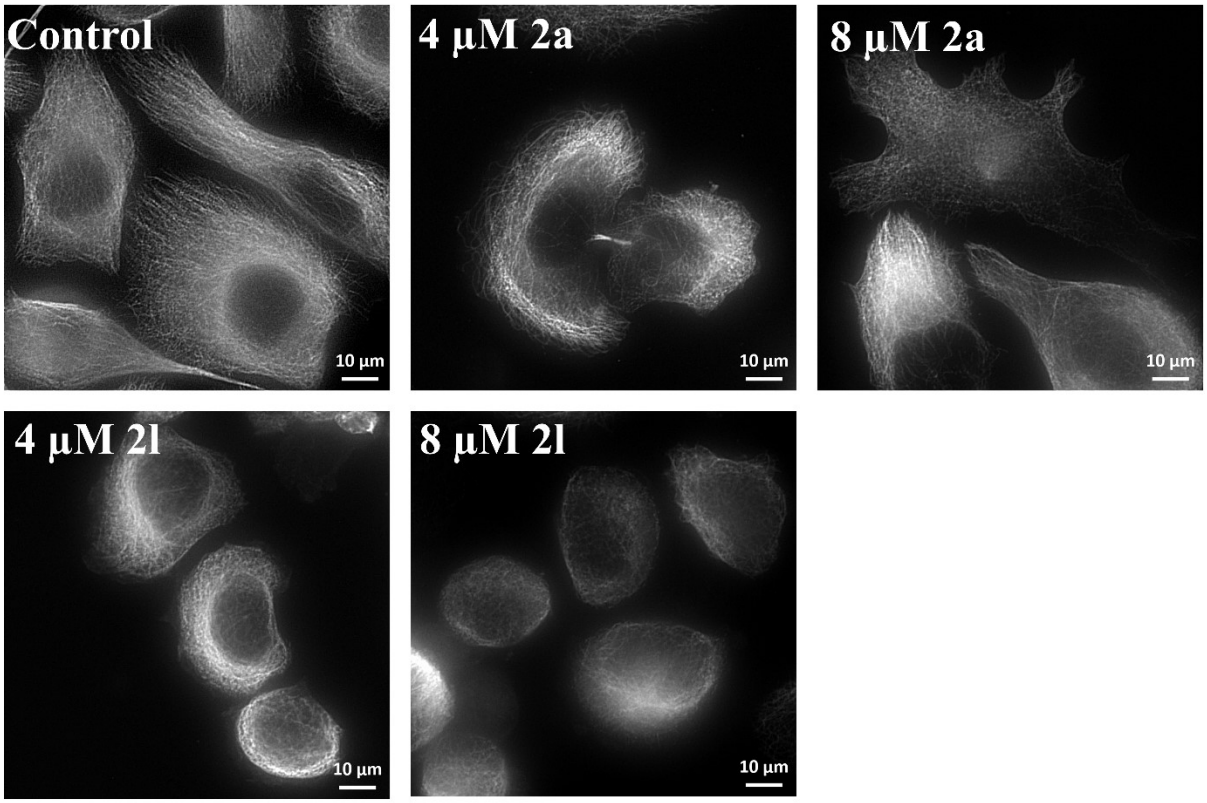

(a)

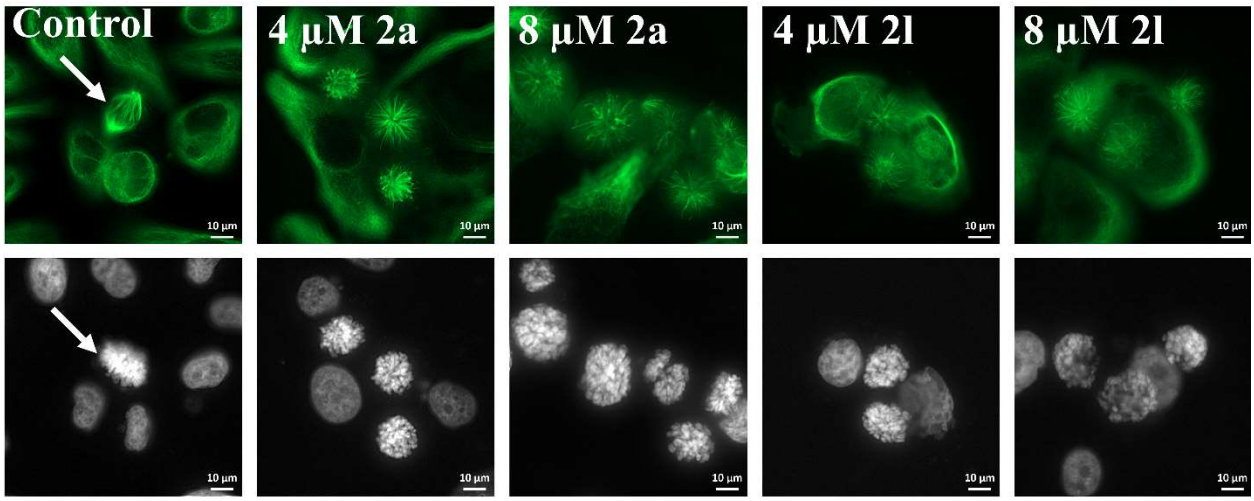

(b)

Figure 6

Molecular Pharmacology Fast Forward. Published on April 2, 2020 as DOI: 10.1124/mol.119.118539
This article has not been copyedited and formatted. The final version may differ from this version.

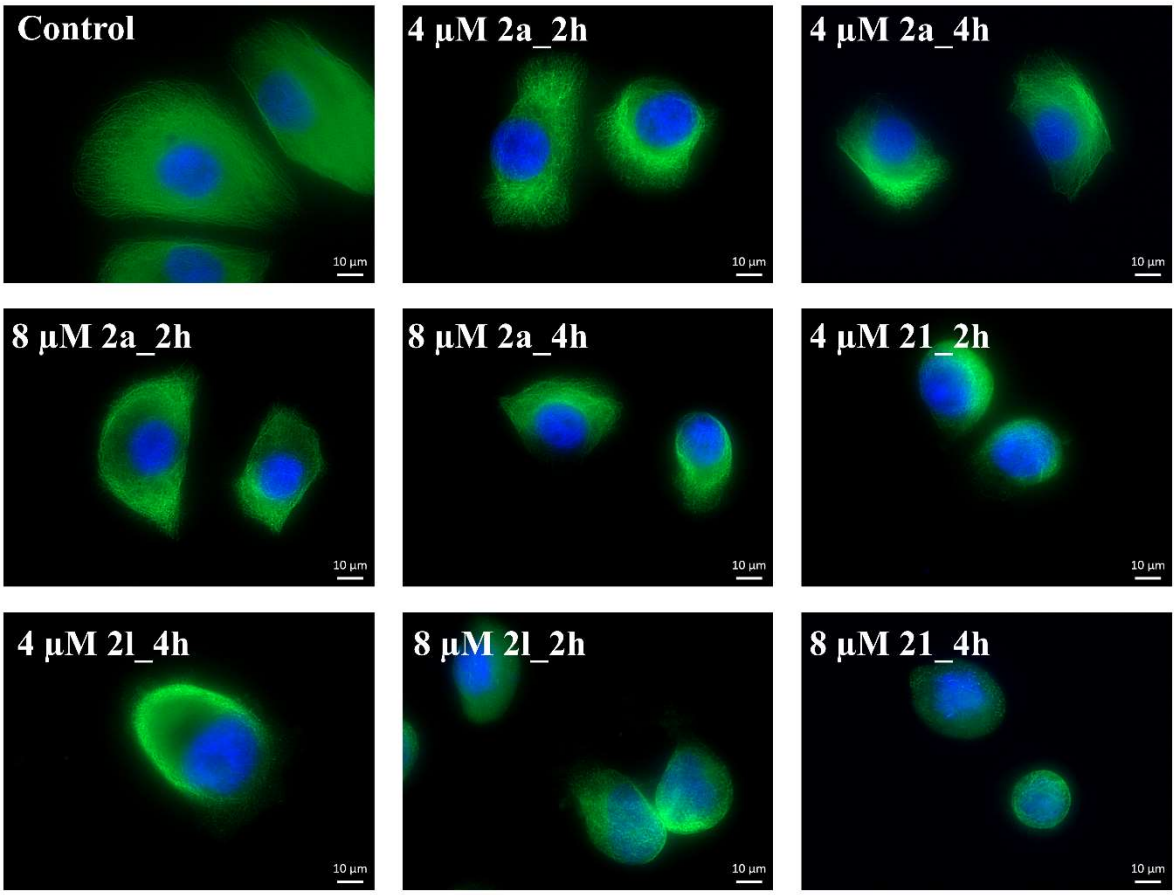

Figure 7

Molecular Pharmacology Fast Forward. Published on April 2, 2020 as DOI: 10.1124/mol.119.118539
This article has not been copyedited and formatted. The final version may differ from this version.

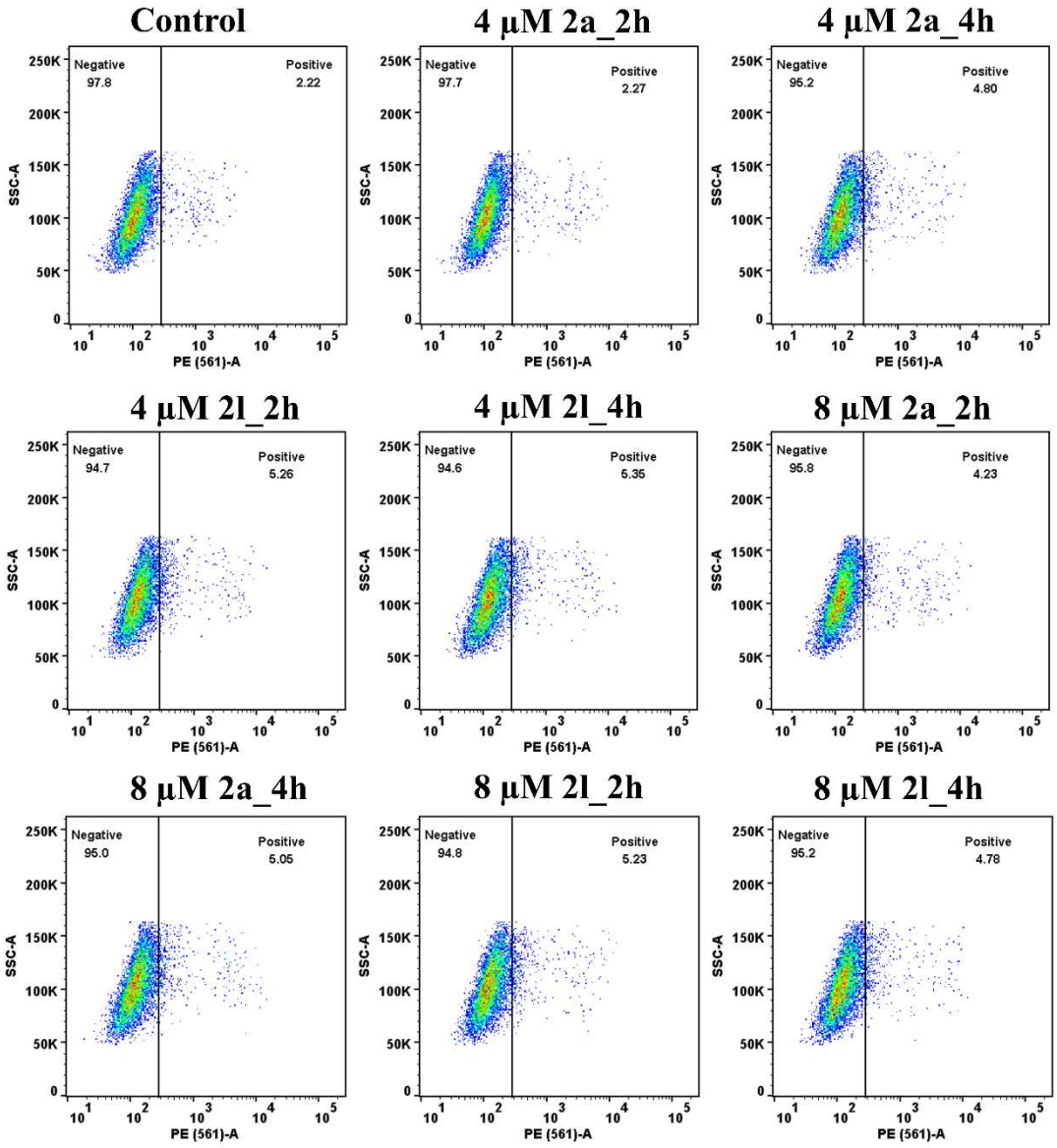

Figure 8

Molecular Pharmacology Fast Forward. Published on April 2, 2020 as DOI: 10.1124/mol.119.118539
This article has not been copyedited and formatted. The final version may differ from this version.

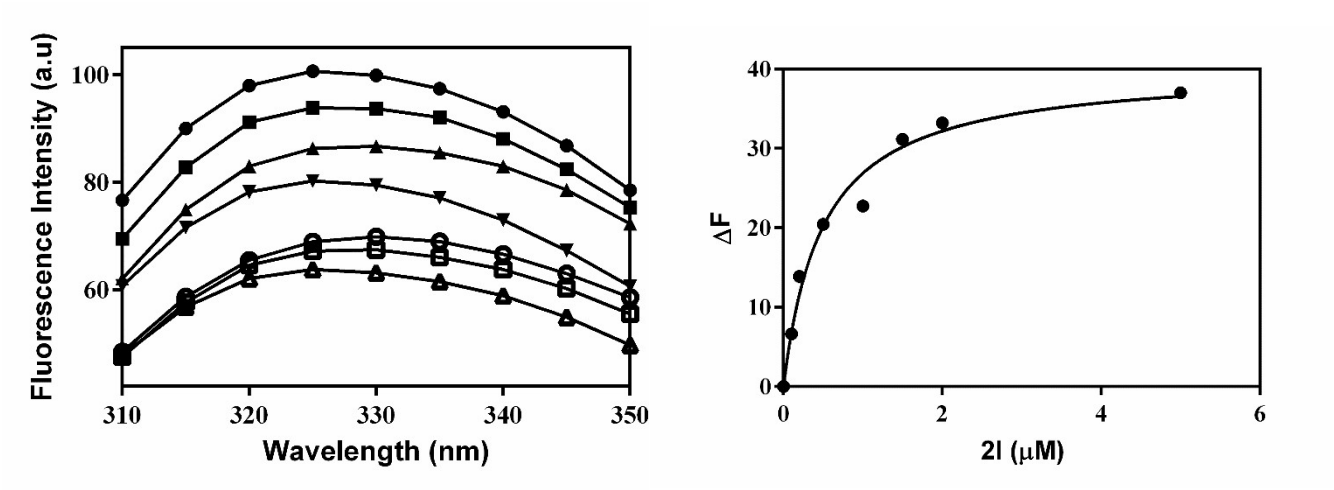

(a) (b)

Figure 9

Molecular Pharmacology Fast Forward. Published on April 2, 2020 as DOI: 10.1124/mol.119.118539
This article has not been copyedited and formatted. The final version may differ from this version.

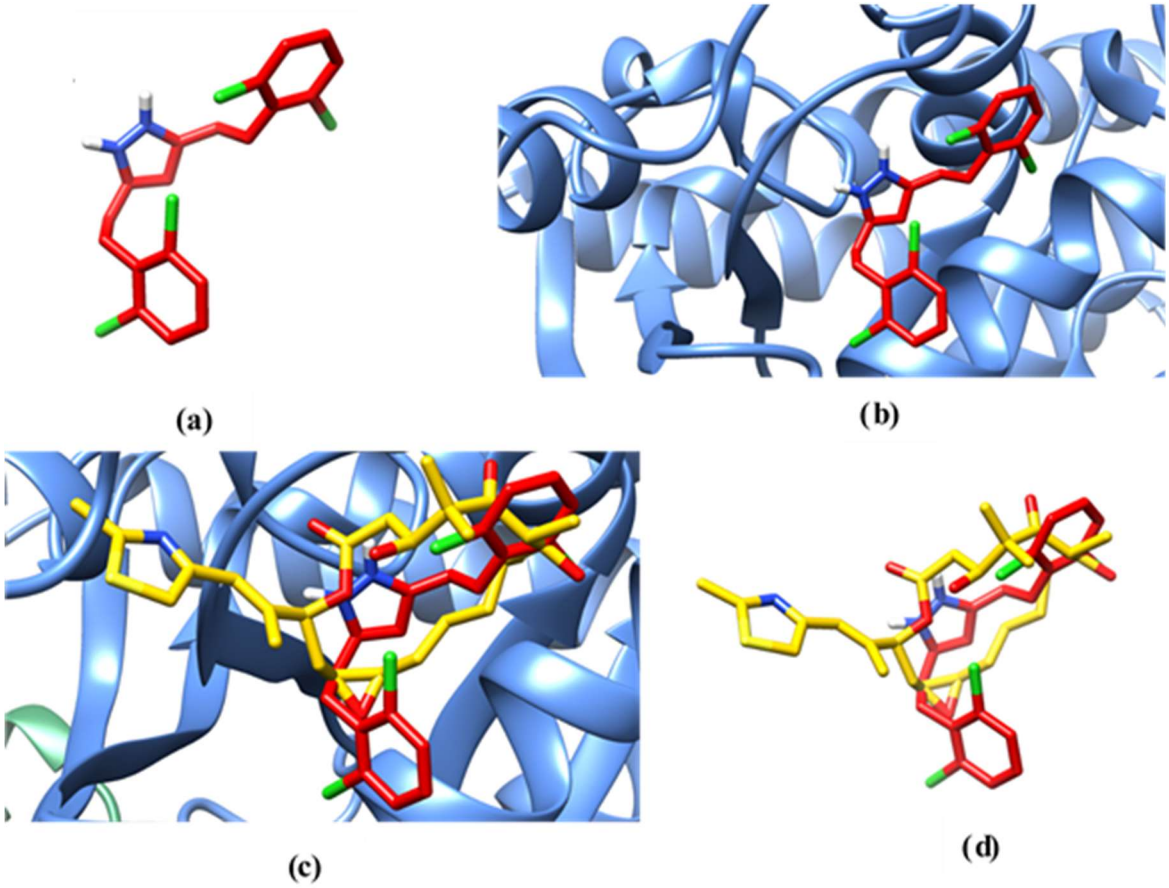

Figure 10

Molecular Pharmacology Fast Forward. Published on April 2, 2020 as DOI: 10.1124/mol.119.118539
This article has not been copyedited and formatted. The final version may differ from this version.

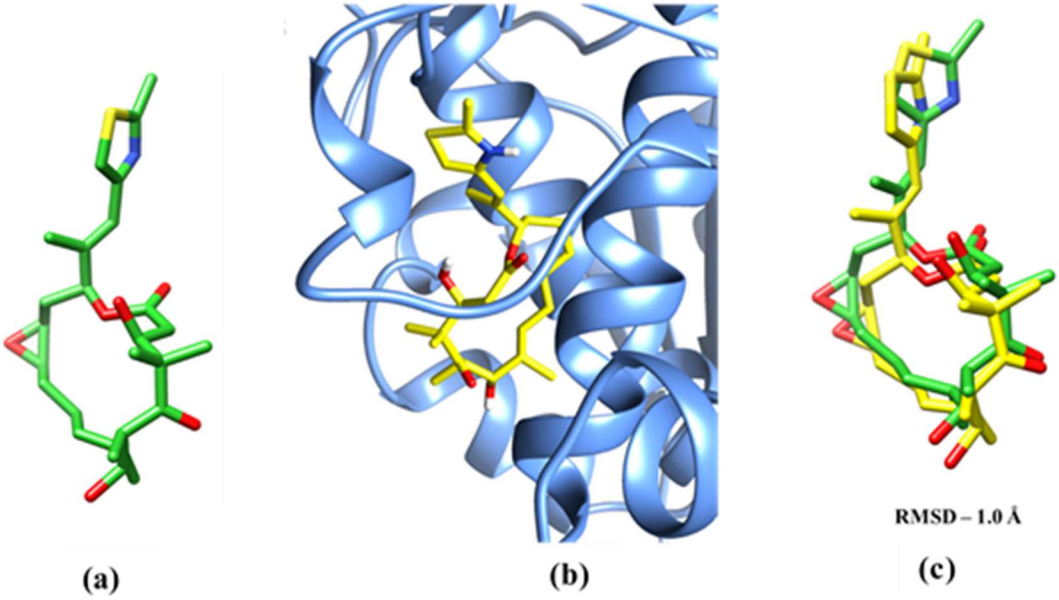

Figure 11

Molecular Pharmacology Fast Forward. Published on April 2, 2020 as DOI: 10.1124/mol.119.118539
This article has not been copyedited and formatted. The final version may differ from this version.

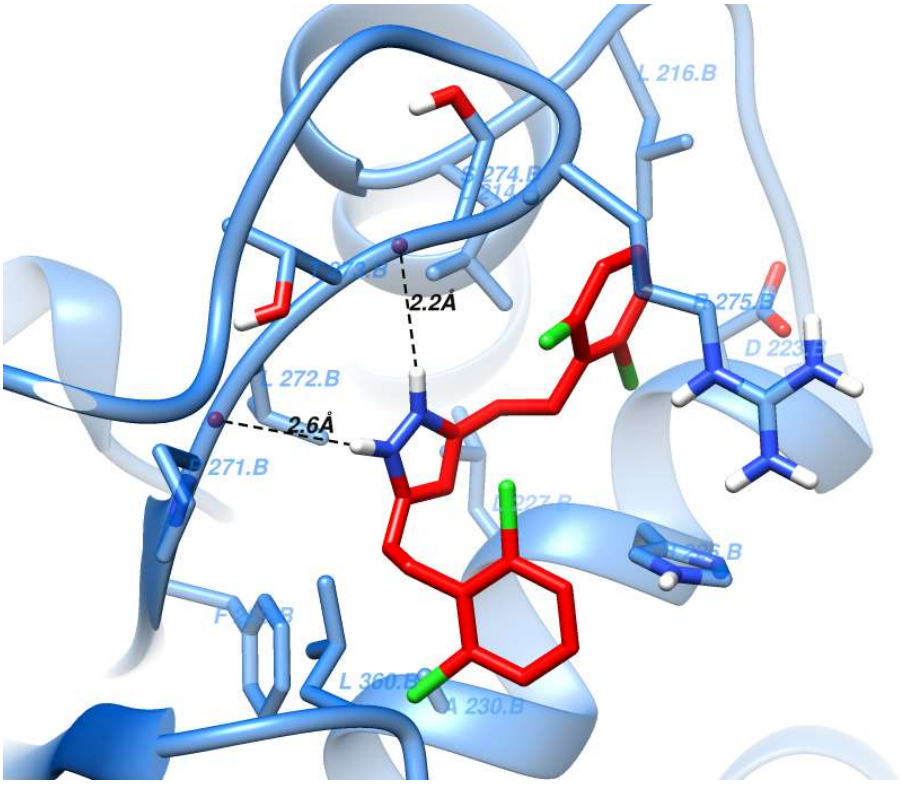

Figure 12

Molecular Pharmacology Fast Forward. Published on April 2, 2020 as DOI: 10.1124/mol.119.118539
This article has not been copyedited and formatted. The final version may differ from this version.

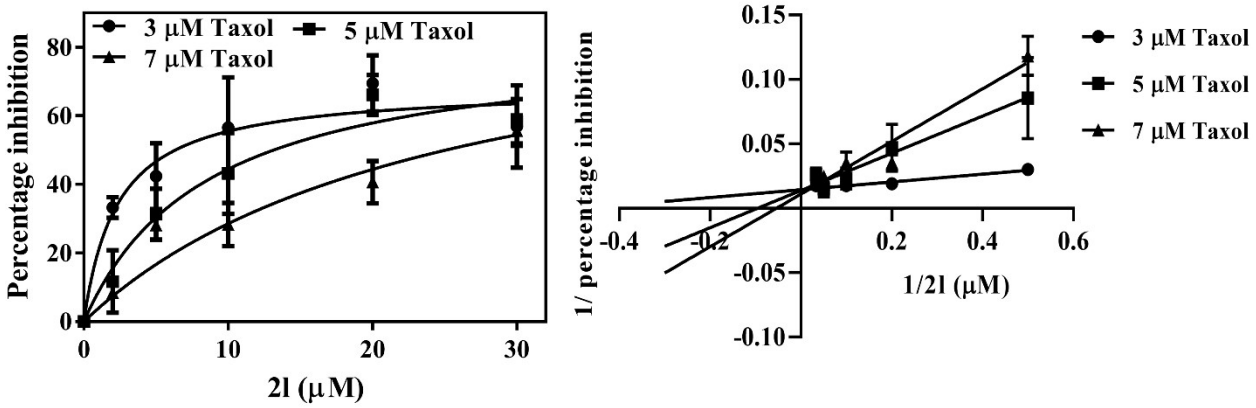

(a) (b)

Figure 13

Molecular Pharmacology Fast Forward. Published on April 2, 2020 as DOI: 10.1124/mol.119.118539
This article has not been copyedited and formatted. The final version may differ from this version.

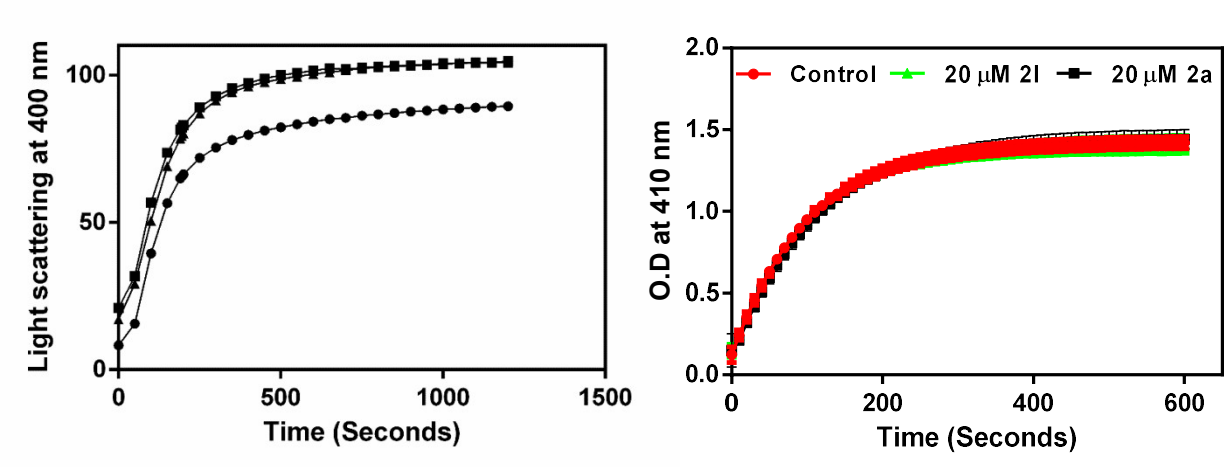

(a) **(b)**

Figure 14

Tubulin-Binding 3,5-Bis(styryl)pyrazoles as Lead Compounds for the Treatment of Castration-Resistant Prostate Cancer

Vivian W.Y. Liao,[#] Anuradha Kumari,[#] Rajeshwar Narlawar, Soma Vignarajan, David E. Hibbs, Dulal Panda, and Paul W. Groundwater

Molecular Pharmacology MOL # 118539

Sydney Pharmacy School, Faculty of Medicine and Health, The University of Sydney, Sydney, NSW 2006, Australia (VWYL, RN, DEH, PWG); Department of Biosciences and Bioengineering, Indian Institute of Technology Bombay, Mumbai 400076, India (AK, DP); Charles Perkins Centre, The University of Sydney, Sydney, NSW 2006, Australia (SV)

[#] These authors contributed equally to this work.

SUPPLEMENTARY INFORMATION

General Synthetic Methods

The 3,5-bis(styryl)pyrazoles **2a-l** were synthesized from the curcuminoids **1** using a CEM Discover SP microwave synthesis system. The spectroscopic and analytical data for pyrazoles **2a** [28,34], **2b** [28] and **2k** [35] were identical to that reported previously. Melting points were determined on a Stuart Scientific SMP10 apparatus. IR spectra were obtained on a FTIR-8400S Shimadzu system, using NaCl plates and values are recorded as wave-numbers (cm^{-1}). ^{1}H and ^{13}C NMR spectra were recorded at 400 and 100 MHz, respectively, on a Varian 400-MR magnetic resonance spectrometer, with chemical shifts (δ) reported in parts per million (ppm). Spectra were acquired in solutions of deuterated solvents and the residual solvent peaks were used as internal references; 7.24 ppm ($CDCl_3$), 2.50 ppm (DMSO-d_6), 2.05 ppm (acetone-d_6) and 3.31 ppm (methanol-d_4). Low resolution electrospray ionization (ESI) mass spectrometry was performed on a TSQ Quantum Access Max LCMS/MS (Thomas R Watson Mass Spectrometry Laboratory, Faculty of Pharmacy, The University of Sydney) and high resolution mass spectroscopy was performed on a Bruker 7T Fourier transform ion cyclotron resonance mass spectrometer (Mass Spectrometry Unit, School of Chemistry, The University of Sydney). Elemental analysis was performed on a Thermo Flash 2000 Elemental Analyser (Campbell Microanalytical Laboratory, University of Otago, New Zealand). All reagents were commercially available and purchased from Sigma Aldrich (Castle Hill, Sydney, Australia), Alfa Aesar (VWR, Australia). Solvents were purchased from Chem-Supply (Australia) and were used as received. Flash column chromatography was performed using Grace Davison (LC604 40-63 µm) Davisil chromatographic silica media. Thin layer chromatography (TLC) was performed using Grace Davidson Reveleris, aluminium-backed TLC plates (UV254).

*3,5-Bis[(1*E*)-2-(3-ethoxy-4-hydroxyphenyl)ethenyl]-1*H*-pyrazole (**2c**).* Yield 57 %, pale yellow crystalline solid, mp 149-153 ˚C. ^{1}H NMR (400 MHz, acetone-d_6) δ 7.19 (2H, d, J = 2.0 Hz, 2 × H-2″), 7.11 (2H, d, J = 16.8 Hz, 2 × H-2′), 7.00-6.96 (4H, m, 2 × H-1′, 2 × H-6″), 6.83 (2H, d, J = 8.0 Hz, 2 × H-5″), 6.65 (1H, s, H-4), 4.17 (4H, q, J = 6.8 Hz, 2 × OCH_2CH_3), 1.40 (6H, t, J = 6.8 Hz, 2 × OCH_2CH_3). ^{13}C NMR (100 MHz, acetone-d_6) δ 148.9 (2 × quat, 2 × C-4″), 148.8 (2 × quat, 2 × C-3″), 131.6 (2 × quat, 2 × C-1″), 131.1 (2 × CH, 2 × C-2′), 122.1 (2 × CH, 2 × C-6″), 116.9 (2 × CH, 2 × C-5″), 111.8 (2 × CH, 2 × C-2″), 100.9 (CH, C-4), 66.0 (2 × OCH_2CH_3), 16.1 (2 × OCH_2CH_3). IR (cm^{-1}) υ_{max} 3535 (OH), 3316 (NH), 1593 (C=N), 1558 (C=C), 1511 (C=C). ESI-MS: *m/z* 393 (100 %) $[M+H]^+$. Anal. Calcd for $C_{23}H_{24}N_2O_4$: C, 70.39; H, 6.16; N, 7.14. Found: C, 70.19; H, 6.43; N, 6.92.

*3,5-Bis[(1*E*)-2-(3-hydroxy-4-methoxyphenyl)ethenyl]-1*H*-pyrazole (**2d**).* Yield 35 %, pale yellow crystalline solid, mp 246-253 ˚C. ^{1}H NMR (400 MHz, acetone-d_6) δ 7.09 (2H, d, J = 2.0 Hz, 2 × H-2″), 7.10 (2H, d, J = 16.4 Hz, 2 × H-2′), 7.00-6.93 (6H, m, 2 × H-1′, 2 × H-5″, 2 × H-6″), 6.69 (1H, s, H-4), 3.86 (6H, s, 2 × OCH_3). ^{13}C NMR (100 MHz, acetone-d_6) δ 149.5 (2 × quat, 2 × C-3″), 148.7 (2 × quat, 2 × C-4″), 132.4 (2 × quat, 2 × C-1″), 131.3 (2 × CH, 2 × C-2′), 120.5 (2 × CH, 2 × C-6″), 114.1 (2 × CH, 2 × C-2″), 113.4 (2 × CH, 2 × C-5″), 101.2 (CH, C-4), 57.3 (2 × OCH_3). IR (cm^{-1}) υ_{max} 3290 (OH), 3229 (NH), 1582 (C=N), 1564 (C=C), 1511 (C=C). ESI-MS: *m/z* 365 (100 %) $[M+H]^+$. Anal. Calcd for $C_{21}H_{20}N_2O_4 \cdot 0.5\ CH_3OH$: C, 67.82; H, 5.83; N, 7.36. Found: C, 67.62; H, 5.74; N, 7.52.

*3,5-Bis[(1*E*)-2-(4-ethoxy-3-methoxyphenyl)ethenyl]-1*H*-pyrazole (**2e**).* Yield 51 %, white crystalline solid, mp 191-193 ˚C. ^{1}H NMR (400 MHz, $CDCl_3$) δ 7.06-7.02 (4H, m, 2 × H-2′, 2 × H-2″), 6.98 (2H, dd, J = 8.0, 1.6 Hz, 2 × H-6″), 6.93 (2H, d, J = 16.4 Hz, 2 × H-1′), 6.80 (2H, d, J = 8.4 Hz, 2 × H-5″), 6.60 (1H, s, H-4), 4.10 (4H, q, J = 6.8 Hz, 2 × OCH_2CH_3), 3.87 (6H, s, 2 ×

OCH_3), 1.47 (6H, t, J = 6.8 Hz, 2 × OCH_2CH_3). ^{13}C NMR (100 MHz, $CDCl_3$) δ 149.3 (2 × quat, 2 × C-4″), 148.5 (2 × quat, 2 × C-3″), 130.6 (2 × CH, 2 × C-2′), 129.5 (2 × quat, 2 × C-1″), 120.0 (2 × CH, 2 × C-6″), 112.4 (2 × CH, 2 × C-5″), 108.8 (2 × CH, 2 × C-2″), 99.5 (CH, C-4), 64.3 (2 × OCH_2CH_3), 55.8 (2 × OCH_3), 14.8 (2 × OCH_2CH_3). IR (cm^{-1}) υ_{max} 3396 (NH), 1595 (C=N), 1577 (C=C), 1507 (C=C). ESI-MS: *m/z* 421 (100 %) $[M+H]^+$. Anal. Calcd for $C_{25}H_{28}N_2O_4$: C, 71.41; H, 6.71; N, 6.66. Found: C, 71.33; H, 6.77; N, 6.66.

*3,5-Bis[(1*E*)-2-(4-methylphenyl)ethenyl]-1*H*-pyrazole (**2f**).* Yield 28 %, yellow crystalline solid, mp 191-193 ˚C. ^{1}H NMR (400 MHz, acetone-d_6) δ 12.18 (1H, bs, H-1), 7.45 (4H, d, J = 8.0 Hz, 2 × H-2″, 2 × H-6″), 7.20-7.17 (6H, m, 2 × H-2′, 2 × H-3″, 2 × H-5″), 7.10 (2H, d, J = 16.8 Hz, 2 × H-1′), 6.75 (1H, s, H-4), 2.33 (6H, s, 2 × CH_3). ^{13}C NMR (100 MHz, acetone-d_6) δ 139.3 (2 × quat, 2 × C-4″), 136.3 (2 × quat, 2 × C-1″), 131.2 (6 × CH, 2 × C-2′, 2 × C-3″, 2 × C-5″), 128.1 (4 × CH, 2 × C-2″, 2 × C-6″), 101.7 (CH, C-4), 22.2 (2 × CH_3). IR (cm^{-1}) υ_{max} 3209 (NH), 1583 (C=N), 1558 (C=C), 1506 (C=C). *m/z* 301 (100 %) $[M+H]^+$. Anal. Calcd for $C_{21}H_{20}N_2$: C, 83.96; H, 6.71; N, 9.33. Found: C, 84.08; H, 6.78; N, 9.50.

*3,5-Bis[(1*E*)-2-(2-methoxyphenyl)ethenyl]-1*H*-pyrazole (**2g**).* Yield 50 %, waxy white solid, mp 92-95 ˚C. ^{1}H NMR (400 MHz, acetone-d_6) δ 7.61 (2H, dd, J = 8.0, 1.6 Hz, 2 × H-6″), 7.49 (2H, d, J = 16.8 Hz, 2 × H-2′), 7.29-7.24 (2H, m, 2 × H-4″), 7.19 (2H, d, J = 16.8 Hz, 2 × H-1′), 7.03 (2H, d, J = 8.0 Hz, 2 × H-3″), 6.97 (2H, m, 2 × H-5″), 6.73(1H, s, H-4), 3.91 (6H, s, 2 × OCH_3). ^{13}C NMR (100 MHz, acetone-d_6) δ 159.0 (2 × quat, 2 × C-2″), 130.7 (2 × CH, 2 × C-4″), 128.3 (2 × CH, 2 × C-6″), 127.7 (2 × quat, 2 × C-1″), 126.4 (2 × CH, 2 × C-2′), 122.5 (2 × CH, 2 × C-5″), 113.0 (2 × CH, 2 × C-3″), 101.5 (CH, C-4), 56.9 (2 × OCH_3). IR (cm^{-1}) υ_{max} 3176 (NH), 1595 (C=N), 1576 (C=C), 1489 (C=C). ESI-MS: *m/z* 333 (100 %) $[M+H]^+$. HRMS (ESI): calcd for $C_{21}H_{21}N_2O_2$ $[M + H]^+$ 333.1603, found 333.1600.

*3,5-Bis[(1*E*)-2-(3-methoxyphenyl)ethenyl]-1*H*-pyrazole (**2h**).* Yield 41 %, white solid, mp 111-113 ˚C. ^{1}H NMR (400 MHz, $CDCl_3$) δ 7.24 (2H, t, J = 8.0 Hz, 2 × H-5″), 7.09 (2H, d, J = 16.4 Hz, 2 × H-1′), 7.07-7.02 (4H, m, 2 × H-2′, 2 × H-6″), 7.00 (2H, s, 2 × H-2″), 6.82 (2H, dd, J = 8.0, 2.0 Hz, 2 × H-4″), 6.66 (1H, s, H-4), 3.81 (6H, s, 2 × OCH_3). ^{13}C NMR (100 MHz, $CDCl_3$) δ 159.8 (2 × quat, 2 × C-3″), 147.1 (2 × quat, C-3, C-5), 137.9 (2 × quat, 2 × C-1″), 130.9 (2 × CH, 2 × C-2′), 129.7 (2 × CH, 2 × C-5″), 119.2 (2 × CH, 2 × H-6″), 117.9 (2 × CH, 2 × C-1′), 113.8 (2 × CH, 2 × C-4″), 111.6 (2 × CH, 2 × C-2″), 100.4 (CH, C-4), 55.2 (2 × OCH_3). IR (cm^{-1}) υ_{max} 3183 (NH), 1597 (C=N), 1588 (C=C), 1481 (C=C). ESI-MS: *m/z* 333 (100 %) $[M+H]^+$. Anal. Calcd for $C_{21}H_{20}N_2O_2$: C, 75.88; H, 6.06; N, 8.43. Found: C, 75.83; H, 6.09; N, 8.56.

*3,5-Bis[(1*E*)-2-(4-methoxyphenyl)ethenyl]-1*H*-pyrazole (**2i**).* Yield 46 %, pale yellow crystalline solid, mp 184-189 ˚C. ^{1}H NMR (400 MHz, $CDCl_3$) δ 7.40(4H, d, J = 8.8 Hz, 2 × H-2″, 2 × H-6″), 7.06 (2H, d, J = 16.4 Hz, 2 × H-2′), 6.92 (2H, d, J = 16.4 Hz, 2 × H-1′), 6.85 (4H, d, J = 8.8 Hz, 2 × H-3″, 2 × H-5″), 6.60 (1H, bs, H-4), 3.82 (6H, s, 2 × OCH_3). ^{13}C NMR (100 MHz, $CDCl_3$) δ 159.5 (2 × quat, 2 × C-4″), 147.4 (2 × quat, C-3, C-5), 130.4 (2 × CH, 2 × C-2′), 129.3 (2 × quat, 2 × C-1″), 127.8 (4 × CH, 2 × C-2″, 2 × C-6″), 115.6 (2 × CH, 2 × C-1′), 114.1 (2 × CH, 2 × C-3″, 2 × C-5″), 99.5 (CH, C-4), 55.3 (2 × OCH_3). IR (cm^{-1}) υ_{max} 3384 (NH), 1601 (C=N), 1569 (C=C), 1507 (C=C). ESI-MS: *m/z* 333 (100 %) $[M+H]^+$. Anal. Calcd for $C_{21}H_{20}N_2O_2$: C, 75.88; H, 6.06; N, 8.43. Found: C, 75.91; H, 6.11; N, 8.52.

*3,5-Bis[(1*E*)-2-(3-hydroxyphenyl)ethenyl]-1*H*-pyrazole (**2j**).* Yield 29 %, beige crystalline solid, mp 207-211 ˚C. ^{1}H NMR (400 MHz, methanol-d_4) δ 7.20-7.16 (2H, m, 2 × H-5″), 7.11 (2H, d, J = 16.4 Hz, 2 × H-2′), 7.03-6.97 (6H, m, 2 × H-1′, 2 × H-2″, 2 × H-6″), 6.73 (1H, s, H-4), 6.73-6.70 (2H, m, 2 × H-4″). ^{13}C NMR (100 MHz, methanol-d_4) δ 158.9 (2 × quat, 2 × C-3″), 139.6 (2 × quat, 2 × C-1″), 132.1 (2 × CH, 2 × C-2″), 130.8 (2 × CH, 2 × C-5″), 119.3 (2 × CH, 2 × C-6″),

116.2 (2 × CH, 2 × C-4″), 113.8 (2 × CH, 2 × C-2″), 101.0 (CH, C-4). IR (cm^{-1}) υ_{max} (OH), 1595 (C=N), 1582 (C=C), 1489 (C=C). ESI-MS: *m/z* 305 (100 %) $[M+H]^+$. Anal. Calcd for $C_{19}H_{16}N_2O_2$: C, 74.98; H, 5.30; N, 9.20. Found: C, 74.72; H, 5.49; N, 9.13.

*3,5-Bis[(1*E*)-2(2,6-dichlorophenyl)ethenyl]-1*H*-pyrazole (**2l**).* Yield 18 %, white fluffy solid, mp 205-210 ˚C. ^{1}H NMR (400 MHz, $CDCl_3$) δ 7.33 (4H, d, J = 8.0 Hz, 2 × H-3″, 2 × H-5″), 7.22-7.17 (4H, m, 2 × C-1′, 2 × C-2′), 7.13-7.09 (2H, m, 2 × H-4″), 6.81 (1H, bs, H-4). ^{1}H NMR (400 MHz, methanol-d_4) δ 7.44 (4H, d, J = 8.4 Hz, 2 × H-3″, 2 × H-5″), 7.27-7.22 (4H, m, 2 × H-2′, 2 × H-4″), 7.12 (2H, d, J = 16.8 Hz, 2 × H-1′), 6.87 (1H, s, H-4). ^{13}C NMR (100 MHz, $CDCl_3$) δ 134.5 (2 × quat, 2 × C-2″, 2 × 6″), 133.6 (2 × quat, 2 × C-1″), 128.6 (4 × CH, 2 × C-3″, 2 × C-5″), 128.4 (2 × CH, 2 × C-4″), 126.0 (2 × CH, 2 × C-1′), 124.6 (2 × CH, 2 × C-2′), 101.2 (CH, C-4). IR (cm^{-1}) υ_{max} 3169 (NH), 1653 (C=N), 1558 (C=C), 1506 (C=C). ESI-MS: *m/z* $C_{19}H_{13}{}^{35}Cl_4N_2$, 409 (71 %) $[M+H]^+$, $C_{19}H_{13}{}^{35}Cl_3{}^{37}ClN_2$, 411 (100 %) $[M+H]^+$, $C_{19}H_{13}{}^{35}Cl_2{}^{37}Cl_2N_2$, 413 (41 %) $[M+H]^+$, $C_{19}H_{13}{}^{35}Cl^{37}Cl_3N_2$, 415 (10 %) $[M+H]^+$. Anal. Calcd for $C_{19}H_{12}Cl_4N_2$: C, 55.64; H, 2.95; N, 6.83. Found: C, 55.67; H, 2.91; N, 6.78.

^{1}H AND ^{13}C SPECTRA OF NOVEL COMPOUNDS

3,5-Bis[(1*E*)-2-(3-ethoxy-4-hydroxyphenyl)ethenyl]-1*H*-pyrazole (**2c**)

3,5-Bis[(1*E*)-2-(3-hydroxy-4-methoxyphenyl)ethenyl]-1*H*-pyrazole (**2d**)

3,5-Bis[(1*E*)-2-(4-ethoxy-3-methoxyphenyl)ethenyl]-1*H*-pyrazole (**2e**)

3,5-Bis[(1*E*)-2-(4-methylphenyl)ethenyl]-1*H*-pyrazole (**2f**)

3,5-Bis[(1*E*)-2-(2-methoxyphenyl)ethenyl]-1*H*-pyrazole (**2g**)

3,5-Bis[(1*E*)-2-(3-methoxyphenyl)ethenyl]-1*H*-pyrazole (**2h**)

3,5-Bis[(1*E*)-2-(4-methoxyphenyl)ethenyl]-1*H*-pyrazole (**2i**)

3,5-Bis[(1*E*)-2-(3-hydroxyphenyl)ethenyl]-1*H*-pyrazole (**2j**)

3,5-Bis[(1E)-2(2,6-dichlorophenyl)ethenyl]-1H-pyrazole (**2l**)

*3,5-Bis[(1*E*)-2-(3-ethoxy-4-hydroxyphenyl)ethenyl]-1*H*-pyrazole (**2c**).* **^{1}H NMR**

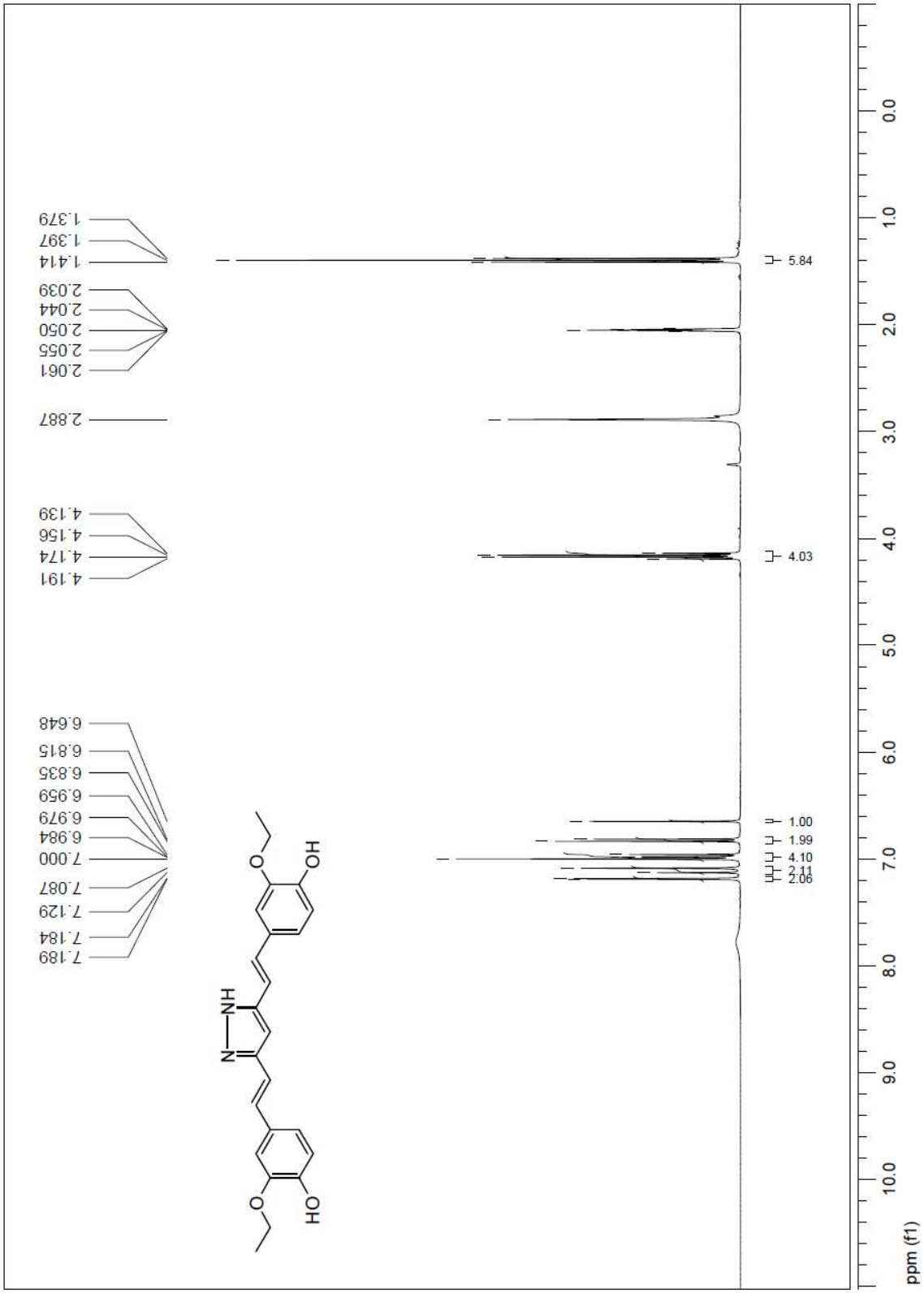

*3,5-Bis[(1*E*)-2-(3-ethoxy-4-hydroxyphenyl)ethenyl]-1*H*-pyrazole (**2c**).* **^{13}C NMR**

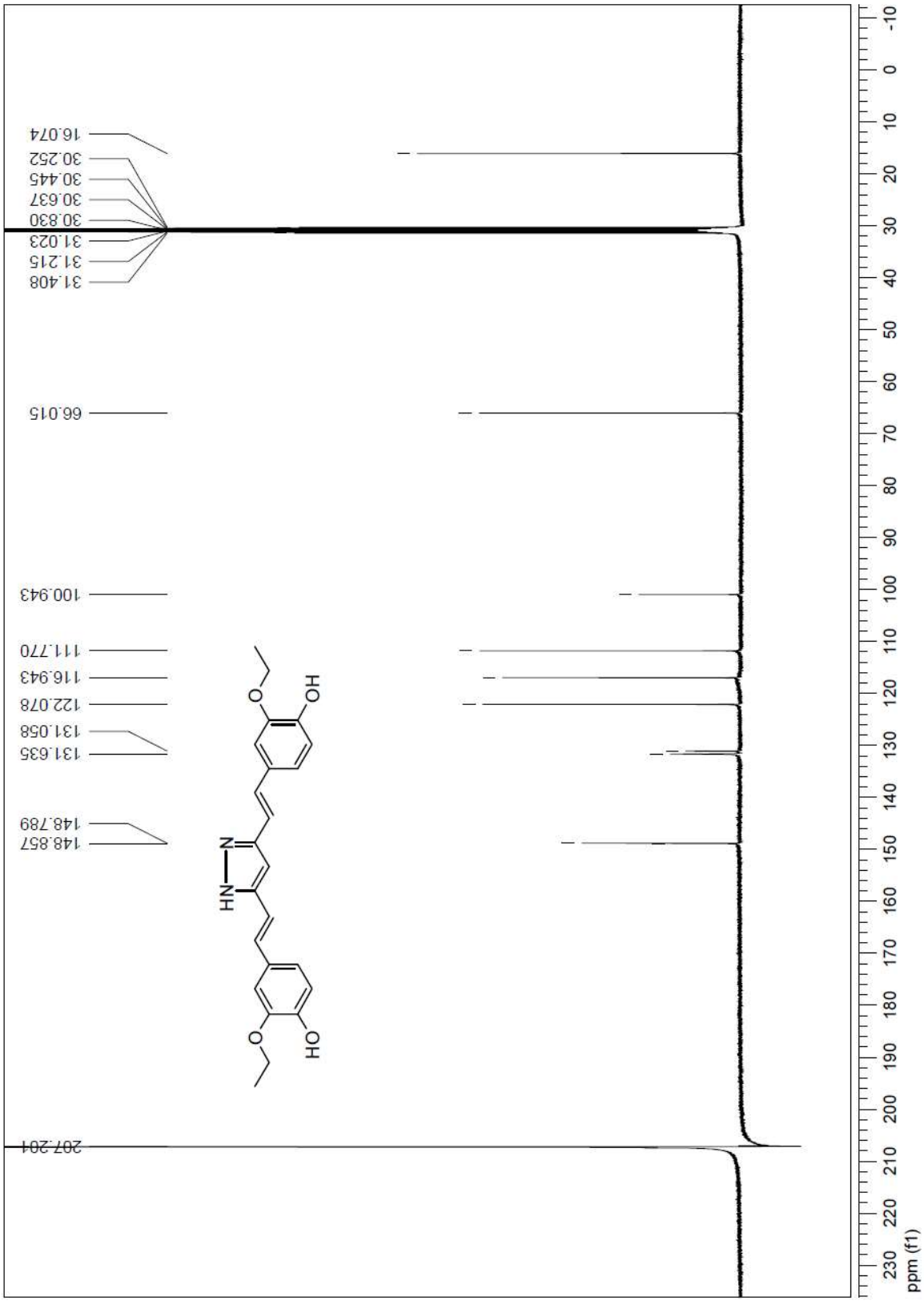

*3,5-Bis[(1*E*)-2-(3-hydroxy-4-methoxyphenyl)ethenyl]-1*H*-pyrazole (**2d**).* **^{1}H NMR**

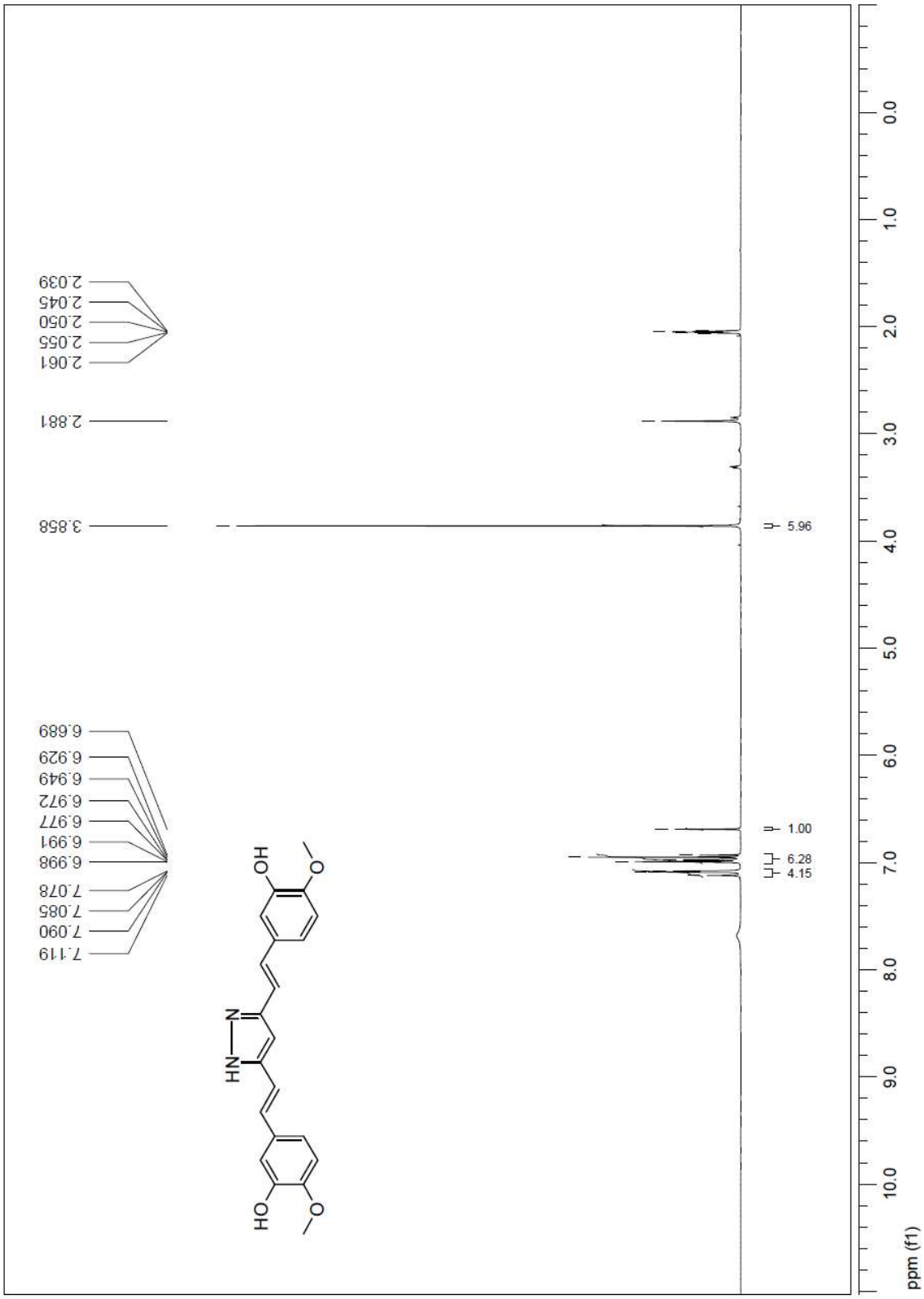

*3,5-Bis[(1*E*)-2-(3-hydroxy-4-methoxyphenyl)ethenyl]-1*H*-pyrazole (**2d**).* **^{13}C NMR**

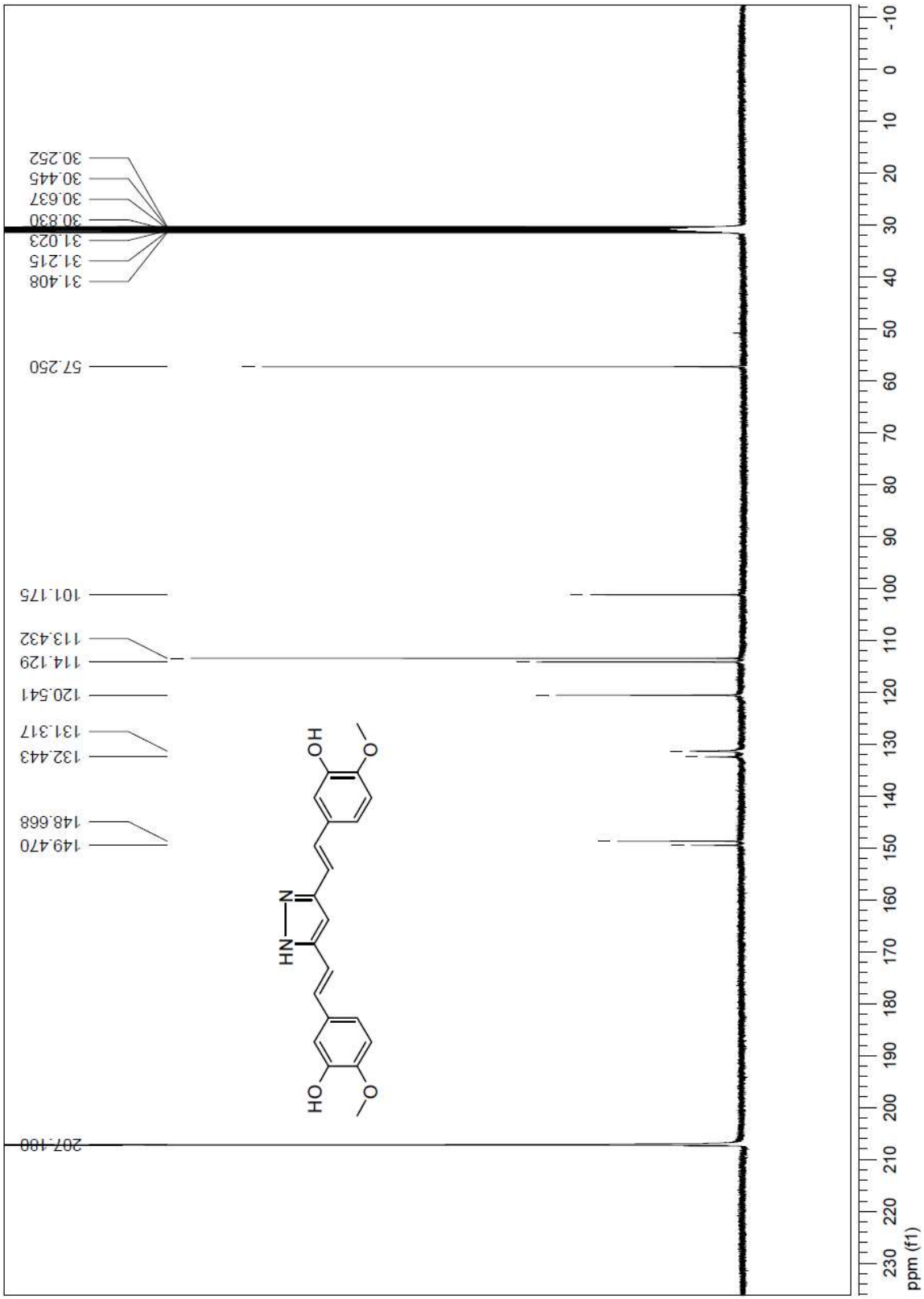

*3,5-Bis[(1*E*)-2-(4-ethoxy-3-methoxyphenyl)ethenyl]-1*H*-pyrazole (**2e**).* **^{1}H NMR**

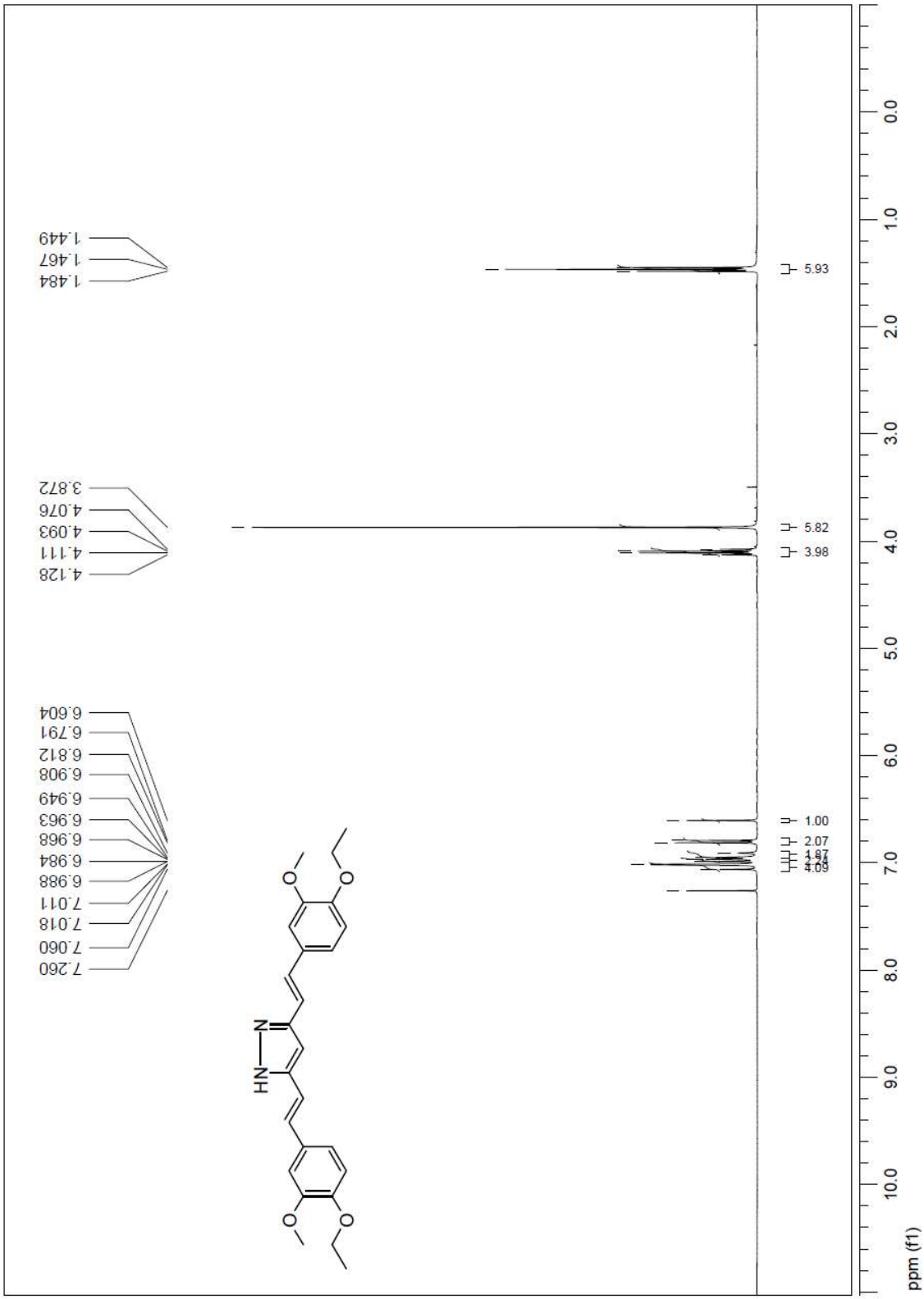

*3,5-Bis[(1*E*)-2-(4-ethoxy-3-methoxyphenyl)ethenyl]-1*H*-pyrazole (**2e**).* **^{13}C NMR**

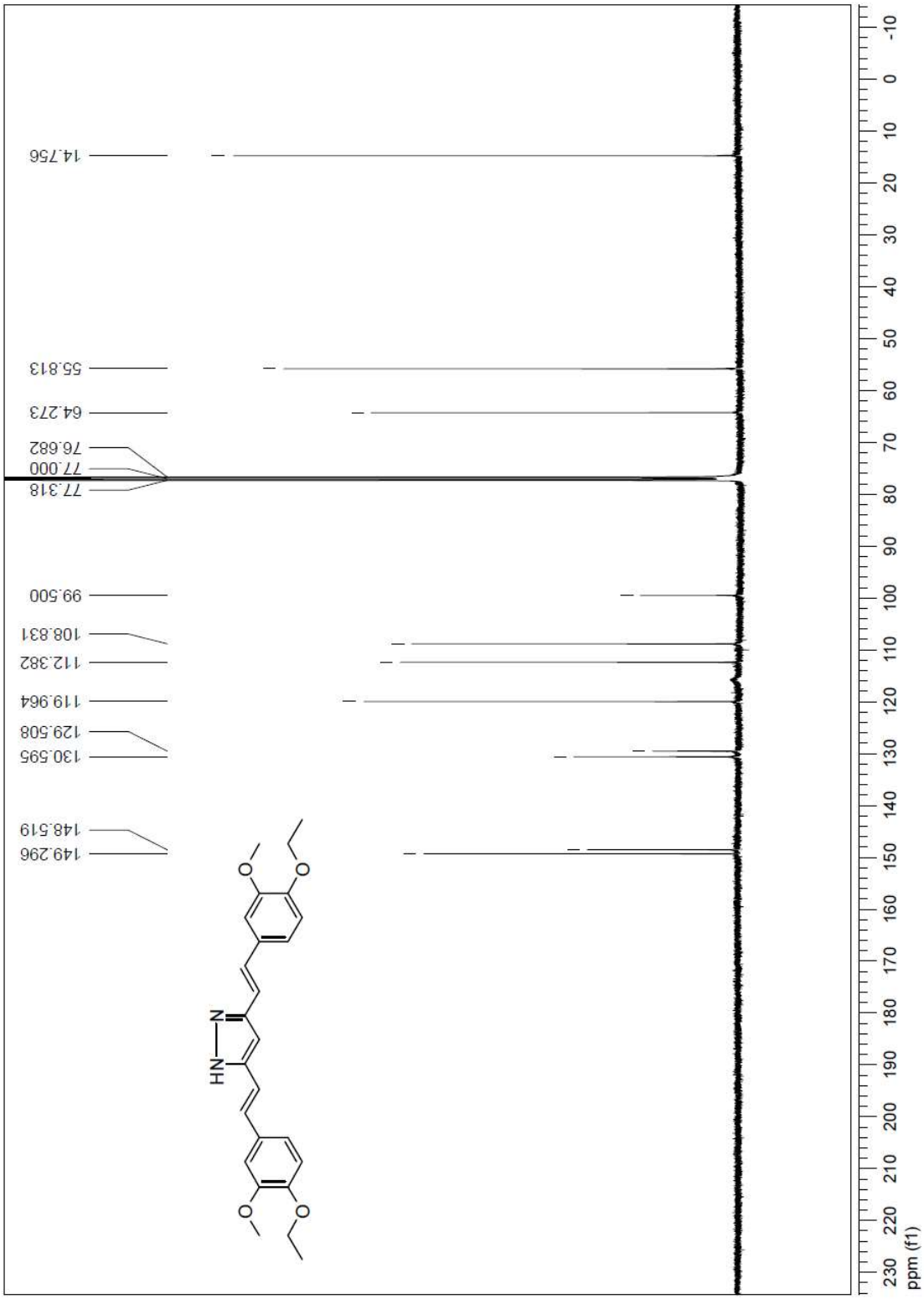

*3,5-Bis[(1*E*)-2-(4-methylphenyl)ethenyl]-1*H*-pyrazole (**2f**).* **^{1}H NMR**

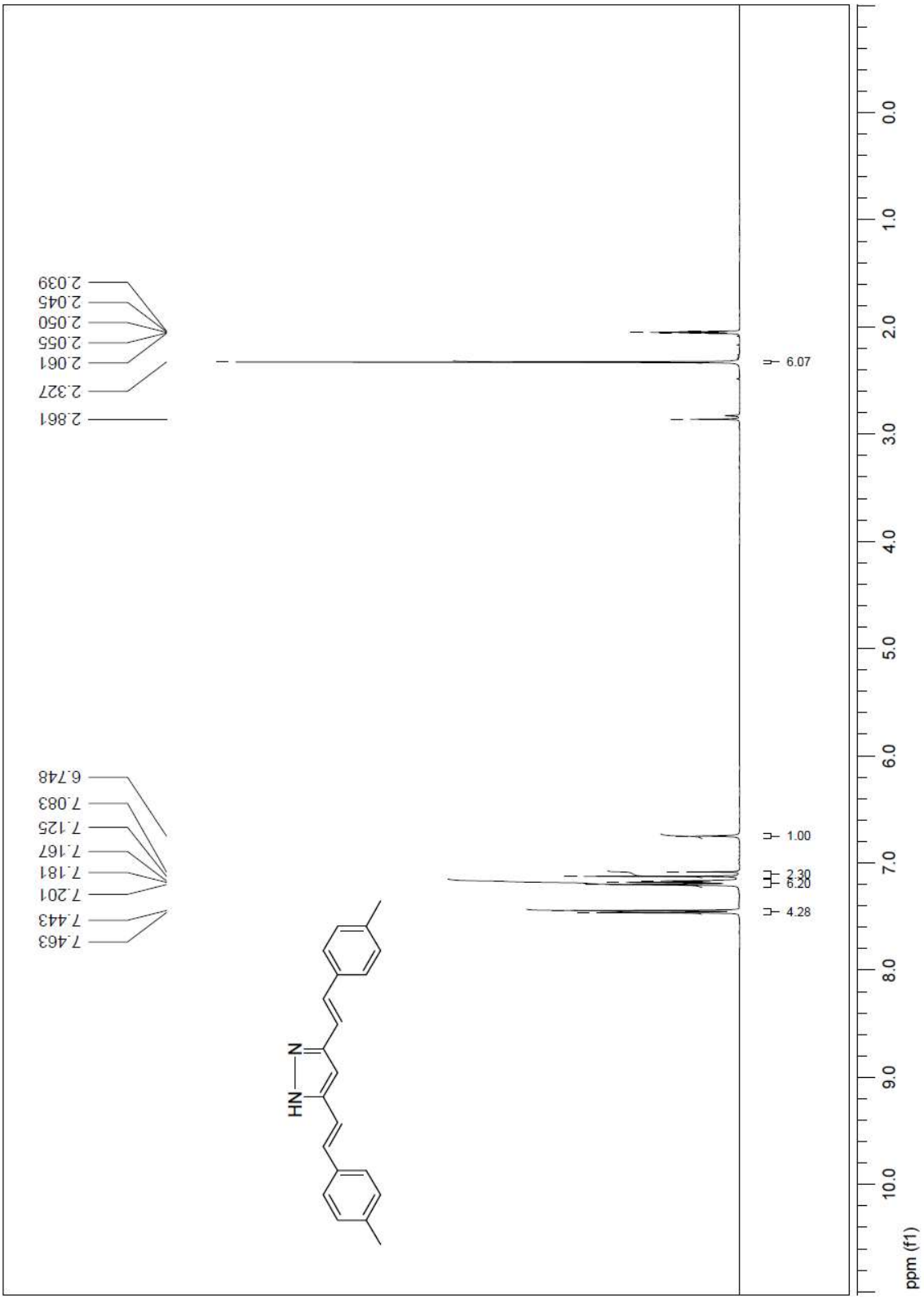

*3,5-Bis[(1*E*)-2-(4-methylphenyl)ethenyl]-1*H*-pyrazole (**2f**).* **^{13}C NMR**

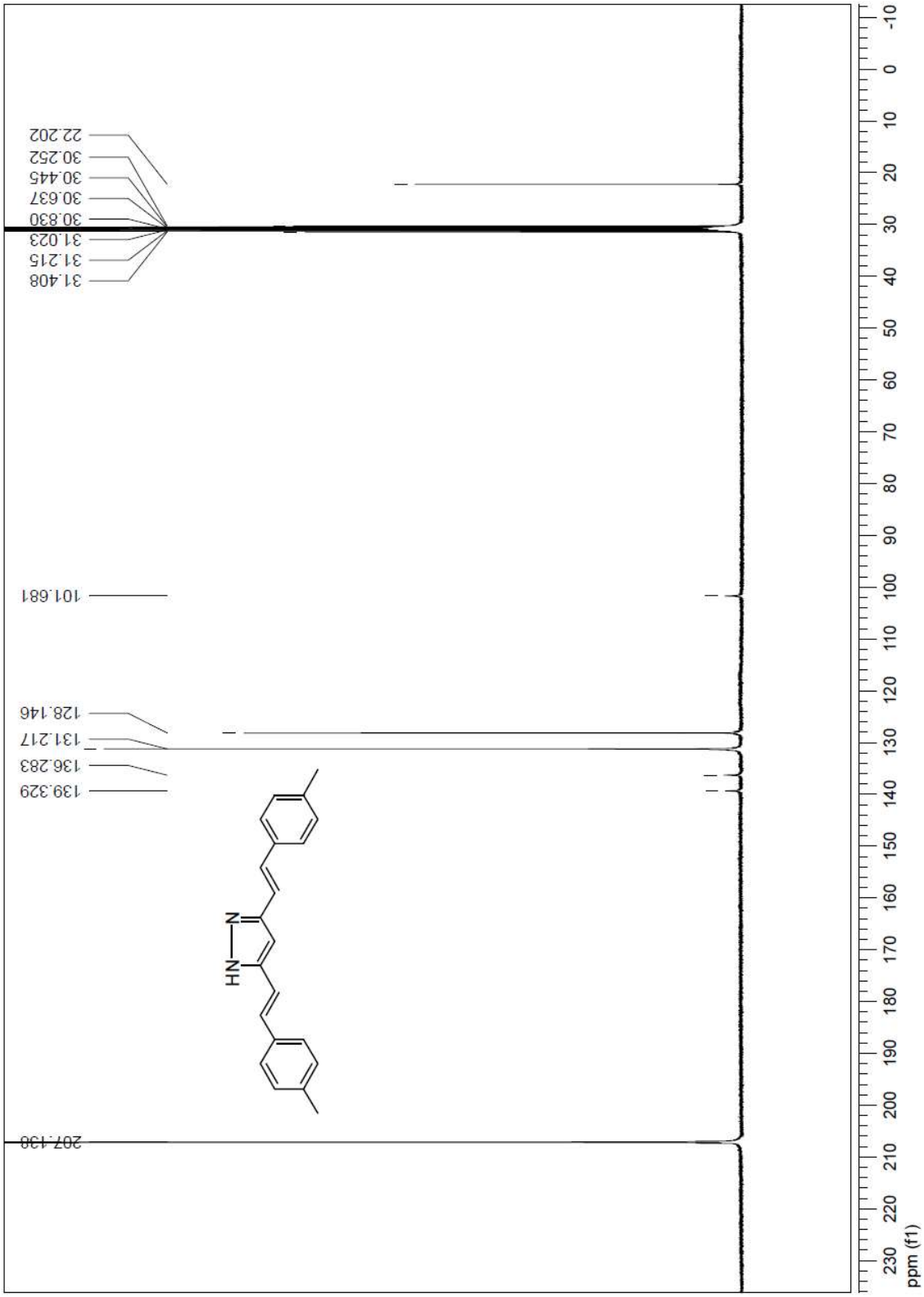

*3,5-Bis[(1*E*)-2-(2-methoxyphenyl)ethenyl]-1*H*-pyrazole (**2g**).* **^{1}H NMR**

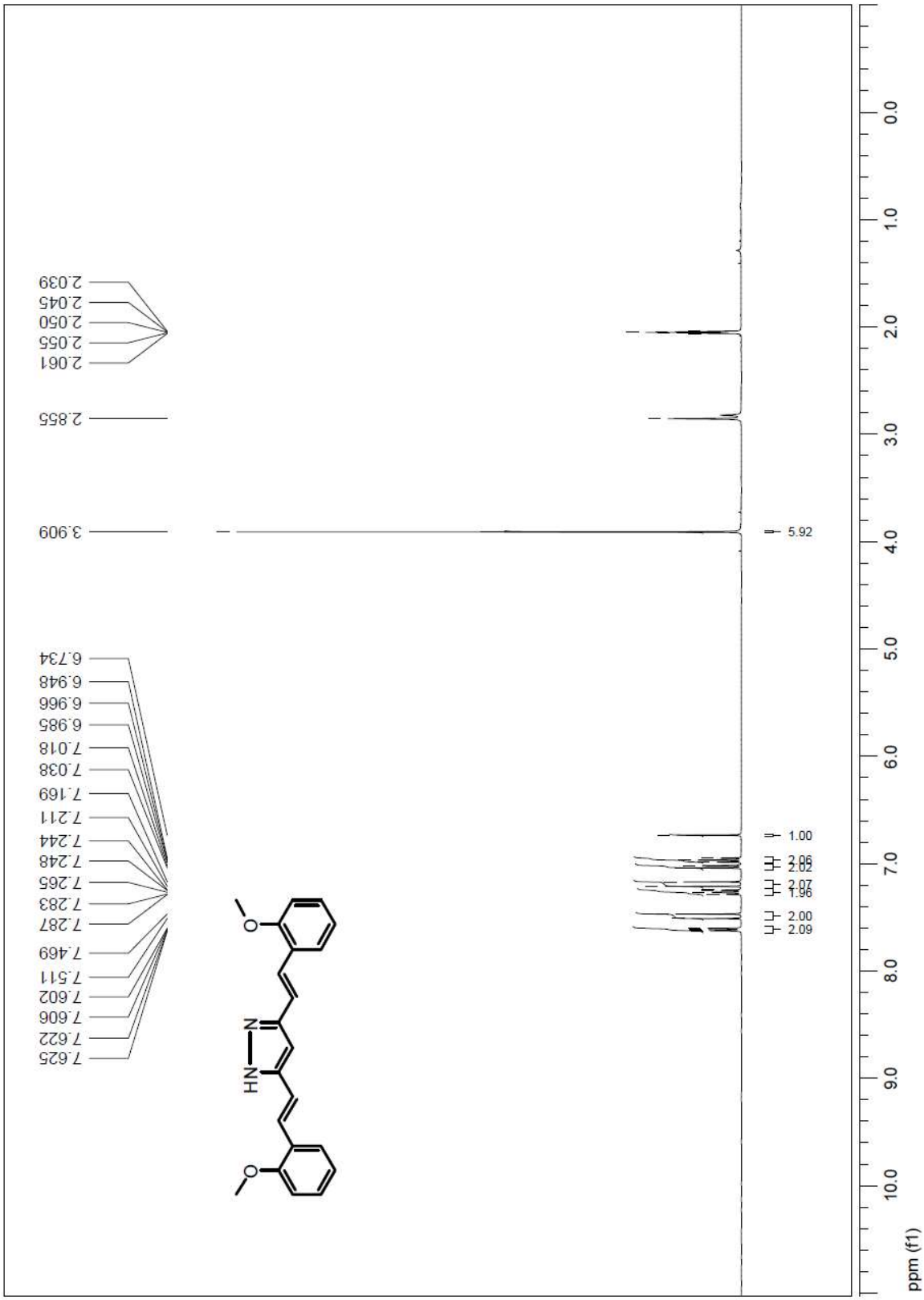

*3,5-Bis[(1*E*)-2-(2-methoxyphenyl)ethenyl]-1*H*-pyrazole (**2g**).* **^{13}C NMR**

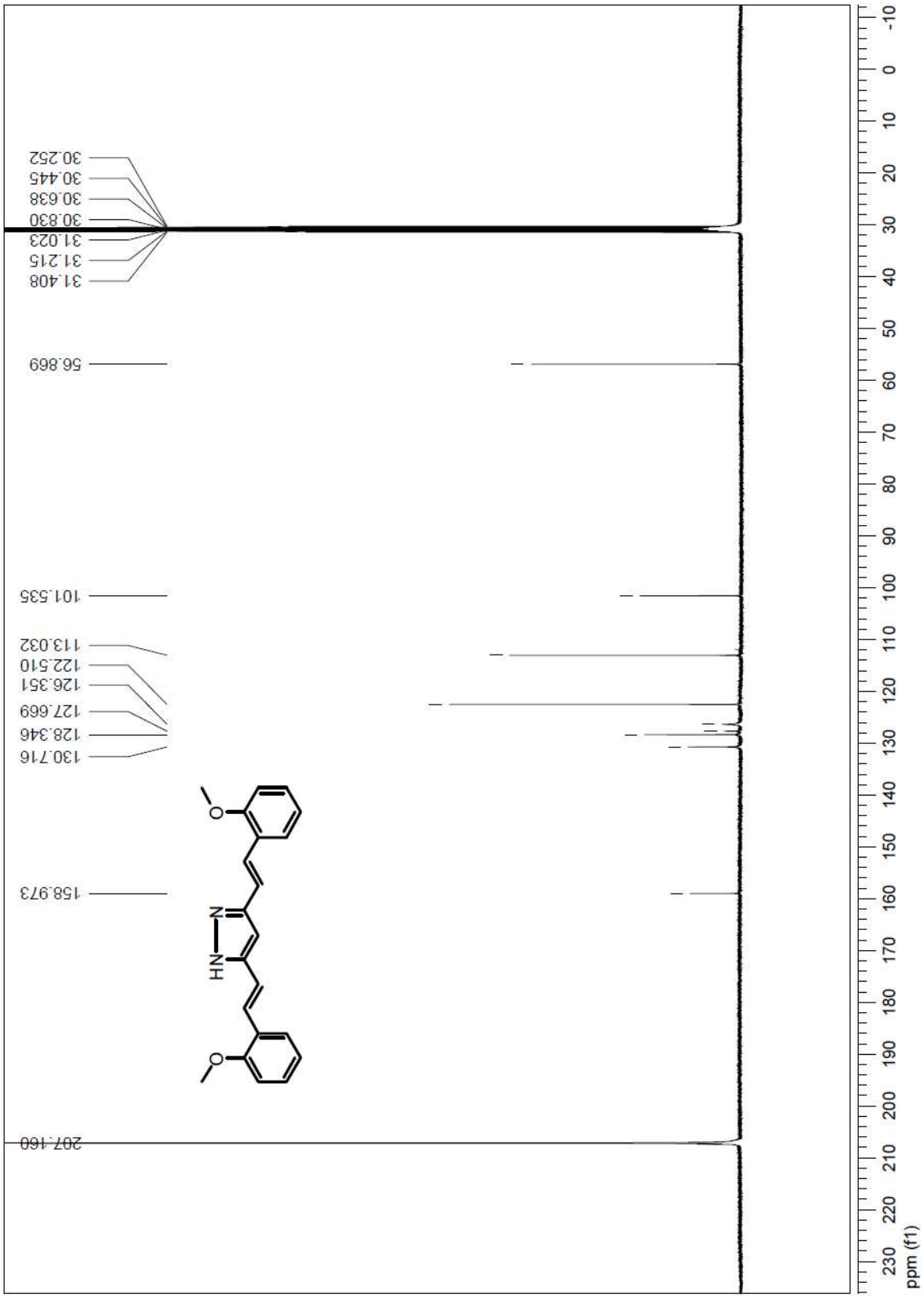

*3,5-Bis[(1*E*)-2-(3-methoxyphenyl)ethenyl]-1*H*-pyrazole (**2h**).* **^{1}H NMR**

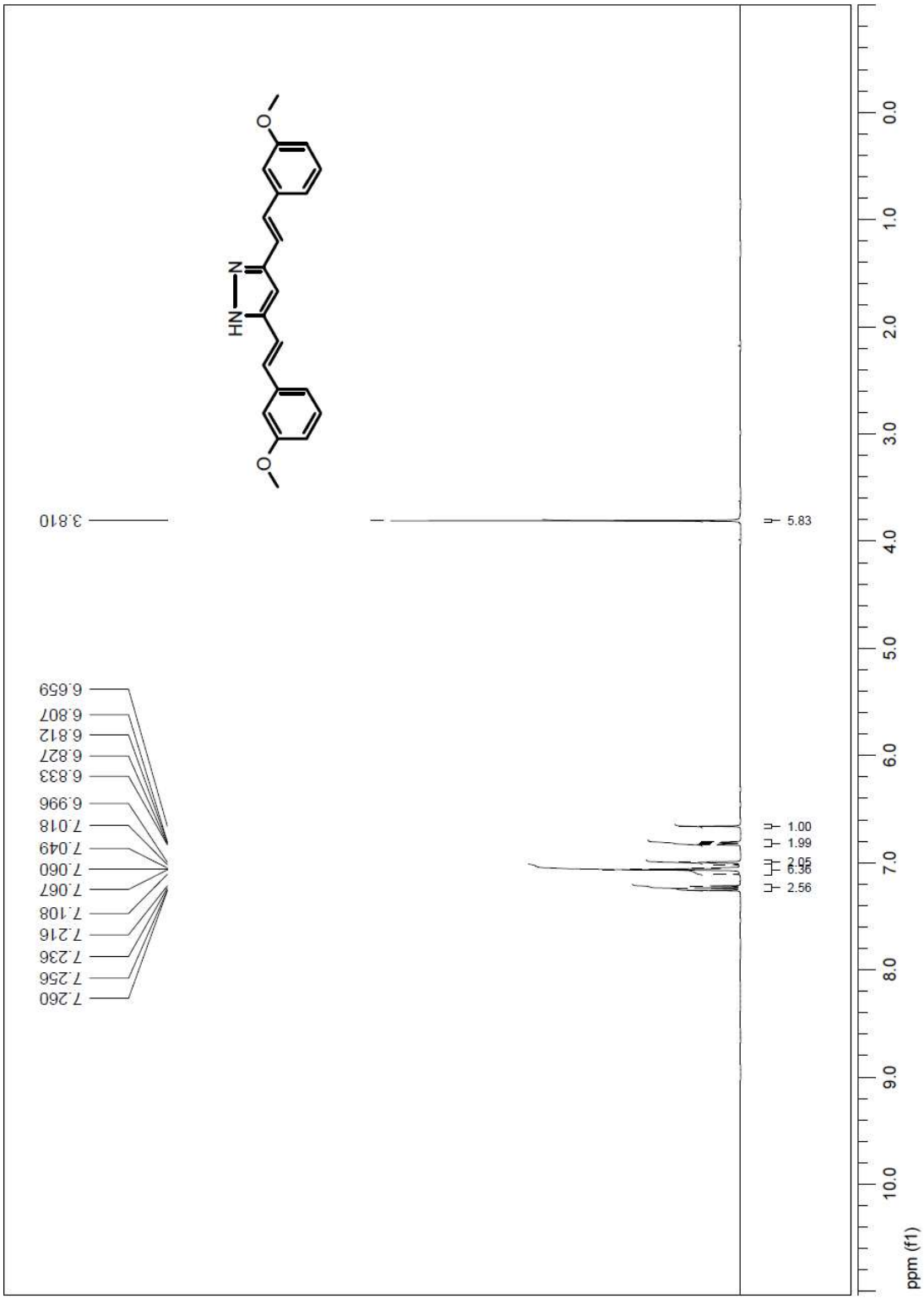

*3,5-Bis[(1E)-2-(3-methoxyphenyl)ethenyl]-1*H*-pyrazole (**2h**).* **^{13}C NMR**

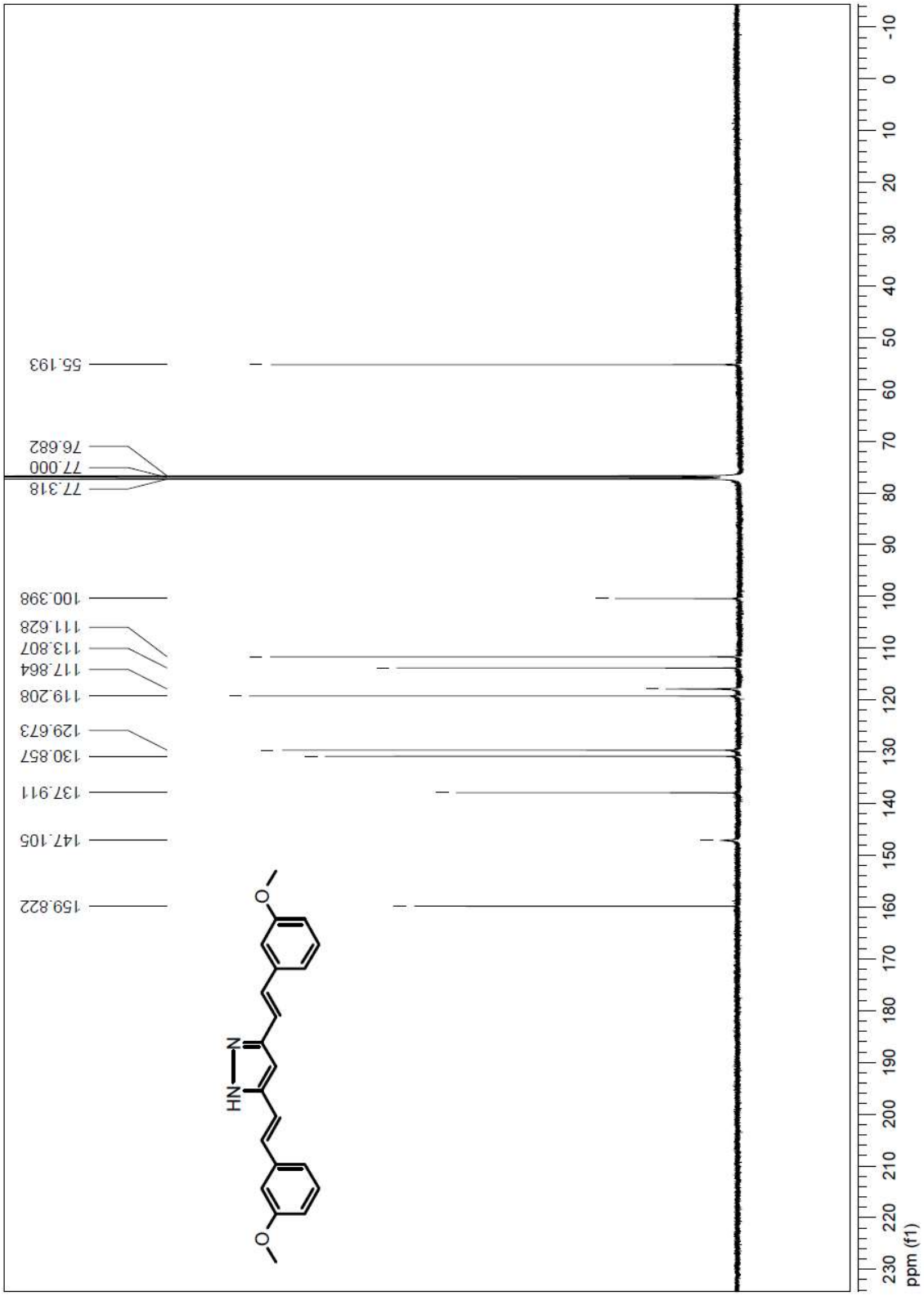

*3,5-Bis[(1*E*)-2-(4-methoxyphenyl)ethenyl]-1*H*-pyrazole (**2i**).* **^{1}H NMR**

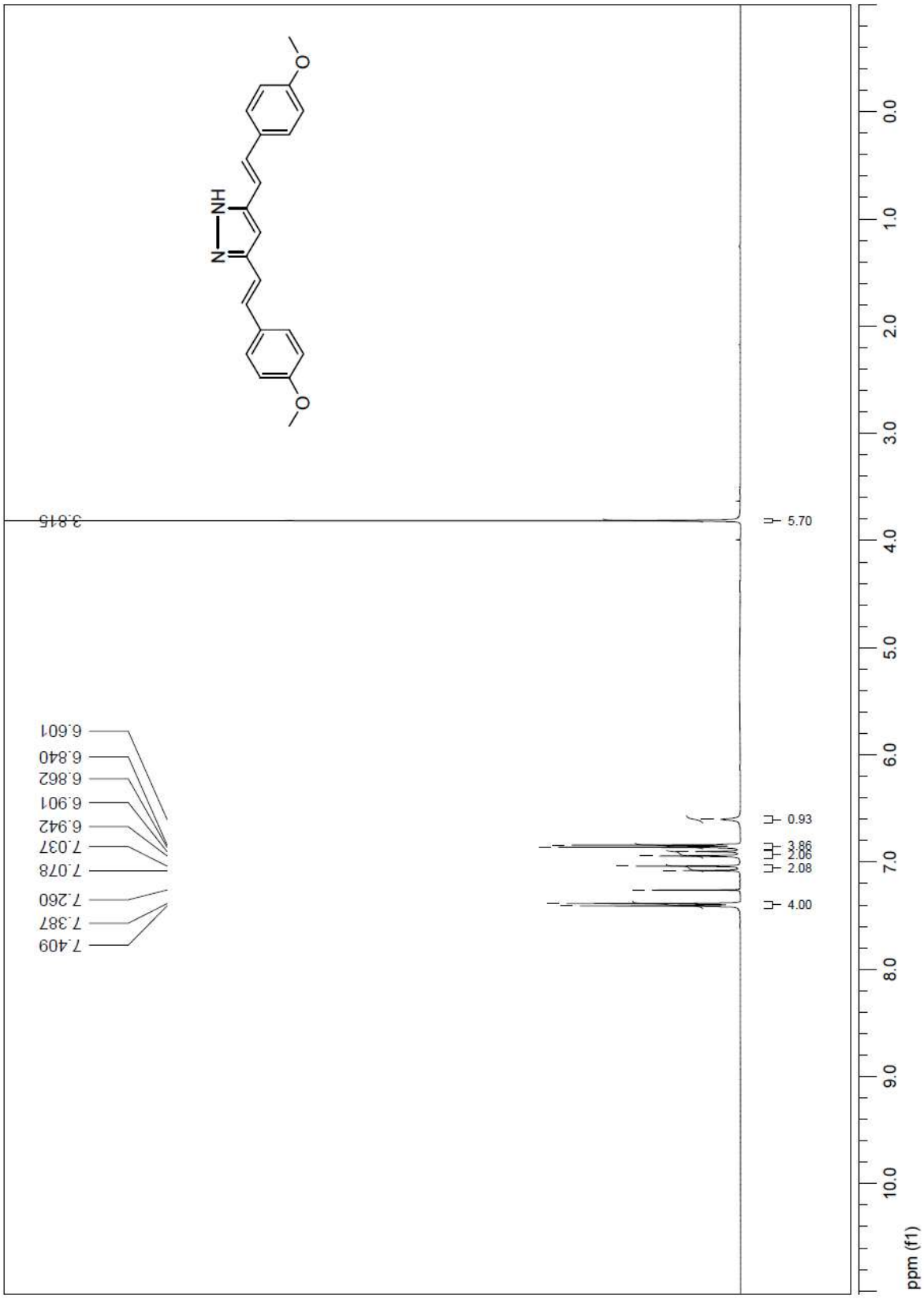

*3,5-Bis[(1*E*)-2-(4-methoxyphenyl)ethenyl]-1*H*-pyrazole (**2i**).* **^{13}C NMR**

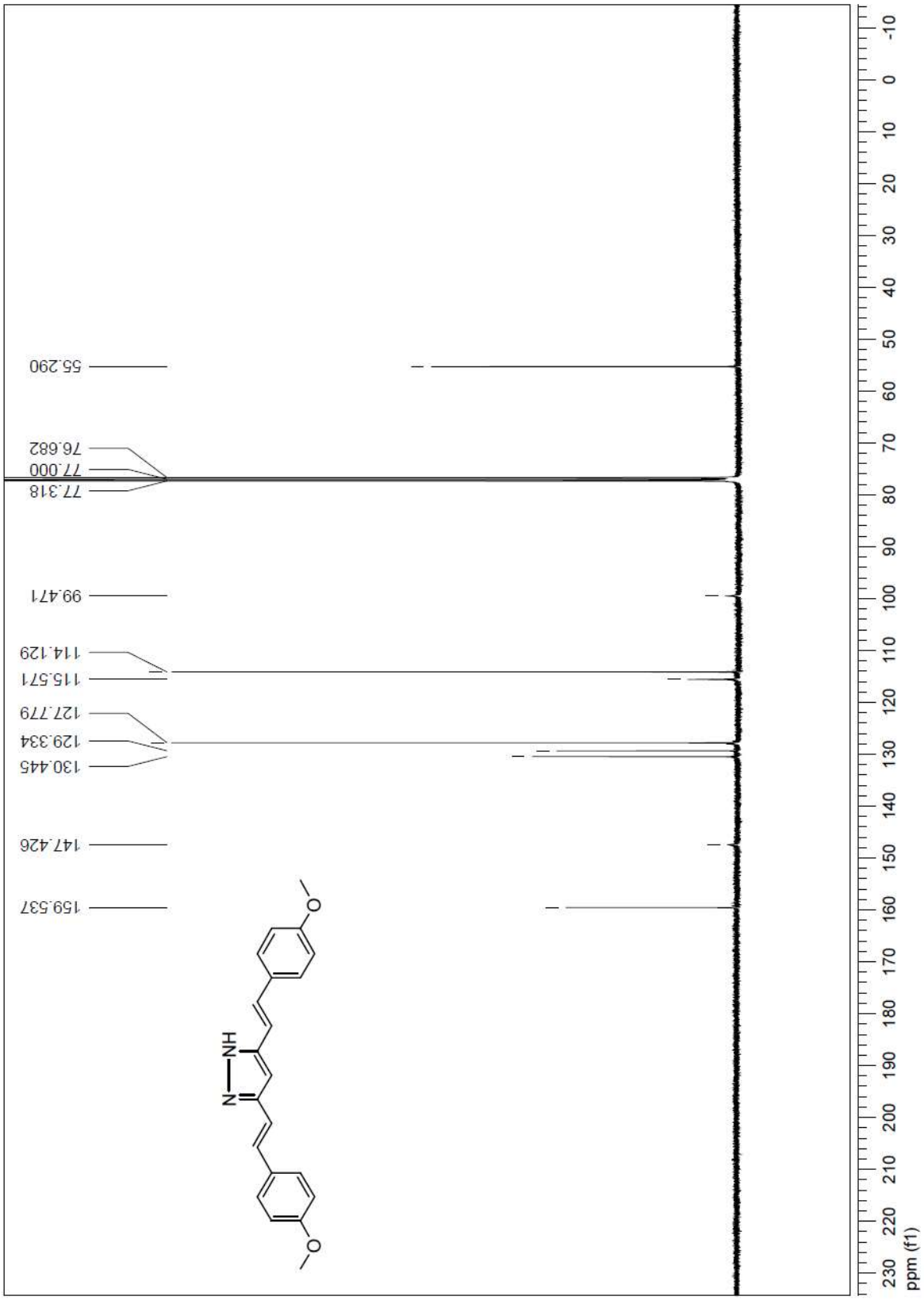

*3,5-Bis[(1*E*)-2-(3-hydroxyphenyl)ethenyl]-1*H*-pyrazole (**2j**).* **^{1}H NMR**

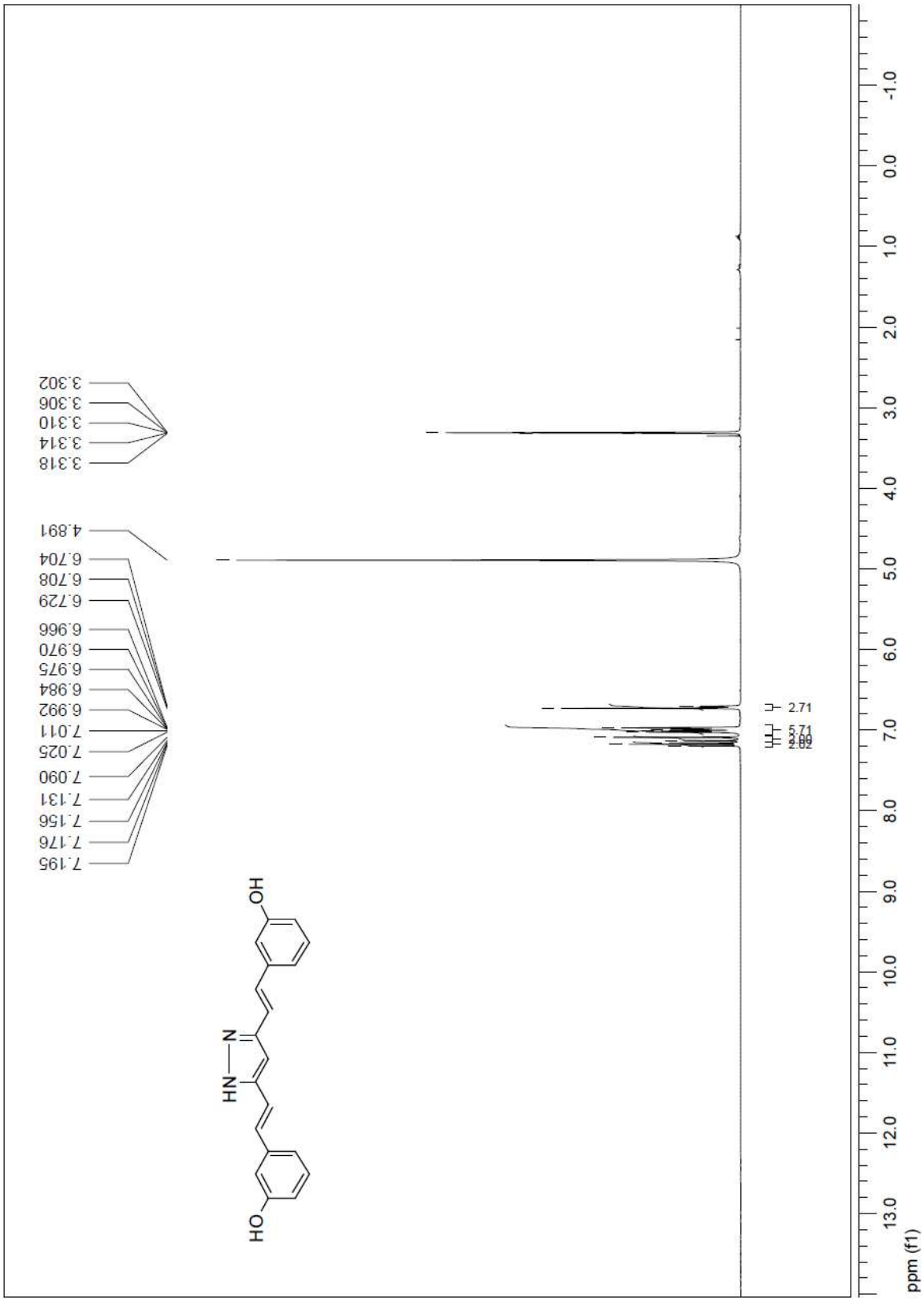

*3,5-Bis[(1*E*)-2-(3-hydroxyphenyl)ethenyl]-1*H*-pyrazole (**2j**).* **^{13}C NMR**

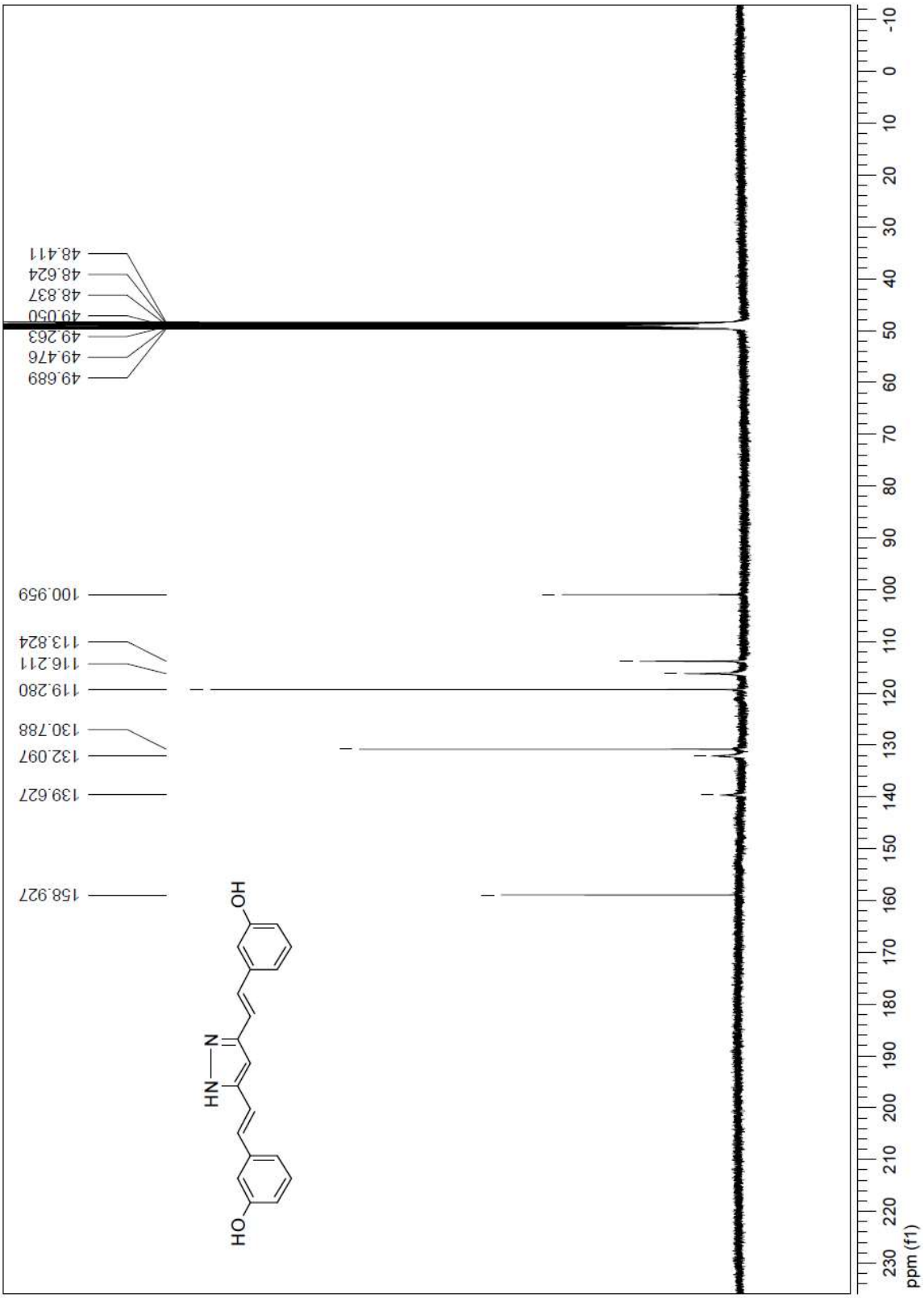

*3,5-Bis[(1*E*)-2-(2,6-dichlorophenyl)ethenyl]-1*H*-pyrazole (**2l**).* **^{1}H NMR CD_3OD**

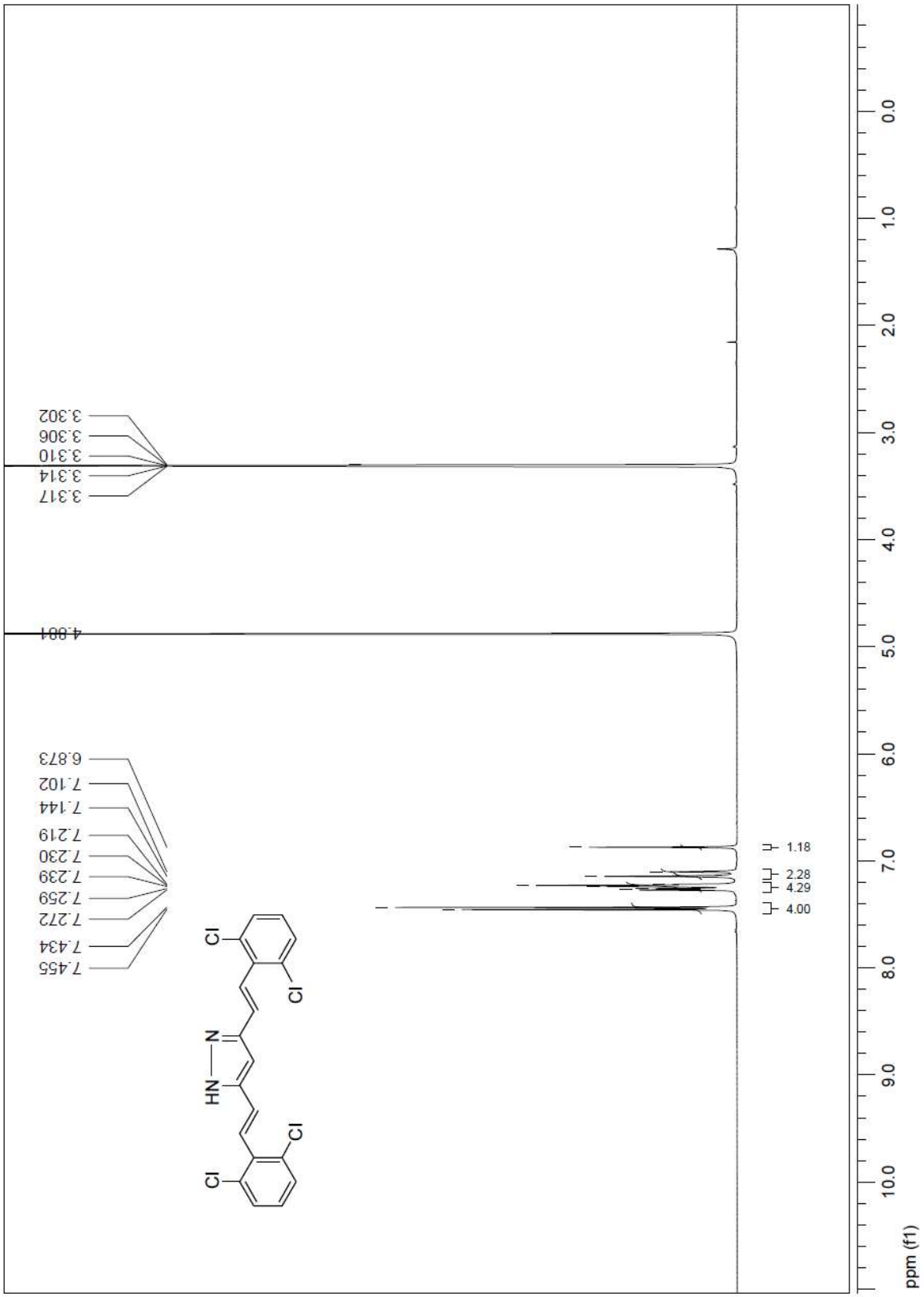

*3,5-Bis[(1*E*)-2(2,6-dichlorophenyl)ethenyl]-1*H*-pyrazole (**2l**).* **^{1}H NMR**

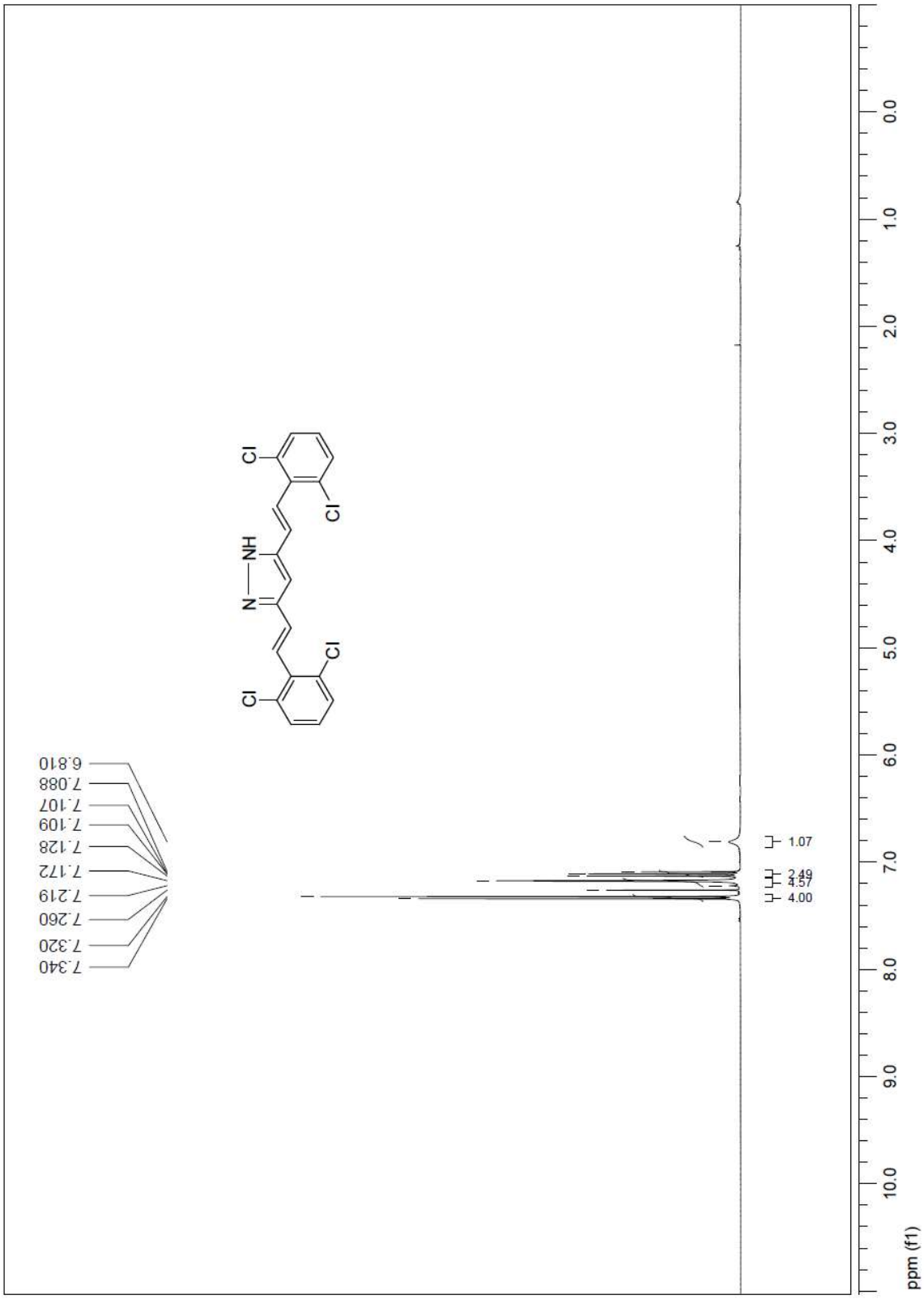

*3,5-Bis[(1*E*)-2(2,6-dichlorophenyl)ethenyl]-1*H*-pyrazole (**2l**).* **^{13}C NMR**

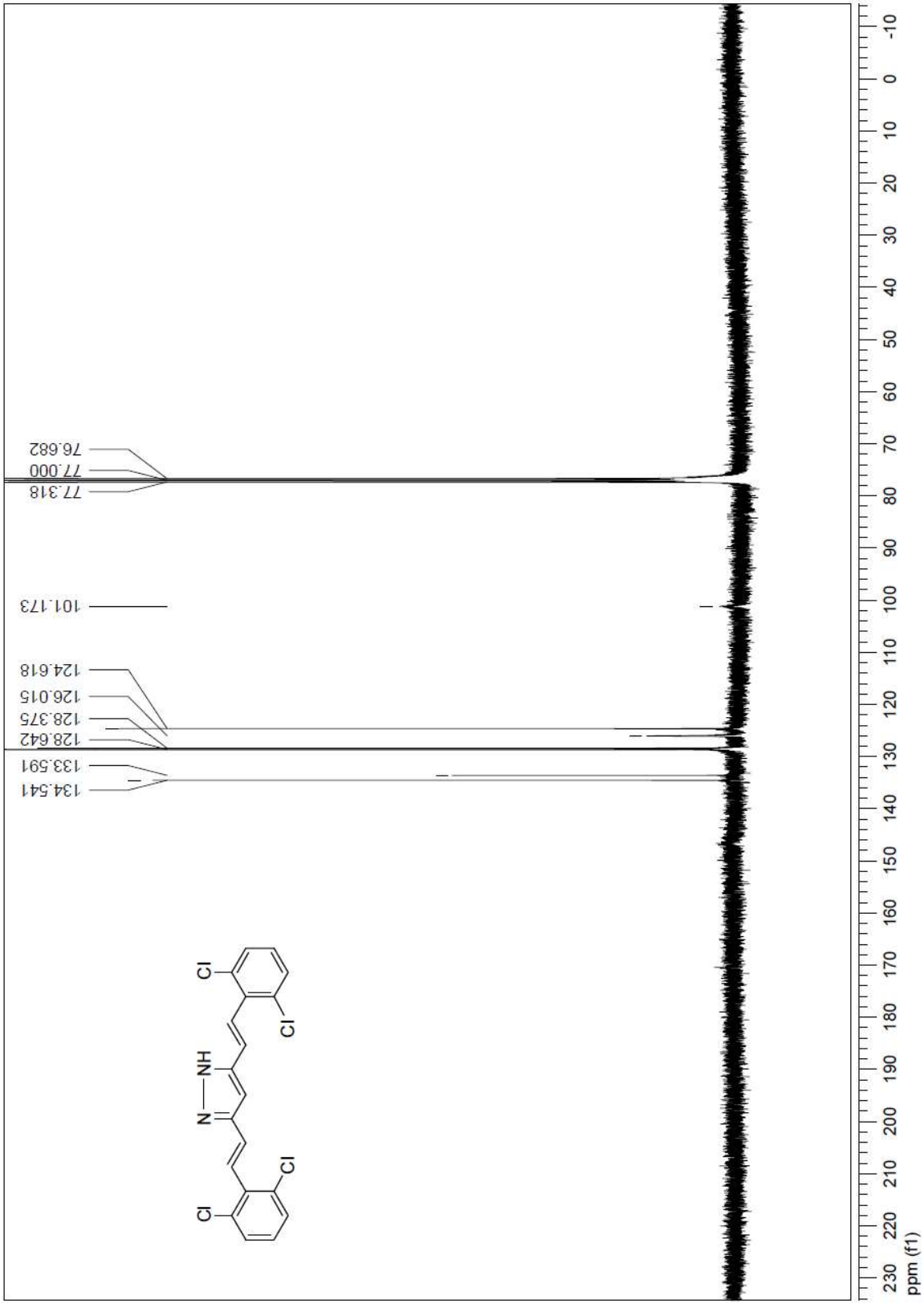

SUPPLEMENTAL TABLE 1

Linearity data for the standard curves for 3,5-bis(styryl)pyrazole **2a**

Standard curve	Slope	95 % confidence interval of slope	Intercept	95 % confidence interval of intercept	R^2
1	$1.623 \times 10^8 \pm 3.792 \times 10^6$	$1.517 \times 10^8 – 1.728 \times 10^8$	$-6.268 \times 10^5 \pm 1.477 \times 10^5$	$-1.037 \times 10^6 – -2.169 \times 10^5$	0.9978
2	$1.604 \times 10^8 \pm 3.908 \times 10^6$	$1.496 \times 10^8 – 1.713 \times 10^8$	$-5.814 \times 10^5 \pm 1.522 \times 10^5$	$-1.004 \times 10^6 – -1.590 \times 10^5$	0.9976
3	$1.616 \times 10^8 \pm 3.121 \times 10^6$	$1.529 \times 10^8 – 1.703 \times 10^8$	$-5.725 \times 10^5 \pm 1.216 \times 10^5$	$-9.099 \times 10^5 – -2.350 \times 10^5$	0.9985
Mean	1.614×10^8		-5.936×10^5		0.9980
SD	9.609×10^5		2.912×10^4		0.0005

The concentration range was between 0.01 - 0.06 mg/mL with six concentrations for each standard curve.

SUPPLEMENTAL TABLE 2

Linearity data for the standard curves for 3,5-bis(styryl)pyrazole **2l**

Standard curve	Slope	95 % confidence interval of slope	Intercept	95 % confidence interval of intercept	R^2
1	$8.090 \times 10^7 \pm 2.609 \times 10^6$	$7.366 \times 10^7 – 8.814 \times 10^7$	$-2.508 \times 10^5 \pm 1.016 \times 10^5$	$-5.328 \times 10^5 – 3.125 \times 10^4$	0.9959
2	$7.988 \times 10^7 \pm 2.507 \times 10^6$	$7.292 \times 10^7 – 8.684 \times 10^7$	$-2.371 \times 10^5 \pm 9.762 \times 10^4$	$-5.081 \times 10^5 – -3.389 \times 10^4$	0.9961
3	$8.127 \times 10^7 \pm 2.608 \times 10^6$	$7.403 \times 10^7 – 8.851 \times 10^7$	$-2.338 \times 10^5 \pm 1.016 \times 10^5$	$-5.158 \times 10^5 – 4.823 \times 10^4$	0.9959
Mean	8.068×10^7		-2.406×10^5		0.9980
SD	7.199×10^5		9.015×10^3		0.0001

The concentration range was between 0.01 - 0.06 mg/mL with six concentrations for each standard curve.

SUPPLEMENTAL TABLE 3

2a and **2l** treatment induced apoptotic cell death in A549, B16F10 and Huh-7 cells.

Compound	**A549** (% dead cells)	**B16F10** (% dead cells)	**Huh-7** (% dead cells)
Control	6.7 ± 0.7	7.2 ± 0.8	4.0 ± 1.9
4 µM 2a	8.0 ± 4.0	19.6 ± 3.1	5.9 ± 1.9
8 µM 2a	18.8 ± 4.1	31.5 ± 5.4	17.3 ± 8.1
4 µM 2l	12.5 ± 2.7	12.1 ± 1.6	30.7 ± 4.5
8 µM 2l	17.3 ± 2.0	55.1 ± 5.2	37.9 ± 2.6

Data represent mean ± standard deviation of four independent replicates (n = 3).

SUPPLEMENTAL TABLE 4

Cell cycle analysis of PC3 cells after treatment with 3,5-bis(styryl)pyrazoles **2a** and **2l** (GI_{50} concentrations) showing the percentage of cells in each phase of the cell cycle.

	G_0/G_1	S	G_2/M
Control	72.2 ± 0.4	10.6 ± 1.1	17.1 ± 1.3
2a	9.2 ± 2.5	3.0 ± 1.2	87.6 ± 5.0
2l	5.3 ± 1.1	5.0 ± 1.2	89.8 ± 1.8

Data represent mean ± standard deviation of four independent replicates (n = 4).

SUPPLEMENTAL TABLE 5

Quantification of live / dead cells after treating PC3 cells with 4 and 8 µM **2a** and **2l** for 2 and 4 hours.

	Compound	PC3 (% dead cells)
	Control	2.7 ± 0.5
	4 µM 2a	3.2 ± 0.8
2 hours	**8 µM 2a**	3.4 ± 0.8
	4 µM 2l	4.0 ± 1.1
	8 µM 2l	3.9 ± 1.2
	4 µM 2a	3.8 ± 0.9
4 hours	**8 µM 2a**	4.1 ± 0.8
	4 µM 2l	4.3 ± 1.0
	8 µM 2l	4.1 ± 0.6

Data represent mean ± standard deviation of four independent replicates (n = 3).

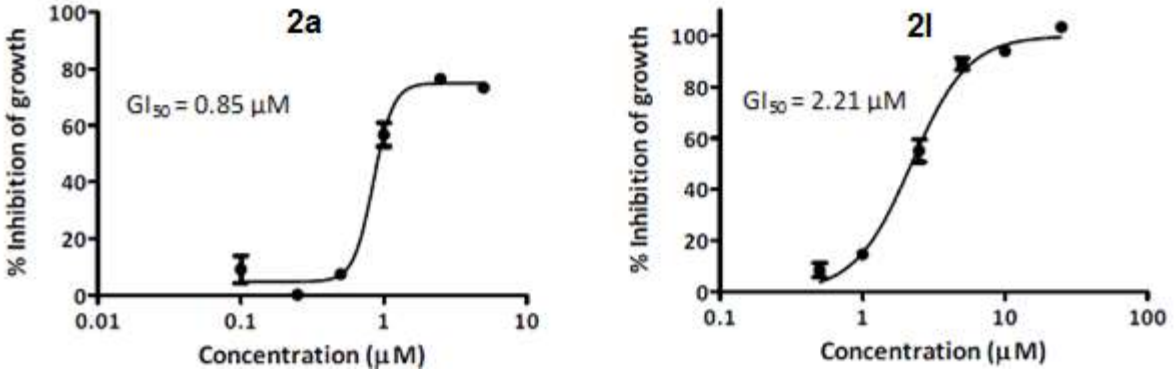

Supplemental Figure 1

Dose-response curves of percentage growth inhibition *vs* log concentrations of 3,5-bis(styryl)pyrazoles **2a** and **2l**. Data represent mean ± standard deviation of three independent replicates (n = 3).

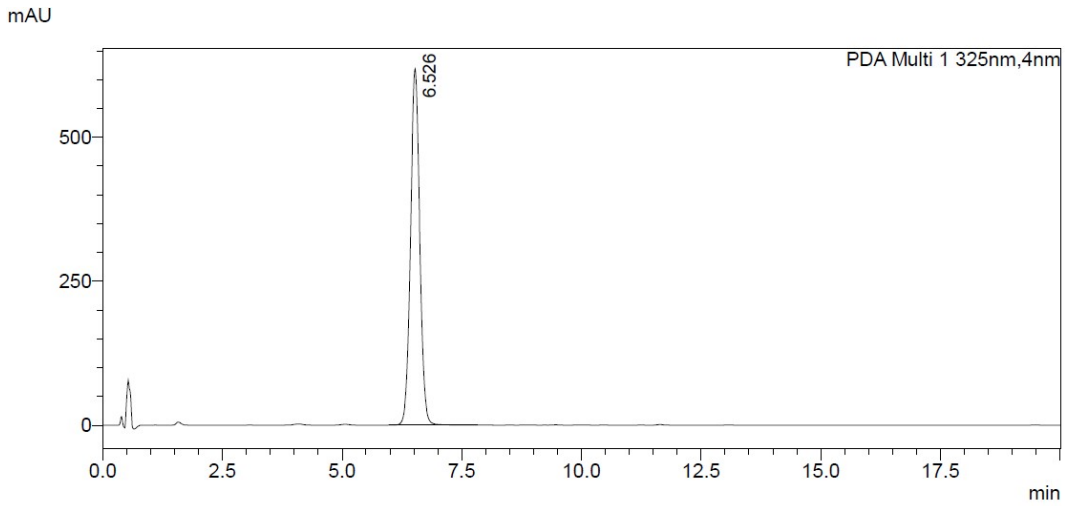

(A)

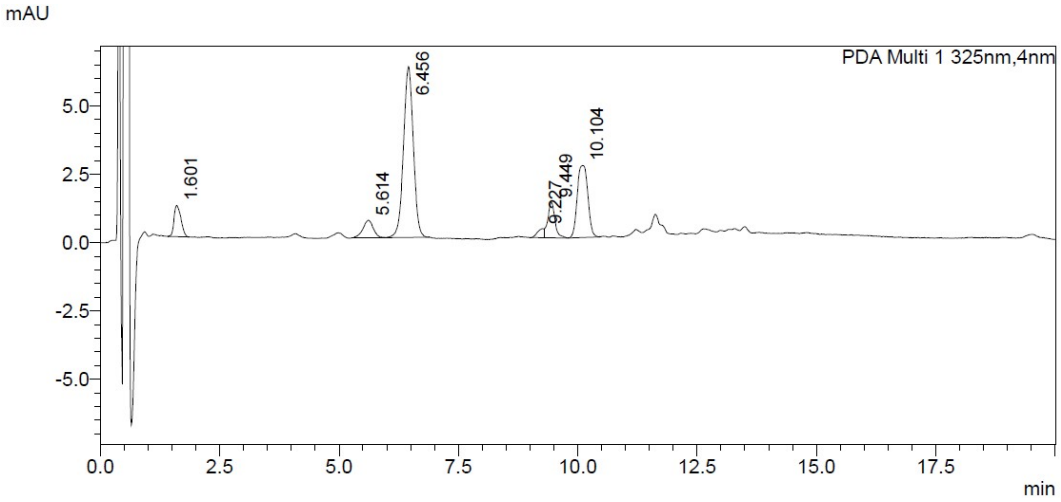

(B)

Supplemental Figure 2

HPLC chromatograms of the stability test for 3,5-bis(styryl)pyrazole **2a**; **(A)** t = 0 and **(B)** t = 72.

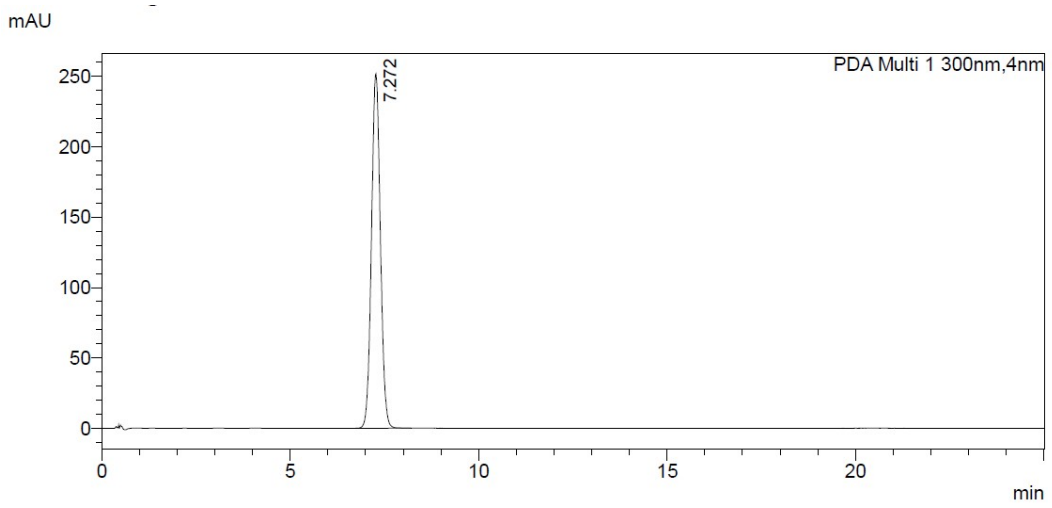

(A)

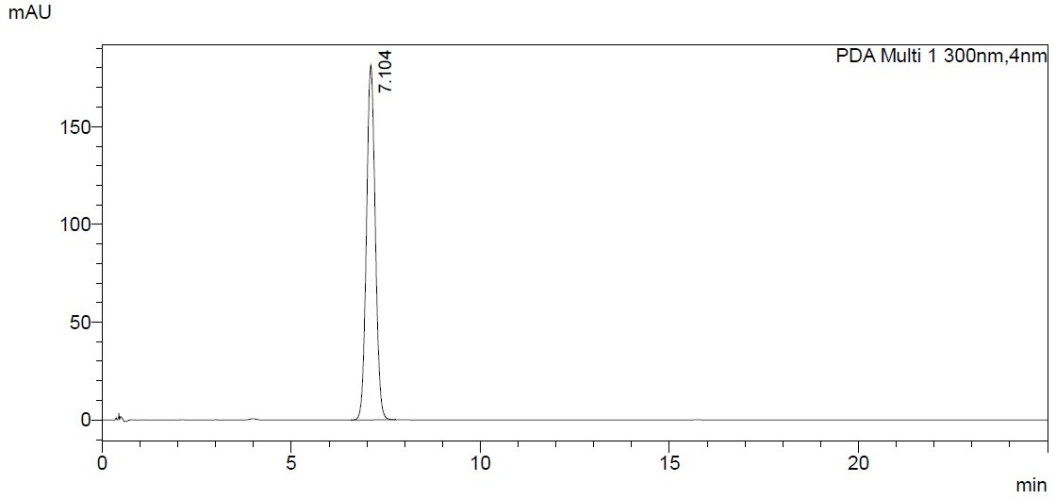

(B)

Supplemental Figure 3

HPLC chromatograms of the stability test for 3,5-bis(styryl)pyrazole **2l**; **(A)** t = 0 and **(B)** t = 72.

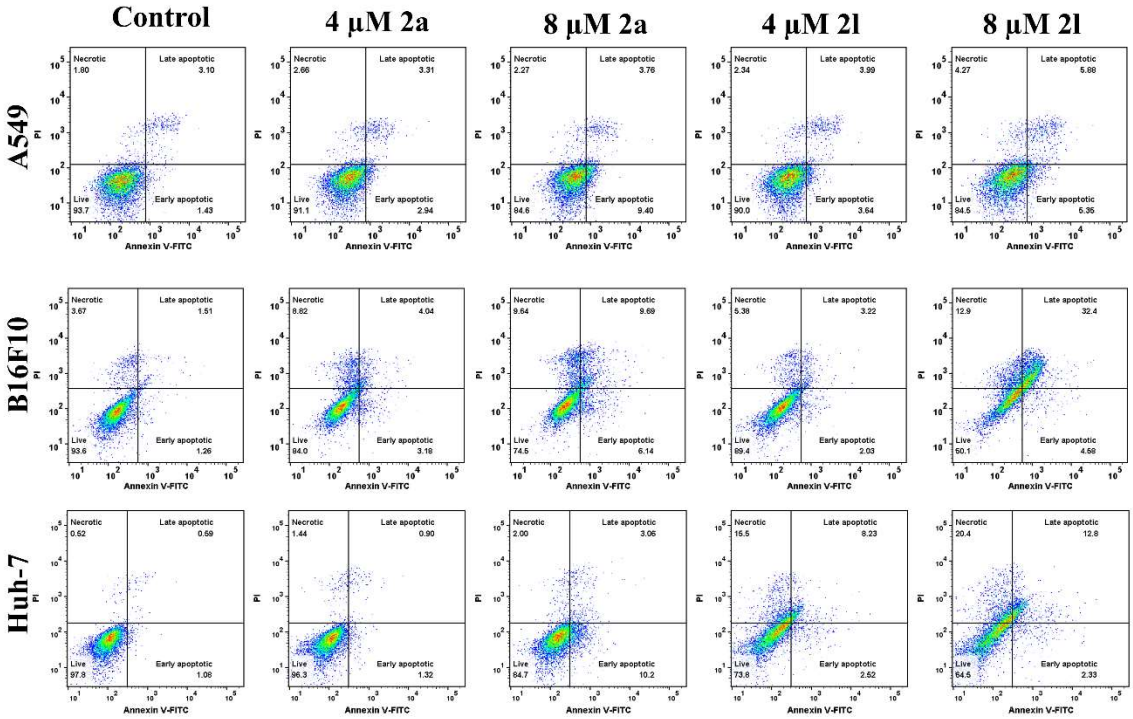

Supplemental Figure 4

Representative dot plots of Annexin-PI staining to determine the percentage of cell death after treatment with 0.1% DMSO (control); **2a** (4 µM); **2a** (8 µM); **2l** (4 µM); and **2l** (8 µM) in three different cell lines (A549, B16F10 and Huh-7) after 24 hours of treatment. The experiment was performed three times.

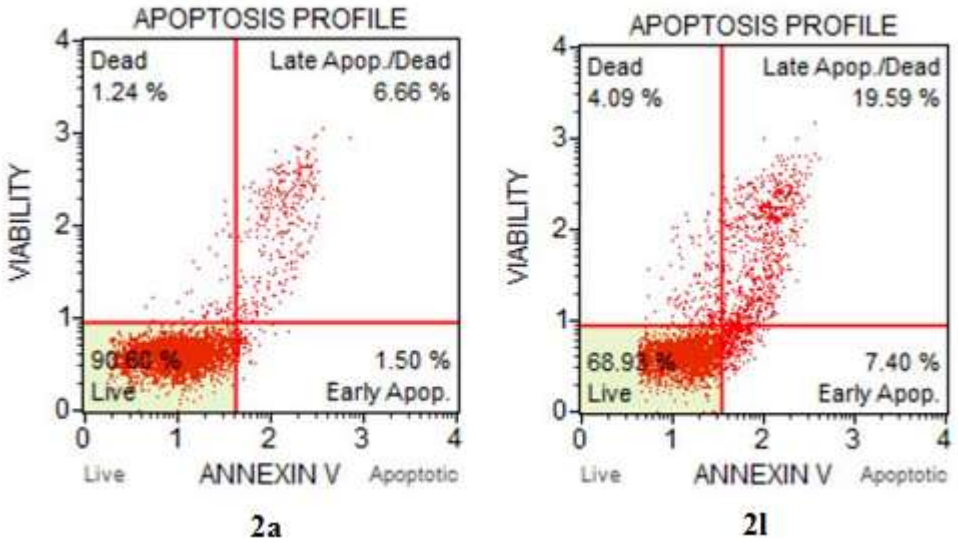

Supplemental Figure 5

Representative dot plot for the annexin V/PI apoptosis assay of PC3 cells 72 hours after the removal of 3,5-bis(styryl)pyrazoles **2a** and **2l** (GI_{50} concentrations).

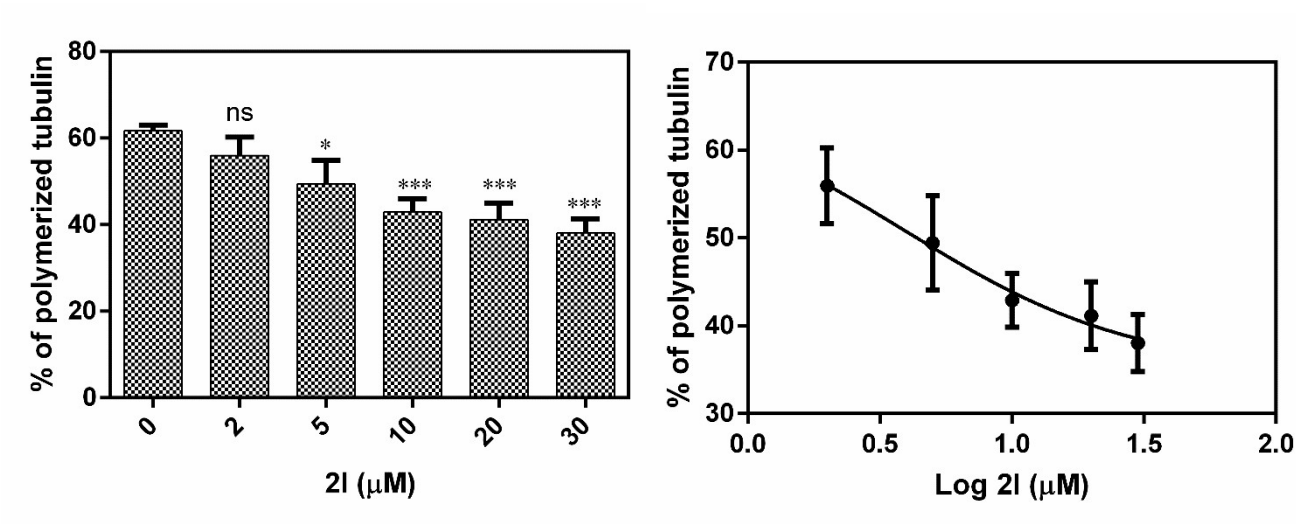

(A) **(B)**

Supplemental Figure 6

Inhibition of tubulin polymerization by 3,-5-bis(styryl)pyrazole **2l** determined by quantifying the amount of microtubules formed in the absence and the presence of different concentrations of **2l** by sedimentation assay; **(A)** percentage of tubulin polymerization quantified by pelleting microtubules at different concentrations of **2l**; **(B)** Determination of IC_{50} of inhibition of tubulin polymerization by **2l** by fitting the data in dose-response inhibition curve in GraphPad Prism software. The experiment was repeated three times and error bars show standard deviations.

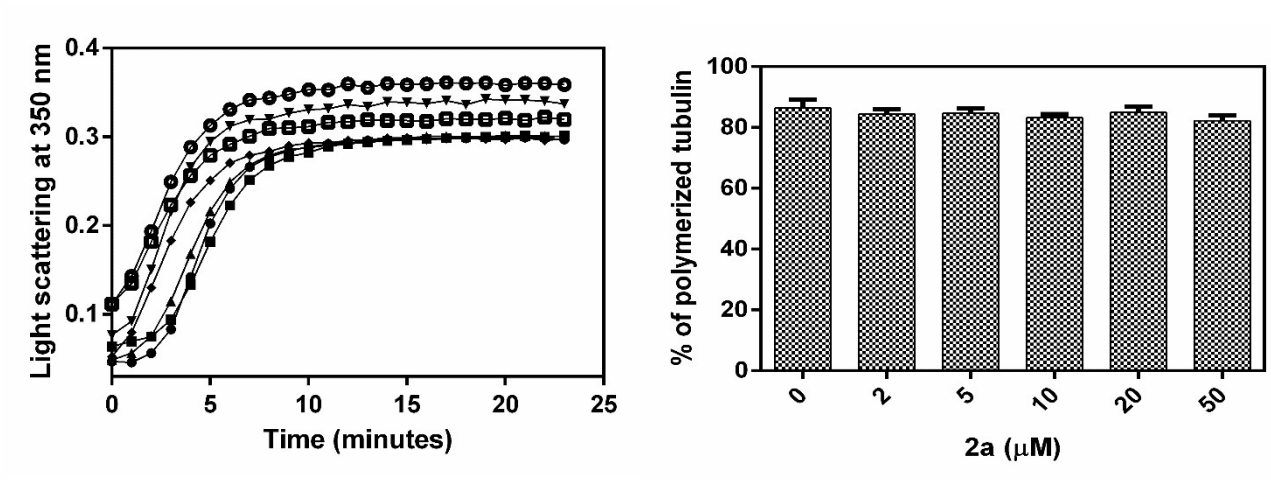

(A) **(B)**

Supplemental Figure 7

Effect of increasing concentrations of **2a** on tubulin polymerization; **(A)** light scattering was observed at similar conditions to **2l**. Tubulin was polymerized without (●) and with 2 (■), 5 (▲), 10 (▼), 20 (♦), 30 (○) and 50 (□) μM of **2a**; **(B)** The amount of polymerized tubulin was determined by sedimentation assay similar to that performed with **2l**. Each experiment was repeated three times and error bar represents standard deviation.

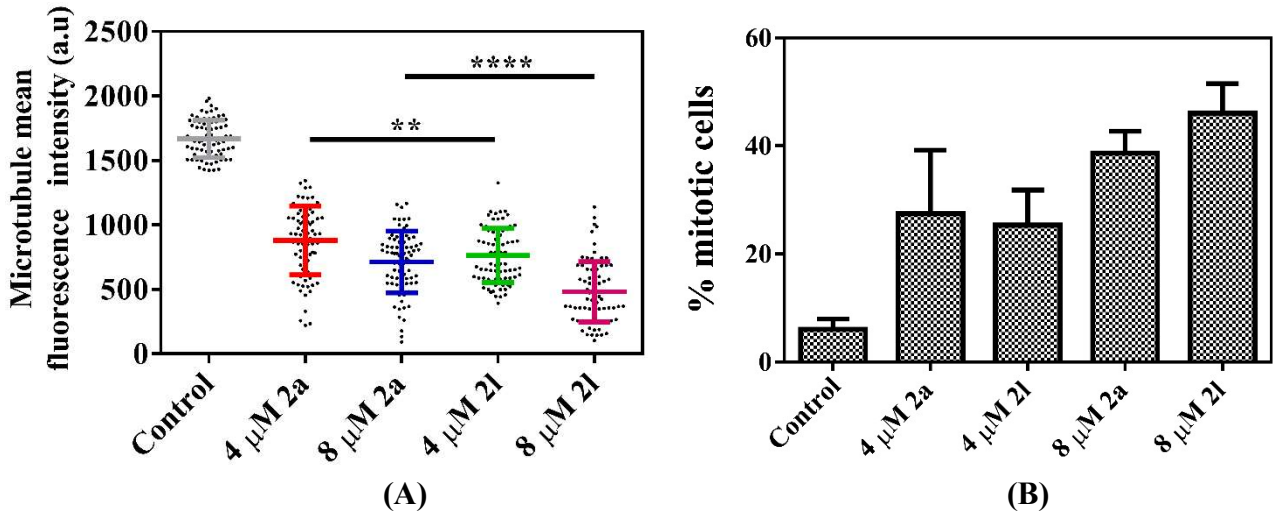

Supplemental Figure 8

(A) The fluorescence intensity of the interphase microtubules in PC3 cells in the absence and presence of 4 and 8 μM of **2a** and **2l.** 200 cells were monitored in each condition. **represents $p < 0.01$; ****represents $p < 0.0001$ by Student's t-test. **(B)** Quantification of percentage of mitotic cells of PC3 cells in the absence and presence of 4 and 8 μM of **2a** and **2l**. Each experiment was repeated three times and error bars represents standard deviation.

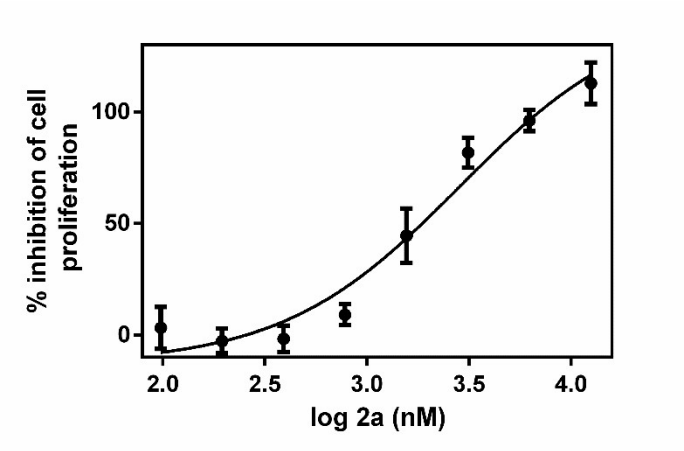
% inhibition of cell proliferation
100
50
0
2.0
2.5
3.0
3.5
4.0
log 2a (nM)

(A)

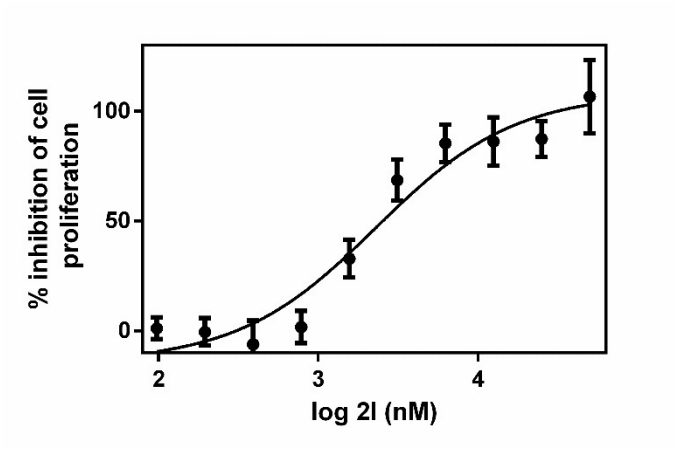
% inhibition of cell proliferation
100
50
0
2
3
4
log 2l (nM)

(B)

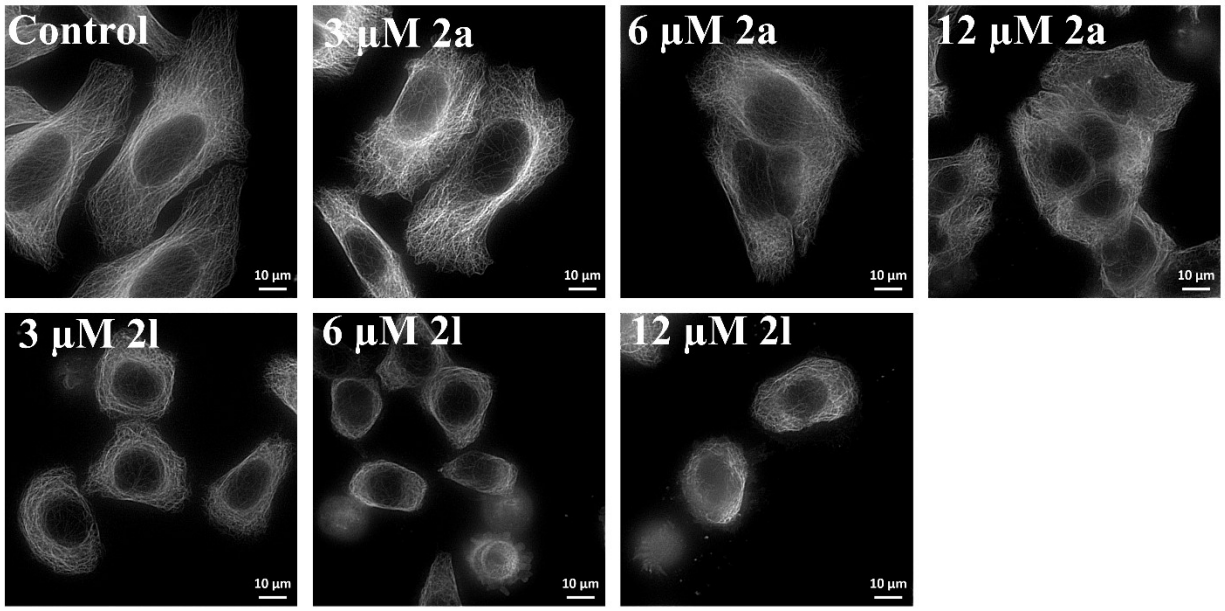
Control
3 µM 2a
6 µM 2a
12 µM 2a
3 µM 2l
6 µM 2l
12 µM 2l
10 µm

(C)

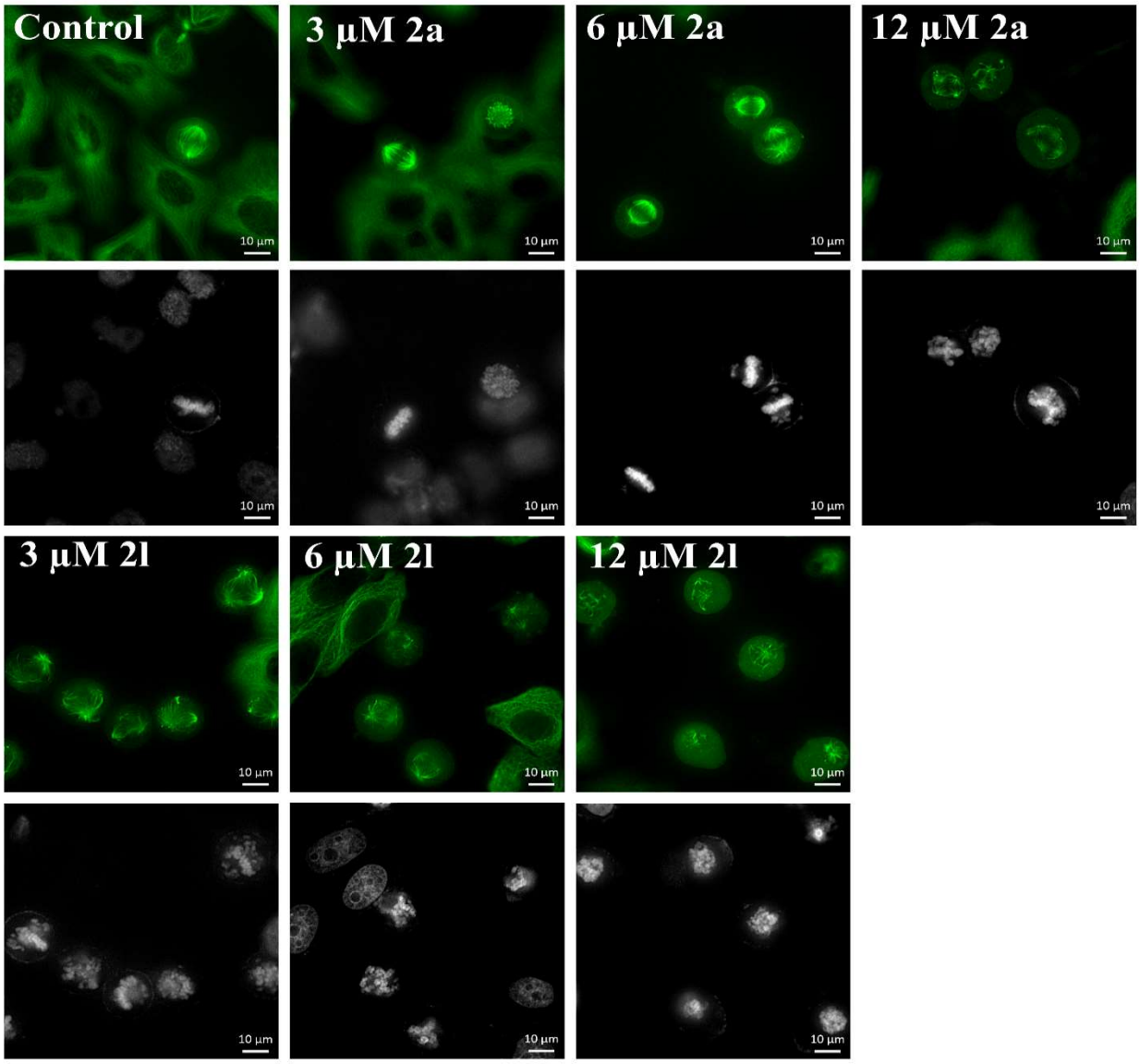

(D)

Supplemental Figure 9

Effect of 3,5-bis(styryl)pyrazoles **2a** and **2l** on HeLa cells. The GI_{50} values for **2a (A)** and **2l (B)** were determined by the Sulphorhodamine B assay. The experiment was performed three times and error bars represent standard deviation. The effect of these compounds on the microtubules of HeLa cells was determined by microtubule staining. Representative fluorescence microscope images of interphase microtubules **(C)** and mitotic microtubules **(D)** are shown after control (0.1 % DMSO treated) and treatment with **2a** and **2l** treatment (3, 6, and 12 μM). The scale bars are shown in the figures.

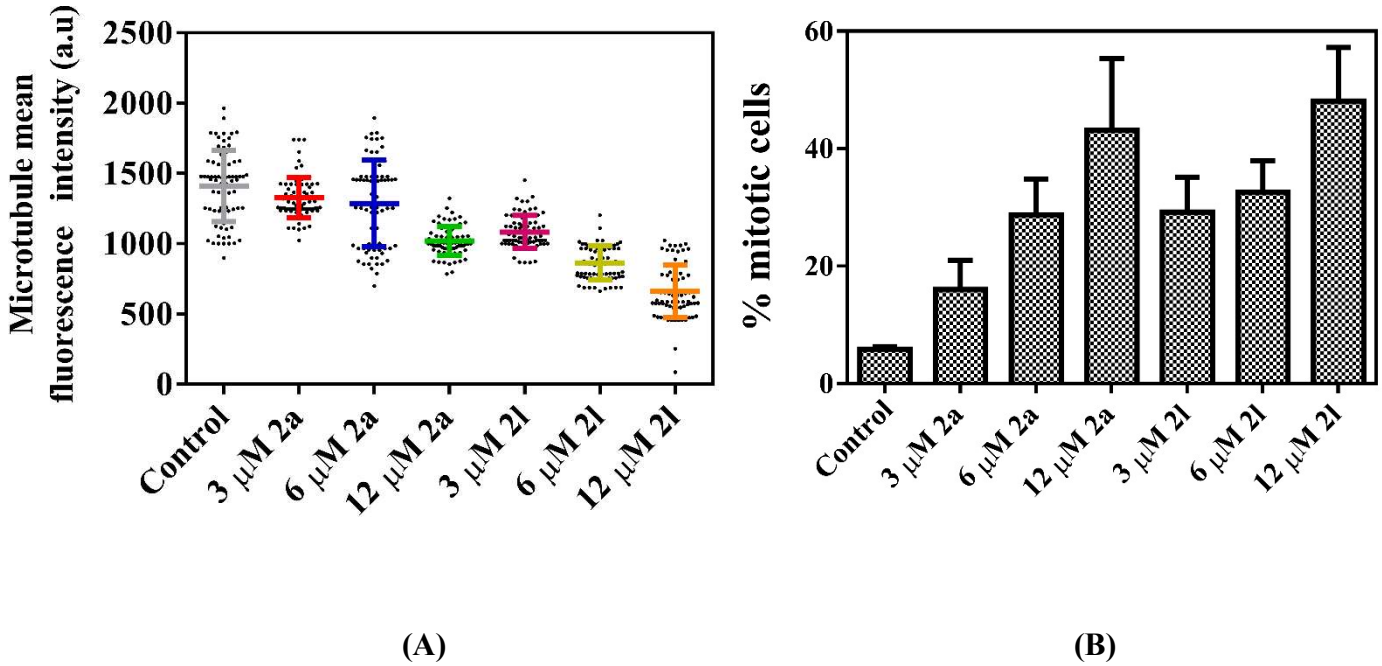

Supplemental Figure 10

(A) Quantification of interphase microtubule intensity of HeLa cells in the absence and presence of 3, 6 and 12 μM of **2a** and **2l**. **(B)** Quantification of percentage of mitotic cells of HeLa cells in the absence and presence of 3, 6 and 12 μM of **2a** and **2l**. Each experiment was repeated three times and error bar represents standard deviation.

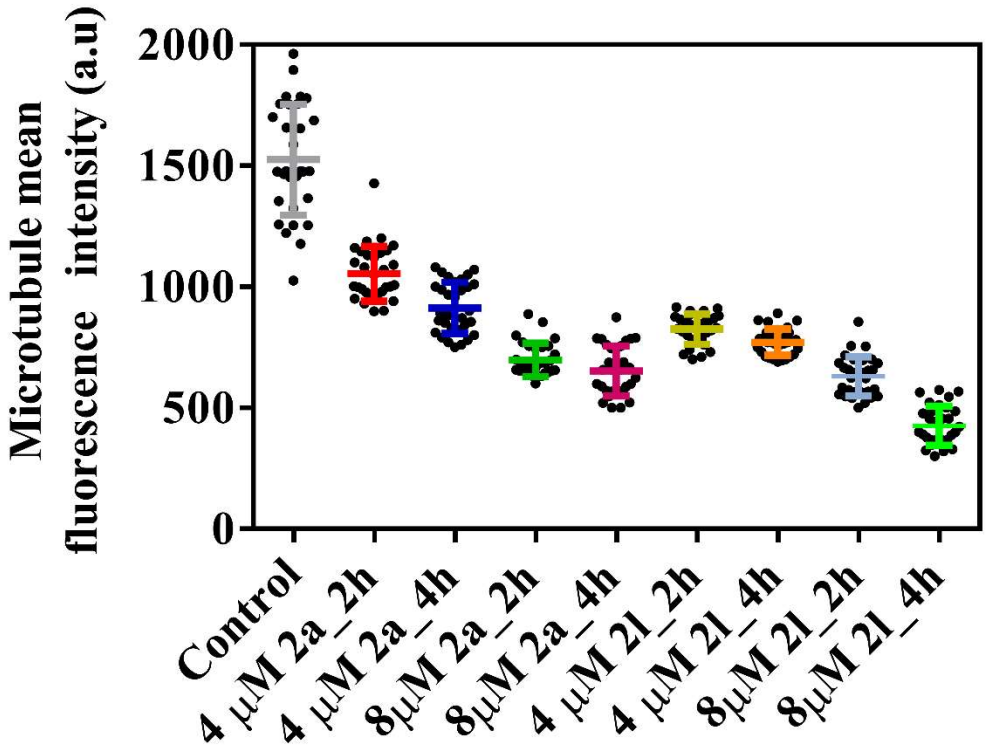

Supplemental Figure 11

Quantification of interphase microtubule intensity of PC3 in the absence and presence of 4 and 12 μM of **2a** and **2l** for 2hours and 4 hours. Experiment was repeated three times and error bar represents standard deviation.

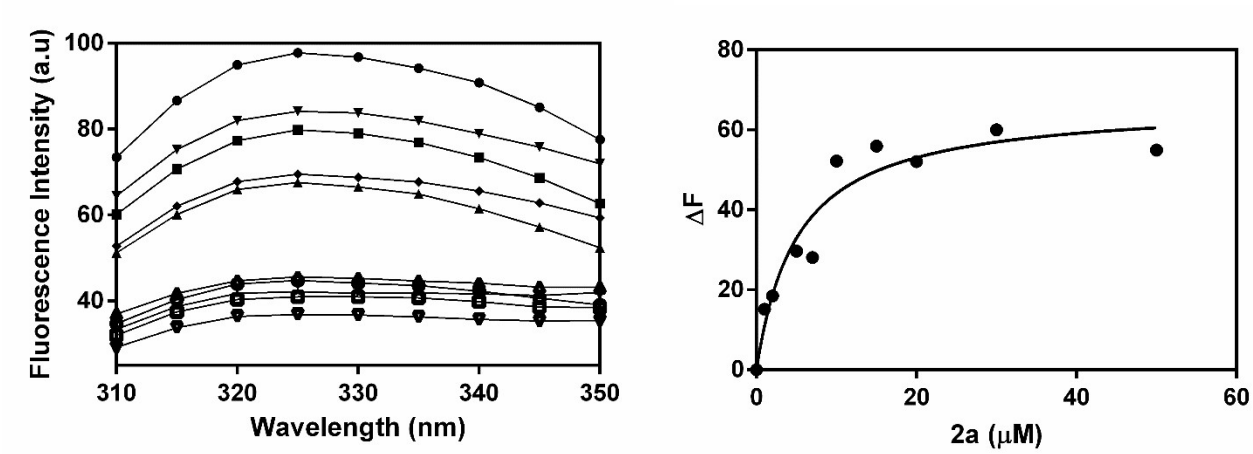

(A) **(b)**

Supplemental Figure 12

Determination of the dissociation constant (K_d) of the tubulin-**2a** complex. **(A)** the fluorescence of tubulin decreases with increasing concentrations of **2a**; 0 (●), 1 (■), 2 (▲), 5 (▼), 7 (♦), 10 (○), 15 (□), 20 (Δ), 30 (⋆) and 50 (◊) μM; **(B)** the line of best fit for the difference in fluorescence at 340 nm at different concentrations was fitted gives the dissociation constant (K_d). The experiment was repeated three times.

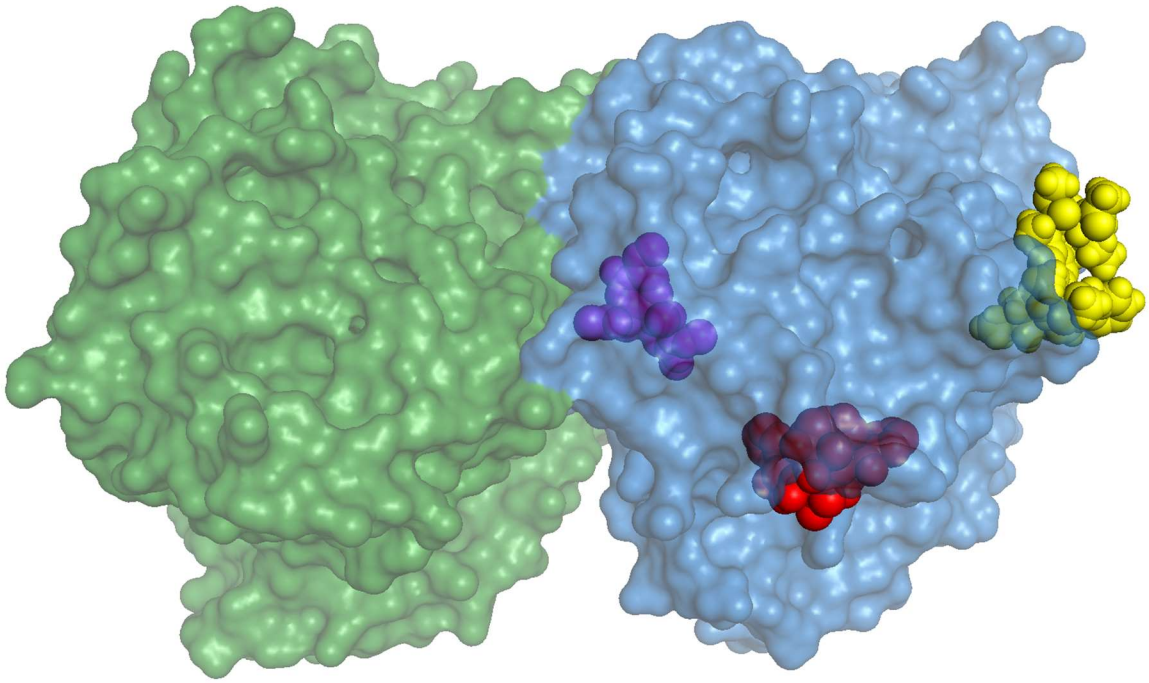

Supplemental Figure 13

Surface representation of α and β tubulin heterodimer with the three major binding sites. Tubulin is taken from the crystal structure of PDB: 5J2T. β-tubulin surface structure is shown in cyan colour while α-tubulin surface structure is shown in green colour. The three main ligands binding on three different binding sites on tubulin are shown by sphere representation. Colchicine is shown as navy blue spheres taken from PDB: 4O2B. Vinblastine is shown as yellow spheres taken from PDB: 5J2T. Taxol is shown as red spheres taken from PDB: 1TUB. The structure was generated using PyMOL.

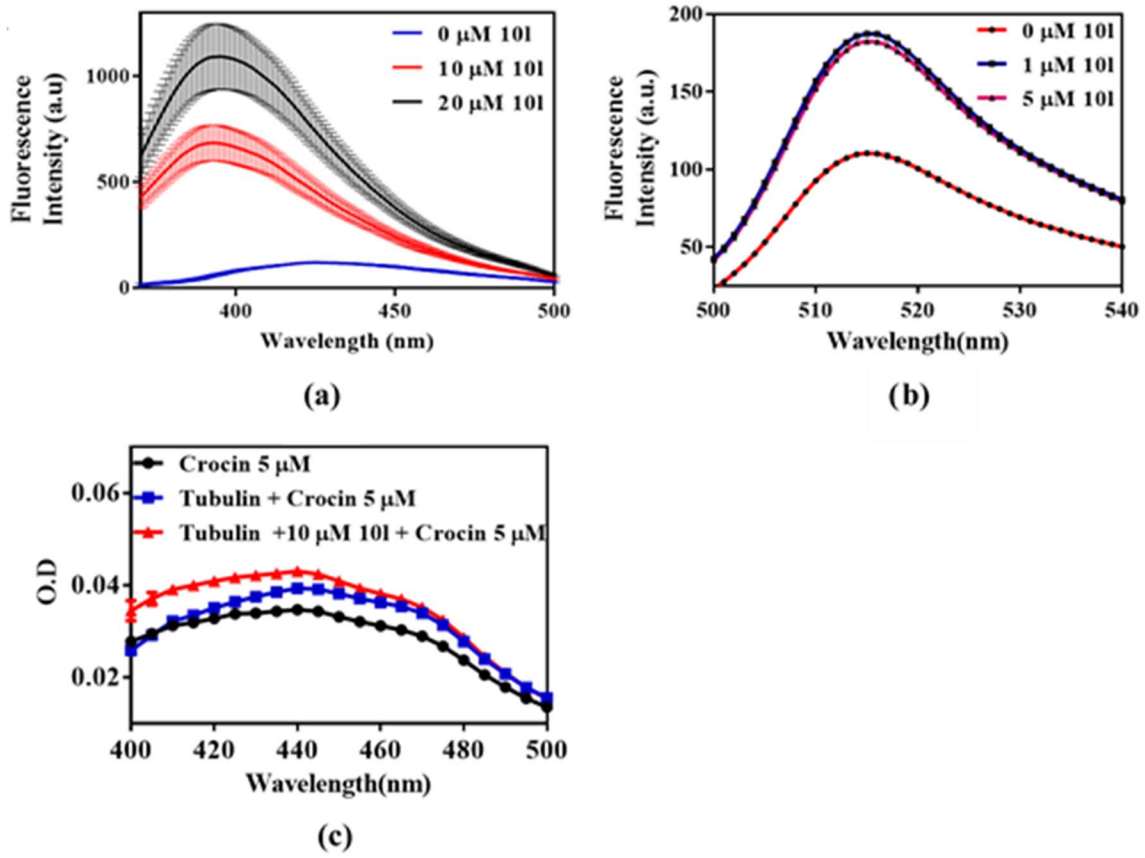

Supplemental Figure 14

Determination of the binding site of **2l** on tubulin; **(A)** the fluorescence of colchicine (blue) increases with increasing concentrations of **2l**; 10 (red) and 20 (black) µM indicating that **2l** does not bind to the colchicine binding site; **(B)** the fluorescence of BODIPY-FL-vinblastine (red) increases with increasing concentrations of **2l**; 1 (blue) and 5 (pink) µM showing **2l** does not bind to the vinblastine binding site ; **(C)** the absorbance of crocin (black) increases upon incubation with tubulin (blue) but remains unchanged (red) in presence of **2l** indicating that **2l** does not bind to the crocin binding site.

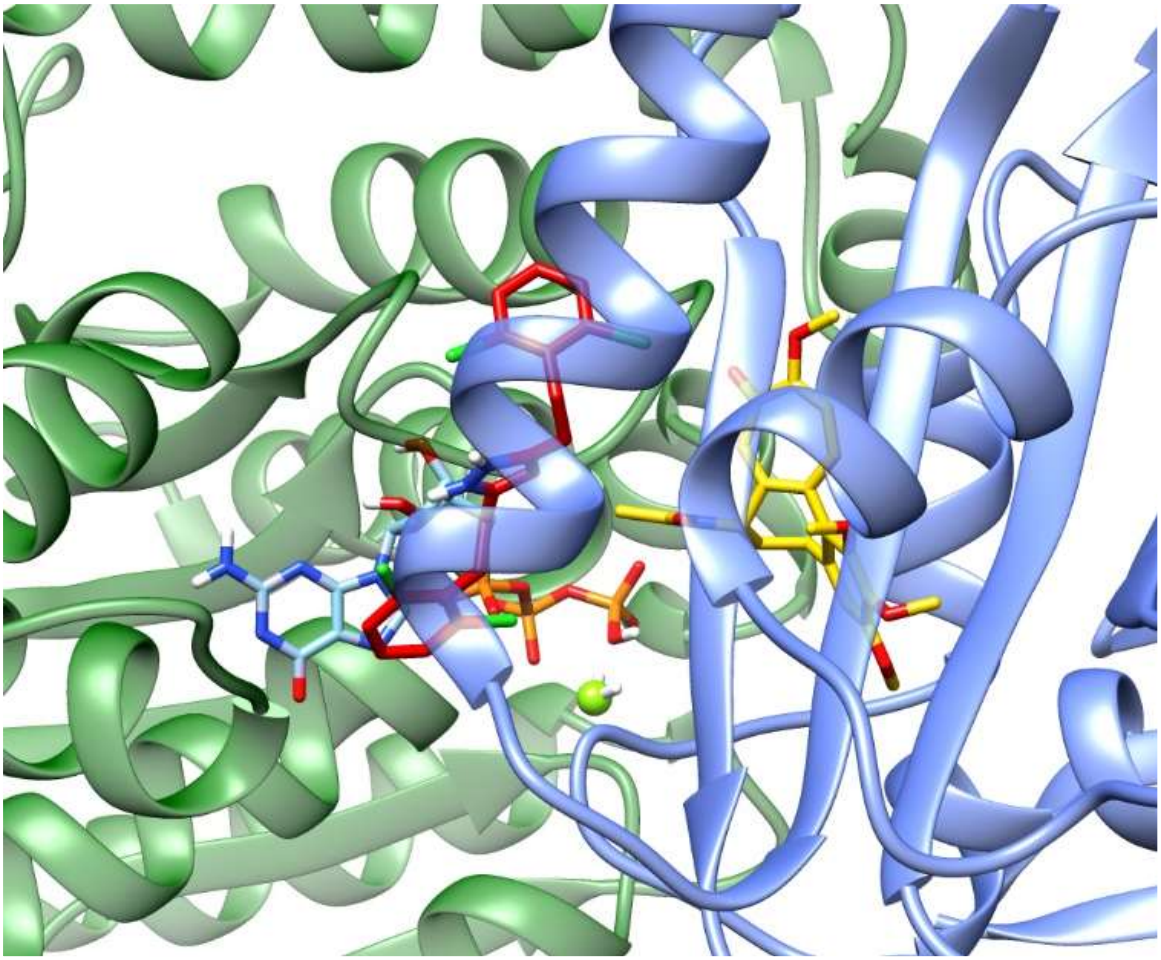

Supplemental Figure 15

Docking of **2l** and colchicine on tubulin; **2l** (red sticks) and colchicine (yellow sticks) are shown to bind at the β-tubulin (blue ribbons) and α-tubulin (green ribbons) heterodimer interface. GTP is shown in blue stick and green ball is magnesium ion.